

MIT Open Access Articles

Measurement of jet charge in dijet events from $\sqrt{s} = 8$ TeV $p p$ collisions with the ATLAS detector

The MIT Faculty has made this article openly available. **Please share** how this access benefits you. Your story matters.

Citation: Aad, G., et al. "Measurement of Jet Charge in Dijet Events from $\sqrt{s} = 8$ TeV $p p$ Collisions with the ATLAS Detector." *Physical Review D*, vol. 93, no. 5, Mar. 2016. © 2016 CERN, for the ATLAS Collaboration

As Published: <http://dx.doi.org/10.1103/PhysRevD.93.052003>

Publisher: American Physical Society

Persistent URL: <http://hdl.handle.net/1721.1/113821>

Version: Final published version: final published article, as it appeared in a journal, conference proceedings, or other formally published context

Terms of Use: Article is made available in accordance with the publisher's policy and may be subject to US copyright law. Please refer to the publisher's site for terms of use.



Measurement of jet charge in dijet events from $\sqrt{s} = 8$ TeV pp collisions with the ATLAS detector

G. Aad *et al.**

(ATLAS Collaboration)

(Received 18 September 2015; published 2 March 2016)

The momentum-weighted sum of the charges of tracks associated to a jet is sensitive to the charge of the initiating quark or gluon. This paper presents a measurement of the distribution of momentum-weighted sums, called *jet charge*, in dijet events using 20.3 fb^{-1} of data recorded with the ATLAS detector at $\sqrt{s} = 8$ TeV in pp collisions at the LHC. The jet charge distribution is unfolded to remove distortions from detector effects and the resulting particle-level distribution is compared with several models. The p_T dependence of the jet charge distribution average and standard deviation are compared to predictions obtained with several leading-order and next-to-leading-order parton distribution functions. The data are also compared to different Monte Carlo simulations of QCD dijet production using various settings of the free parameters within these models. The chosen value of the strong coupling constant used to calculate gluon radiation is found to have a significant impact on the predicted jet charge. There is evidence for a p_T dependence of the jet charge distribution for a given jet flavor. In agreement with perturbative QCD predictions, the data show that the average jet charge of quark-initiated jets decreases in magnitude as the energy of the jet increases.

DOI: [10.1103/PhysRevD.93.052003](https://doi.org/10.1103/PhysRevD.93.052003)

I. INTRODUCTION

Quarks and gluons produced in high-energy particle collisions hadronize before their electric charge can be directly measured. However, information about the electric charge is embedded in the resulting collimated sprays of hadrons known as jets. One jet observable sensitive to the electric charge of quarks and gluons is the momentum-weighted charge sum constructed from charged-particle tracks in a jet [1]. Called the *jet charge*, this observable was first used experimentally in deep inelastic scattering studies [2–8] to establish a relationship between the quark model and hadrons. Since then, jet charge observables have been used in a variety of applications, including tagging the charge of b -quark jets [9–19] and hadronically decaying W bosons [20–25] as well as distinguishing hadronically decaying W bosons from jets produced in generic quantum chromodynamic (QCD) processes [25] and quark jets from gluon jets [24,26–28].

The study presented in this paper is a measurement of the jet charge distribution in inclusive dijet events from pp collisions at the LHC. Inclusive dijet events provide a useful environment for measuring the jet charge as they are an abundant source of gluon-initiated and quark-initiated jets. There are fewer theoretical ambiguities from close-by jets and large-angle radiation associated with assigning the

jet flavor in events with two jets than in events with higher jet multiplicities. Furthermore, the transverse momentum (p_T) range accessible in dijet events is broad, $\mathcal{O}(10)$ GeV up to $\mathcal{O}(1000)$ GeV. Since the initial state at the LHC has a net positive charge, the probability for positively charged quarks to be produced in pp collisions is higher than that for negatively charged quarks. The probability for collisions to involve a positively charged valence up quark in the proton increases with the parton center-of-mass energy $\sqrt{\hat{s}}$. Thus the average jet charge in inclusive dijet events is expected to increase with $\sqrt{\hat{s}}$ if it is correlated with the quark charge. The parton distribution functions (PDFs) encode the probabilities to find gluons and certain flavors of quarks at given momentum fractions x of the proton. The momentum fractions of the two initial partons x_1, x_2 , and the proton and parton center-of-mass energies \sqrt{s} and $\sqrt{\hat{s}}$ are related by $\sqrt{\hat{s}} = \sqrt{x_1 x_2 s}$. The PDFs are fairly well constrained [29–33] in the x range relevant for this study, 0.005–0.5. However, if the jet charge is directly sensitive to the parton flavor, its p_T dependence can provide a consistency check using new information beyond the jet p_T , which is currently used in PDF fits. The PDFs are not the only nonperturbative input needed to model the jet charge distribution and its evolution with $\sqrt{\hat{s}}$. As a momentum-weighted sum over jet constituents, the jet charge is sensitive to the modeling of fragmentation. Previous studies have shown that there are qualitative differences between the charged-particle track multiplicities of jets in data and as predicted by the leading models of hadron production [26]. Thus, a measurement of the jet charge distribution

*Full author list given at the end of the article.

Published by the American Physical Society under the terms of the [Creative Commons Attribution 3.0 License](https://creativecommons.org/licenses/by/3.0/). Further distribution of this work must maintain attribution to the author(s) and the published article's title, journal citation, and DOI.

with a range of quark/gluon compositions can provide a constraint on models of jet formation.

While the change in jet parton flavor due to the PDF x dependence predicts most of the variation in the jet charge distribution as a function of \sqrt{s} , there is a second contribution due to the energy dependence of the fragmentation functions. Ratios of the charge distribution moments at different values of \sqrt{s} can be calculated perturbatively. Recent calculations [34,35] in the context of soft collinear effective theory [36–39] show a significant reduction in the magnitude of the average jet charge for a given jet flavor as a function of jet energy. Information from PDFs can be used to extract the energy dependence of the average jet charge in the data for direct comparisons to the predictions.

This paper presents a measurement of the p_T dependence of the jet charge distribution's mean and standard deviation in dijet events in pp collisions at $\sqrt{s} = 8$ TeV with the ATLAS detector. The jet p_T is a measurable quantity that is strongly related to \sqrt{s} . The average jet charge is extracted for both the leading and subleading jet and they are distinguished based on their relative orientation in rapidity.¹ After a description of the ATLAS detector (Sec. II), the data and simulated samples (Sec. III) and the detector- and particle-level objects and selections used in the analysis (Sec. IV), Sec. V details the construction of the jet charge and some of its properties. In order for the measured jet charge distribution to be compared with particle-level models, the data are unfolded to remove distortions from detector effects, as described in Sec. VI. Systematic uncertainties in the measured jet charge spectra are discussed in Sec. VII and the results are presented in Sec. VIII.

II. THE ATLAS DETECTOR

ATLAS [40] is a general-purpose detector designed to measure the properties of particles produced in high-energy pp collisions with nearly a full 4π coverage in solid angle. The innermost subsystem of the detector is a series of tracking devices used to measure charged-particle trajectories bent in a 2 T axial field provided by a solenoid whose axis is parallel with the beam direction. This inner detector (ID) consists of a silicon pixel detector surrounded by a semiconductor microstrip detector (SCT) and a straw-tube

¹ATLAS uses a right-handed coordinate system with its origin at the nominal interaction point (IP) in the center of the detector and the z axis along the beam pipe. The x axis points from the IP to the center of the LHC ring, and the y axis points upward. Cylindrical coordinates (r, ϕ) are used in the transverse plane, with ϕ being the azimuthal angle around the beam pipe. The pseudorapidity is defined in terms of the polar angle θ as $\eta = -\ln \tan(\theta/2)$. The variable $\Delta R = \sqrt{(\Delta\phi)^2 + (\Delta\eta)^2}$ is a measure of how close two objects are in the (η, ϕ) plane. The rapidity of a four-vector is defined as $y = 0.5 \ln\left(\frac{E+p_z}{E-p_z}\right)$, where E is the energy and p_z is the component of the momentum parallel to the beam axis.

tracker. It has full coverage in ϕ and can detect particles with $|\eta| < 2.5$. Charged-particle tracks are reconstructed from all three ID components, providing measurements of the transverse momentum of tracks with a resolution $\sigma_{p_T}/p_T = 0.05\% \times p_T/\text{GeV} \oplus 1\%$. The track reconstruction algorithm fits five track parameters: d_0 , z_0 , ϕ , θ , and q/p , where d_0 and z_0 are the transverse and longitudinal impact parameters, respectively, q is the track charge and p is the track momentum. Excellent spatial precision is required to maintain a well-performing track reconstruction out to and exceeding charged-particle p_T of 1 TeV, where track sagittas are $\lesssim 0.2$ mm.

Surrounding the ID and solenoid are electromagnetic and hadronic calorimeters to measure showers from charged and neutral particles. The high-granularity liquid-argon (LAr) sampling electromagnetic calorimeter is located just beyond the solenoid and spans the range $|\eta| < 3.2$. Beyond the electromagnetic calorimeter is the two-component hadronic calorimeter that uses scintillator-tile sampling technology in the range $|\eta| < 1.7$ and LAr sampling technology for $1.5 < |\eta| < 3.2$. Additional calorimeters are located in the forward region. Surrounding the calorimeters is a muon spectrometer, with trigger and precision chambers, and incorporating three large toroid magnets composed of eight coils each.

Due to the large event rate, not every collision can be recorded for processing offline. Events are selected using a three-level trigger system [41] that is hardware based at the first level and software based for the two following levels. An event must satisfy all three trigger levels to be recorded for further processing. At each stage of the trigger, energy thresholds are placed on jet-like objects, with the similarity between online and offline jets increasing with each level. The first level makes decisions based on low-granularity calorimeter towers with thresholds that are typically less than half of the energy required by jets at the second level. A simple jet reconstruction algorithm is used at the second level in regions around the jets identified by the first level. The third level (known as the Event Filter) clusters jets with the same algorithm as used offline over the entire detector with thresholds that are typically 20–30 GeV higher than at level two. The single-jet trigger thresholds increase at each level due not only to differences in the jet reconstruction and calibrations, but also to meet the different bandwidth requirements at each trigger level. For low- p_T dijets, the event rate is far too large to save every event that passes the trigger selection and so most of the jet triggers are *prescaled* to artificially lower their recording rate.

III. DATA AND SIMULATED SAMPLES

This measurement uses the full data set of pp collisions recorded by the ATLAS detector in 2012, corresponding to an integrated luminosity of 20.3 fb^{-1} at a center-of-mass energy of $\sqrt{s} = 8$ TeV. Events are only considered if they are collected during stable beam conditions and satisfy all

TABLE I. The single-jet trigger menu used to collect dijet events with the 2012 data set. The first column is the level-three (Event Filter) jet p_T threshold and the second column is the offline leading-jet p_T range corresponding to the given trigger. The luminosity collected with each trigger is in the last column. The total 2012 data set was 20.3 fb^{-1} ; the highest- p_T trigger is not prescaled.

Trigger threshold [GeV]	Offline selection [GeV]	Luminosity [fb^{-1}]
25	[50, 100]	7.84×10^{-5}
55	[100, 136]	4.42×10^{-4}
80	[136, 190]	2.32×10^{-3}
110	[190, 200]	9.81×10^{-3}
145	[200, 225]	3.63×10^{-2}
180	[225, 250]	7.88×10^{-2}
220	[250, 300]	2.61×10^{-1}
280	[300, 400]	1.16
360	≥ 400	20.3

data-quality requirements [42]. To reject noncollision events, there must be a primary vertex reconstructed from at least two tracks each with $p_T > 400 \text{ MeV}$ [43]. Due to the high instantaneous luminosity and the large total inelastic proton-proton cross section, on average there are about 21 simultaneous (*pileup*) collisions in each bunch crossing.

A set of single-jet triggers is used to collect dijet events with high efficiency. Table I shows the collected luminosity for each trigger as well as the offline jet p_T ranges used, chosen such that the trigger is fully efficient. The highest- p_T trigger is not prescaled.

Monte Carlo (MC) simulated events are generated in p_T slices in order to ensure a large number of events over a broad range of reconstructed jet p_T , given constraints on the available computing resources. The p_T slices span the interval 0 to 5 TeV in ranges that approximately double with each increasing slice, starting with a range of size 8 GeV and ending with a range of size 2240 GeV. The baseline sample used for the measurement is generated with PYTHIA 8.175 [44] with the AU2 [45] set of tuned parameters (tune) and the next-to-leading-order (NLO) PDF set² CT10 [48,49]. Another large sample of events is generated with HERWIG++ 2.63 [50,51] with tune EE3 [52] and leading-order (LO) PDF set CTEQ6L1 [53] (particle-level samples with CT10 and EE4 are also used for comparisons). Both PYTHIA and HERWIG++ are LO in perturbative QCD for the $(2 \rightarrow 2)$ matrix element and resum the leading logarithms in the parton shower. However, the ordering of emissions in the MC resummation in the shower differs between these two generators: PYTHIA implements p_T -ordered showers [54] whereas

²A discussion on the use of NLO PDF sets with LO matrix elements is given in Refs. [46,47].

HERWIG++ uses angular ordering [55]. The phenomenological modeling of the nonperturbative physics also differs between PYTHIA and HERWIG++. In addition to different underlying-event models (Ref. [56] for PYTHIA and an eikonal model [57] for HERWIG++) the hadronization models differ between PYTHIA (Lund string model [58]) and HERWIG++ (cluster model [59]). These two schemes are known [26] to predict different numbers of charged particles within jets and different distributions of the charged-particle energies within jets, both of which are important for the jet charge. All tunes of the underlying event that are used with PYTHIA and HERWIG++ in this analysis use LHC data as input. As discussed in Sec. I, the corrected data are compared to models with various PDF sets; for consistency, each set has a dedicated underlying-event tune constructed in the same way from a fixed set of data inputs (AU2) described in detail in Ref. [45]. The PDF sets include LO sets CTEQ6L1 [53] and MSTW08LO [29] as well as NLO sets CT10 [48,49], NNPDF21 NLO [60], and MSTW2008NLO [29]. A sample generated with a NLO matrix element from POWHEG-BOX R2262 [61–64] (henceforth referred to as POWHEG) with PDF set CT10 interfaced with PYTHIA 8.175 and the AU2 tune is also used for comparisons.

All MC samples are processed using the full ATLAS detector simulation [65] based on GEANT4 [66].

IV. OBJECT RECONSTRUCTION AND EVENT SELECTION

The reconstructed objects used for the jet charge as well as for the event selection are described in Sec. IV A. The fiducial definition of the measurement, unfolded to particle level, is given in Sec. IV B.

A. Object reconstruction at detector level

Jets are clustered using the anti- k_r jet algorithm [67] with radius parameter $R = 0.4$ implemented in Fastjet [68] from topological calorimeter-cell clusters [69], calibrated using the local cluster weighting algorithm [70,71]. An overall jet energy calibration accounts for residual detector effects as well as contributions from pileup [72] in order to make the reconstructed jet energy an unbiased measurement of the particle-level jet energy. Jets are required to be central ($|\eta| < 2.1$) so that their charged particles are within the $|\eta| < 2.5$ coverage of the ID.

When more than one primary vertex is reconstructed, the one with the highest $\sum p_T^2$ of tracks is selected as the hard-scatter vertex. Events are further required to have at least two jets with $p_T > 50 \text{ GeV}$ and only the leading two jets are considered for the jet charge measurement. To select dijet topologies, the two leading jets must have $p_T^{\text{lead}}/p_T^{\text{sublead}} < 1.5$, where p_T^{lead} and p_T^{sublead} are the transverse momenta of the jets with the highest and second-highest p_T , respectively. The jet with the smaller (larger)

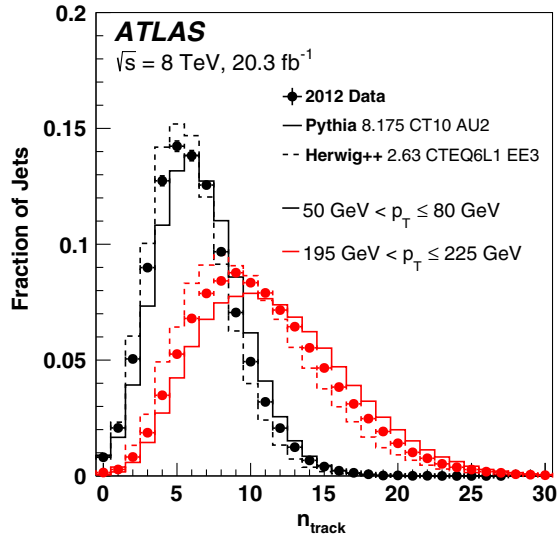


FIG. 1. The distribution of the number of tracks associated with a jet in two example jet p_T ranges.

absolute pseudorapidity $|\eta|$ is classified as the more central (more forward) jet. A measurement of the more forward and more central jet charge distributions can exploit the rapidity dependence of the jet flavor to extract information about the jet charge for a particular flavor. This is discussed in more detail in Sec. IV B.

Tracks used to calculate the jet charge are required to have $p_T \geq 500$ MeV, $|\eta| < 2.5$, and a χ^2 per degree of freedom (resulting from the track fit) less than 3.0. Additional quality criteria are applied to select tracks originating from the collision vertex and reject fake tracks reconstructed from random hits in the detector. In particular, tracks must be well matched to the hard-scatter vertex with $|z_0 \sin(\theta)| < 1.5$ mm and $|d_0| < 1$ mm, where z_0 and d_0 are calculated with respect to the primary vertex. Tracks must furthermore have at least one hit in the pixel detector and at least six hits in the SCT. The matching of tracks with the calorimeter-based jets is performed via the ghost-association technique [73]: the jet clustering process is repeated with the addition of *ghost* versions of measured tracks that have the same direction but infinitesimally small p_T , so that they do not change the properties of the calorimeter jets. A track is associated with a jet if its ghost version is contained in the jet after reclustering. The distribution of the number of tracks in two representative jet p_T ranges is shown in Fig. 1. The number of tracks increases with jet p_T and the data fall between the predicted distributions of PYTHIA and HERWIG++.

B. Object definitions at particle level

The measurement is carried out within a fiducial volume matching the experimental selection to avoid extrapolation into unmeasured kinematic regions that have additional model dependence and related uncertainties. Particle-level

definitions of the reconstructed objects are chosen to be as close as possible to those described in Sec. IV A. Particle-level jets are clustered from generated stable particles with a mean lifetime $\tau > 30$ ps, excluding muons and neutrinos. As with the detector-level jets, particle-level jets are clustered with the anti- k , $R = 0.4$ algorithm. In analogy to the ghost association of tracks to jets performed at detector level, any charged particle clustered in a particle-level jet is considered for the jet charge calculation.³ There must be at least two jets with $|\eta| < 2.1$ and $p_T > 50$ GeV. The two highest- p_T jets must satisfy the same p_T -balance requirement between the leading and subleading jet as at detector level ($p_T^{\text{lead}}/p_T^{\text{sublead}} < 1.5$). Due to the high-energy and well-separated nature of the selected jets, the hard-scatter quarks and gluons can be cleanly matched to the outgoing jets. While it is possible to classify jets as quark- or gluon-initiated beyond leading order in $m_{\text{jet}}/E_{\text{jet}}$ [74], the classification is algorithm dependent and unnecessary for the present considerations. In this analysis, the flavor of a jet is defined as that of the highest-energy parton in simulation within a $\Delta R < 0.4$ cone around the particle-jet axis. The jet flavor depends on rapidity and so the two selected jets are classified as either more forward or more central; the more forward jet tends to be correlated to the higher- x parton and is less likely to be a gluon jet. Figure 2 shows the flavor fraction for the more forward and more central particle-level jets passing the event selection. The p_T evolution of the sum of the flavor fractions weighted by the sign of the parton charge is shown in Fig. 2(b). The forward-central differences between the flavor fractions are largest at low p_T , but the highest quark-jet purity occurs at high jet p_T .

V. CONSTRUCTING THE JET CHARGE

There is no unique way to define the jet charge. The most naive construction is to add up the charge of all tracks associated with a jet. However, this scheme is very sensitive to lost or extraneous soft radiation. Therefore, a weighting scheme is introduced to suppress fluctuations. Using the tracks assigned to a jet by ghost association, the jet charge Q_J of a jet J is calculated using a transverse-momentum-weighting scheme [1]:

$$Q_J = \frac{1}{(p_{TJ})^\kappa} \sum_{i \in \text{Tracks}} q_i \times (p_{T,i})^\kappa, \quad (1)$$

where Tracks is the set of tracks associated with jet J , q_i is the charge (in units of the positron charge) of track i with associated transverse momentum $p_{T,i}$, κ is a free regularization parameter, and p_{TJ} is the transverse momentum of the calorimeter jet. The distributions of Q_J for various jet flavors are shown in Fig. 3 for $\kappa = 0.3$. In the simulation,

³There is no $p_T > 500$ MeV threshold applied to charged particles. The impact of applying such a threshold is negligible for all p_T bins except the first two where effects of up to 1% are observed in the mean and standard deviation of the jet charge.

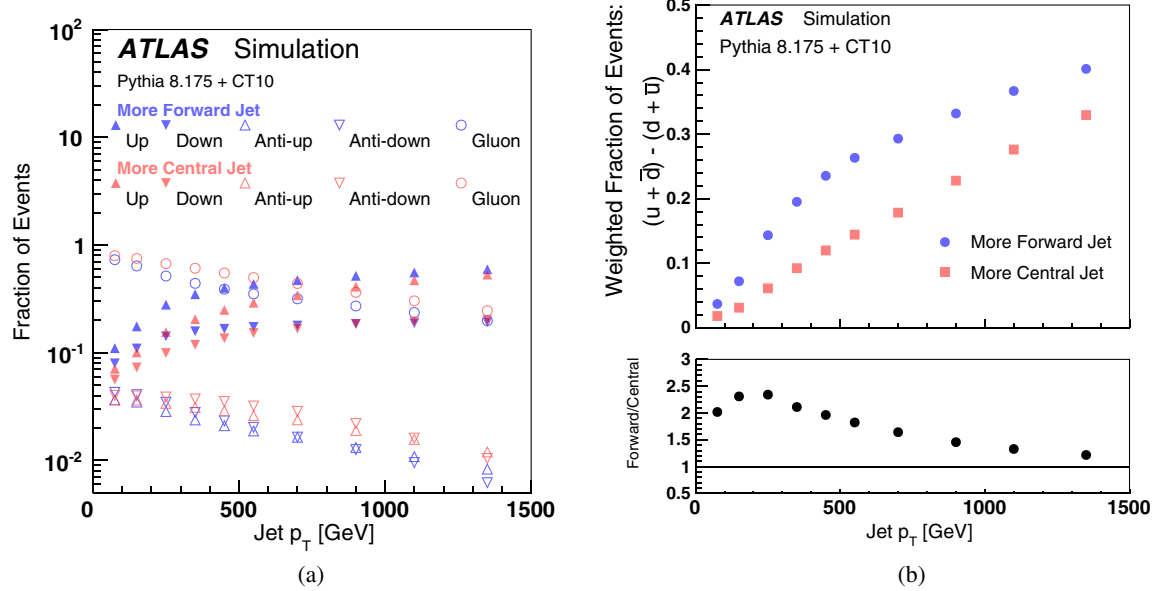


FIG. 2. For a given jet flavor, (a) shows the fraction f of jets with that flavor in events passing the particle-level event selection and (b) shows the p_T evolution of the flavor fractions weighted by charge sign: $f_{\text{up}} + f_{\text{anti-down}} - f_{\text{anti-up}} - f_{\text{down}}$. The forward-central differences between the flavor fractions are largest at low p_T , but the highest quark-jet purity occurs at high jet p_T . The markers for the more forward and central jets are distinguished by their blue and red colors, respectively.

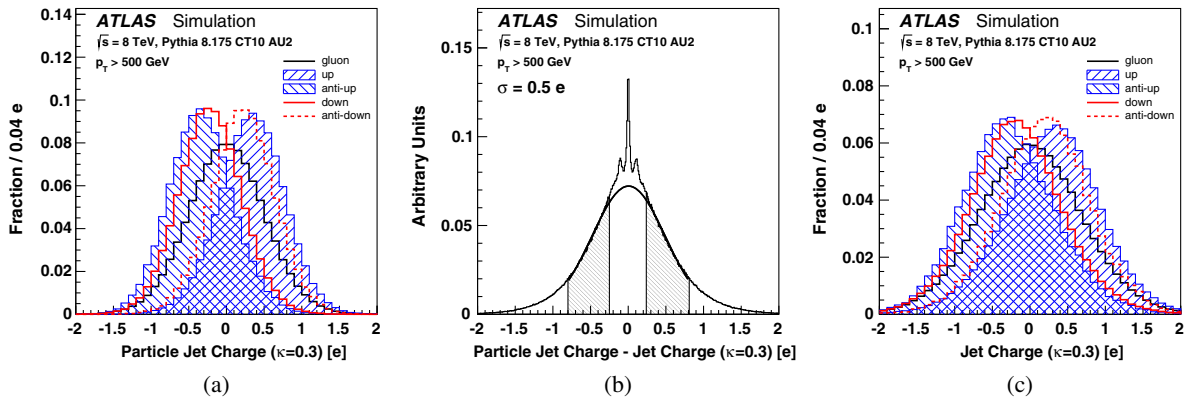


FIG. 3. The (a) particle-level and (c) detector-level jet charge distribution for various jet flavors in a sample of jets with $p_T > 500$ GeV for $\kappa = 0.3$. (b): The distribution of the jet-by-jet difference between the particle-level and detector-level jet charge distributions. The shaded region is used to fit a Gaussian function to extract the bulk response resolution, which is $\sigma \sim 0.5 e$, where e is the positron charge.

there is a clear relationship between the jet charge and the initiating parton's charge, as up-quark jets tend to have a larger jet charge than gluon jets. Furthermore, gluon jets tend to have a larger jet charge than down-quark jets. However, the jet charge distribution is already broad at particle level and the jet charge response ($Q_{\text{particle-level}} - Q_{\text{detector-level}}$) resolution is comparable to the differences in the means of the distributions for different flavors, so one can expect only small changes in the inclusive jet charge distribution for changes in the jet flavor composition. The three narrow distributions on top of the bulk response distribution in Fig. 3(b) are due to cases in which only one or two charged particles dominate the jet charge calculation at particle level. The two

off-center peaks are due to cases in which one of the two high- p_T -fraction tracks is not reconstructed and the widths of the two off-center and central peaks are due to the (single) track and jet p_T resolutions. The bulk response is fit to a Gaussian function with standard deviation $\sigma \sim 0.5 e$ (units of the positron charge).

The parameter κ in Eq. (1) regulates the sensitivity of the jet charge to soft radiation. For $\kappa > 0$, the jet charge is infrared safe.⁴ Low values of κ enhance the contribution to the jet charge from low- p_T particles while in the $\kappa \rightarrow \infty$

⁴The jet charge is never collinear safe for $\kappa > 0$ and not even the sign of the jet charge is Lorentz invariant, although it is clearly invariant under longitudinal boosts.

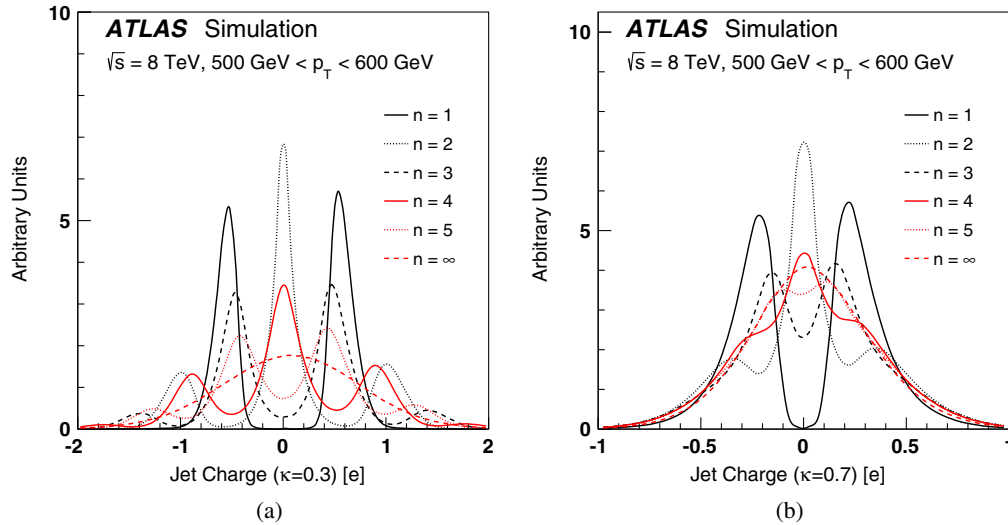


FIG. 4. The distribution of the jet charge built from the leading n tracks ($Q_{J,n}$) for (a) $\kappa = 0.3$ and (b) $\kappa = 0.7$ in a sample of jets with $500 \text{ GeV} < p_T < 600 \text{ GeV}$. The horizontal axis ranges are not the same. In this p_T range, the median number of tracks is about 15.

limit, only the highest- p_T track contributes to the sum in Eq. (1). The dependence on the highest- p_T tracks is demonstrated with the plots in Fig. 4 with the variable $Q_{J,n}$, which is the jet charge in Eq. (1), but built from the leading n tracks. The variable $Q_{J,1}$ is simply the weighted fragmentation function of the leading-track p_T to the jet p_T with weight κ . The usual Q_J is recovered in the limit $n \rightarrow \infty$. Figure 4 shows the sequence $Q_{J,n}$ for $\kappa = 0.3$ and $\kappa = 0.7$. For lower values of κ , many tracks are required for the sequence of distributions to converge to the full jet charge. However, for $\kappa = 0.7$, the distribution converges quickly, indicating that only the highest- p_T tracks are contributing. All reconstructed tracks are henceforth used when computing the jet charge, but the plots in Fig. 4 give an indication of the contribution of (relatively) high- and low- p_T tracks. Dedicated studies [24] agree with theoretical predictions [34] that suggest that $\kappa \sim 0.5$ is the most sensitive to the charge of the parton initiating a jet. Therefore, the measurement presented in this paper uses $\kappa = 0.5$ in addition to $\kappa = 0.3$ and $\kappa = 0.7$ in order to maintain a broad sensitivity to both hard and soft radiation inside jets.

The reconstructed jet charge distributions for $\kappa = 0.3$ and $\kappa = 0.7$ are shown in Fig. 5 for events passing the selection described in Sec. IV. Section VI describes how the jet charge moments are corrected for detector resolution and acceptance effects through an unfolding procedure.

VI. UNFOLDING

The particle-level jet charge distribution's mean and standard deviation are measured as a function of jet p_T . This is accomplished by unfolding a discretized two-dimensional distribution of the jet charge and the jet p_T and then computing the first two moments of the jet charge

distribution in each bin of p_T . The jet charge distribution is discretized into 15 bins in each of ten bins of the jet p_T . The jet charge mean is robust against the bias introduced from the discretization procedure, where fewer than five charge bins per p_T bin is required to ensure negligible bias after recovering the mean from the discretized distribution. However, the standard deviation of the jet charge distribution is sensitive to the discretization and requires about 15 charge bins⁵ in order for the inherent bias due to discretization to be negligible. The jet charge spans the range $|Q_J| < 1.8$ for $\kappa = 0.3$, $|Q_J| < 1.2$ for $\kappa = 0.5$ and $|Q_J| < 0.9$ for $\kappa = 0.7$. Events in the overflow of the jet charge distribution are placed in the first or last bins. The p_T binning is given by [50,100), [100, 200), [200, 300), [300, 400), [400, 500), [500, 600), [600, 800), [800, 1000), [1000, 1200), and [1200, 1500] GeV. Figure 6 displays the p_T dependence of the jet charge distribution's mean and standard deviation for detector-level data and simulation and for particle-level simulation. The differences between the simulated detector- and particle-level distributions give an indication of the corrections required to account for detector acceptance and resolution effects in the unfolding procedure. The growing difference between the particle- and detector-level average jet charge is due to the loss of charged-particle momentum inside jets as a result of track merging. At particle level, the standard deviation of the jet charge distribution decreases with increasing p_T , but at detector level it increases with p_T due to resolution effects.

There is no unique way to extract the particle-level distribution of the jet charge and jet p_T from the reconstructed distributions. An iterative Bayesian (IB) technique [75], implemented in the RooUnfold framework [76], is used

⁵Fifteen is the number used in the unfolding and differs from the number shown for illustration in e.g. Fig. 5.

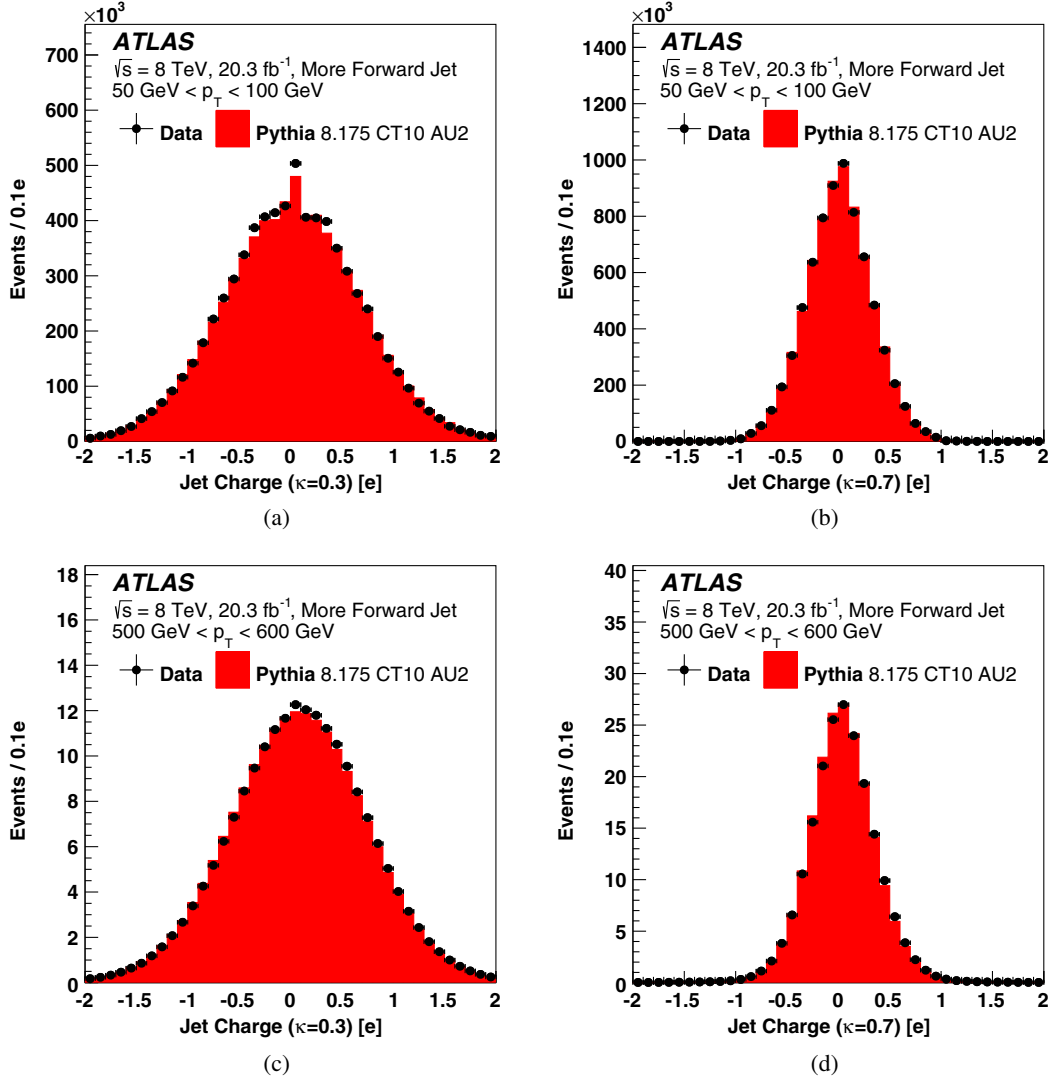


FIG. 5. The detector-level jet charge distributions for (a),(b) $50 \text{ GeV} < p_T < 100 \text{ GeV}$ and (c), (d) $500 \text{ GeV} < p_T < 600 \text{ GeV}$ for the more forward jet and (a), (c) $\kappa = 0.3$ and (b), (d) $\kappa = 0.7$. The peak at zero in the top left plot is due to jets without any tracks.

to unfold the two-dimensional jet charge and jet p_T distribution. In the IB unfolding technique, the number of iterations and the prior distribution are the input parameters. In the first step, the raw data are corrected using the simulation to account for events that pass the fiducial selection at detector level, but not the corresponding selection at particle level; this correction is the *fake factor*. Then, the IB method iteratively applies Bayes' theorem using the *response matrix* to connect the prior to posterior at each step, with the nominal PYTHIA sample used for the initializing prior. The response matrix describes the bin migrations between the particle-level and detector-level two-dimensional jet charge and jet p_T distributions. While the response matrix is nearly diagonal, the resolution degrades at high p_T where more bin-to-bin migrations from particle level to detector level occur. The number of iterations in the IB method trades off unfolding bias with statistical fluctuations. An optimal value of four

iterations is obtained by minimizing the bias when unfolding pseudodata HERWIG++ with PYTHIA as a test of the methodology. The last step of the unfolding applies another correction from simulation to the unfolded data to account for the differential rate of events passing the particle-level selection but not the detector-level selection; this correction is the *inefficiency factor*.

VII. SYSTEMATIC UNCERTAINTIES

All stages of the jet charge measurement are sensitive to sources of potential bias. The three stages of the measurement are listed below, with an overview of the systematic uncertainties that impact the results at each stage:

Correction factors: Fake and inefficiency factors are derived from simulation to account for the fraction of events that pass either the detector-level or particle-level fiducial selection, but not both. These factors are generally

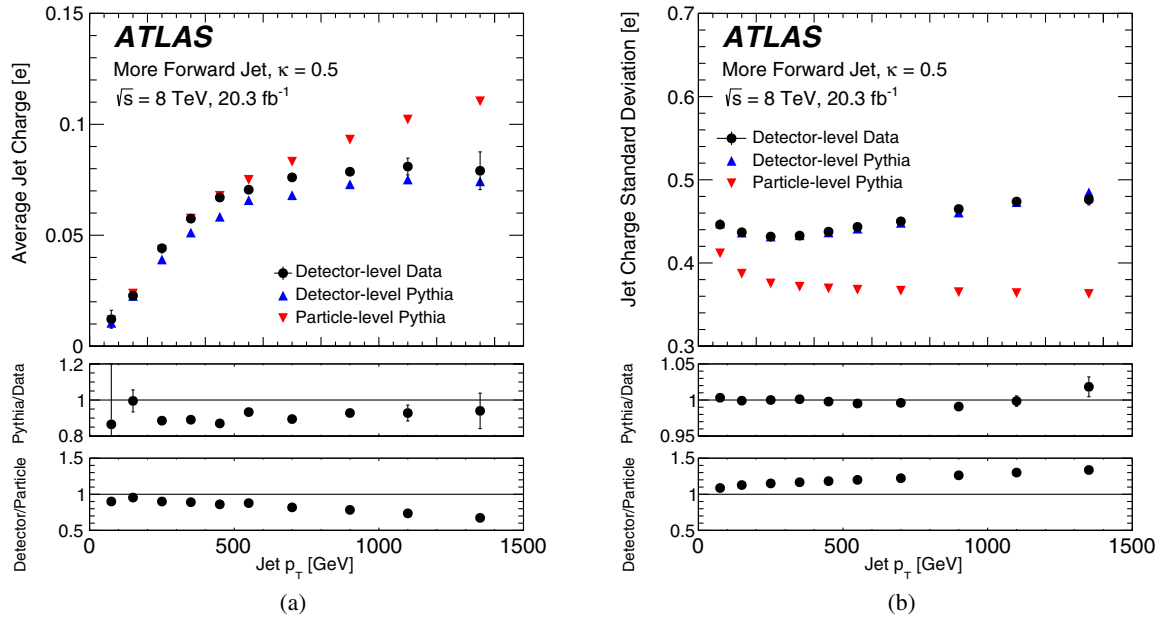


FIG. 6. The detector-level (data and simulation) and particle-level jet charge distribution's (a) average and (b) standard deviation as a function of the jet p_T for the more forward jet. The ratios in the bottom panel are constructed from the simulation, and show the prediction of detector-level PYTHIA over the data (top ratio), and detector-level PYTHIA over particle-level PYTHIA (bottom ratio). Bars on the data markers represent only the statistical uncertainties. For both (a) and (b), $\kappa = 0.5$.

between 0.9 and 1.0 except in the first p_T bin, where threshold effects introduce corrections that can be as large as 20%. Experimental uncertainties correlated with the detector-level selection acceptance, such as the jet energy scale uncertainty, result in uncertainties in these correction factors. An additional source of uncertainty on the correction factors is due to the explicit dependence on the particle-level jet charge and jet p_T spectra. A comparison of particle-level models (PYTHIA and HERWIG++) is used to estimate the impact on the correction factors.

Response matrix: For events that pass both the detector-level and particle-level fiducial selections, the response matrix describes migrations between bins when moving between the detector level and the particle level. The response matrix is taken from simulation and various experimental uncertainties on the jet charge and jet p_T spectra result in uncertainties in the matrix. Uncertainties can be divided into two classes: those impacting the calorimeter jet p_T and those impacting track reconstruction inside jets.

Unfolding procedure: A data-driven technique is used to estimate the potential bias from a given choice of prior and number of iterations in the IB method [77]. The particle-level spectrum is reweighted using the response matrix so that the simulated detector-level spectrum has significantly improved agreement with data. The modified detector-level distribution is unfolded with the nominal response matrix and the difference between this and the reweighted particle-level spectrum is an indication of the bias due to the unfolding method (in particular, the choice of prior).

The following two subsections describe the impact of the detector-related sources of systematic uncertainty in more detail. Uncertainties on the calorimeter jet p_T are described in Sec. VII A and the uncertainties related to tracking are described in Sec. VII B. Summaries of the systematic uncertainties for the more forward jet and $\kappa = 0.5$ are found in Tables II and III for the average jet charge and the jet charge distribution's standard deviation, respectively.⁶ The uncertainties for the more central jet are similar.

A. Calorimeter jet uncertainties

Jets are calibrated so that the detector-level p_T is an unbiased measurement of the particle-level jet p_T and various data-driven techniques are used to derive *in situ* estimates of the difference in this calibration between the data and the simulation. Uncertainties in the energy scale and resolution of calibrated jets impact the jet charge in the normalization of Eq. (1) (but preserve the jet charge sign) as well as the binning for the two-dimensional distribution. Complete details of this source of uncertainty can be found in Ref. [78]. There are many components of the jet energy scale uncertainty. The *in situ* correction is derived from data using the momentum balance in events with Z bosons (low p_T) or photons (moderate p_T) produced in association with jets as well as the balance of multijet (high p_T) and dijet (high $|\eta|$) systems. Uncertainties on this method stem from

⁶The uncertainties on the first p_T bin of the average jet charge are much larger than on the other bins because the mean is small compared to the resolution.

TABLE II. A summary of all the systematic uncertainties and their impact on the mean jet charge for $\kappa = 0.5$ and the more forward jet. The correction factors are the fake and inefficiency corrections applied before/after the response matrix. The Other Tracking category includes uncertainty on the track reconstruction efficiency, track momentum resolution, charge misidentification, and fake track rate. All numbers are given in percent.

Average Jet Charge	Jet p_T Range [100 GeV]									
	Systematic Uncertainty [%]	[0.5,1]	[1,2]	[2,3]	[3,4]	[4,5]	[5,6]	[6,8]	[8,10]	[10,12]
Total Jet Energy Scale	+8.4	+3.8	+0.9	+0.8	+1.1	+1.1	+0.7	+0.7	+0.4	+0.9
Jet Energy Resolution	-13.6	-3.5	-5.0	-0.3	-1.6	-1.1	-1.0	-0.9	-0.7	-0.3
Charged Energy Loss	+6.8	+2.3	+0.7	+0.7	+0.3	+0.3	+0.1	+0.1	+0.1	+0.3
Other Tracking	-6.8	-2.3	-0.7	-0.7	-0.3	-0.3	-0.1	-0.1	-0.1	-0.3
Track Multiplicity	+0.0	+0.0	+0.0	+0.0	+1.7	+1.5	+1.5	+1.5	+1.6	+3.6
Correction Factors	-0.0	-0.0	-0.0	-0.0	-0.0	-0.0	-0.0	-0.0	-0.0	-0.0
Unfolding Procedure	+3.3	+0.0	+0.9	+0.7	+0.5	+1.4	+0.7	+1.2	+1.1	+0.9
Total Systematic	-1.6	-0.4	-0.2	-0.1	-0.4	-0.6	-0.9	-1.2	-1.3	-1.7
Data Statistics	+0.0	+0.1	+0.0	+0.0	+0.0	+0.0	+0.0	+0.0	+0.0	+0.0
Total Uncertainty	-1.5	-0.0	-0.6	-1.1	-0.8	-0.6	-1.2	-1.4	-2.1	-2.9
Measured Value [e]	+23	+0.9	+0.8	+1.0	+0.3	+0.6	+0.1	+0.3	+0.2	+0.1
	-23	-0.9	-0.8	-1.0	-0.3	-0.6	-0.1	-0.3	-0.2	-0.1
	+28	+2.4	+0.3	+0.2	+0.2	+0.3	+1.1	+1.0	+1.6	+0.6
	-28	-2.4	-0.3	-0.2	-0.2	-0.3	-1.1	-1.0	-1.6	-0.6
Total Systematic	+39	+5.1	+1.7	+1.6	+2.1	+2.4	+2.1	+2.3	+2.6	+3.8
Data Statistics	-38	-4.9	-5.2	-1.7	-1.9	-1.6	-2.1	-2.3	-3.0	-3.4
Total Uncertainty	28	7.4	1.4	0.7	0.3	0.6	0.9	2.0	4.2	7.0
Measured Value [e]	+48	+9.0	+2.2	+1.8	+2.1	+2.5	+2.3	+3.0	+5.0	+8.0
	-47	-8.9	-5.4	-1.9	-1.9	-1.7	-2.3	-3.0	-5.2	-7.8

TABLE III. A summary of all the systematic uncertainties and their impact on the jet charge distribution's standard deviation for $\kappa = 0.5$ and the more forward jet. The correction factors are the fake and inefficiency corrections applied before/after the response matrix. The Other Tracking category includes uncertainty on the track reconstruction efficiency, track momentum resolution, charge misidentification, and fake track rate. All numbers are given in percent.

Standard Deviation	Jet p_T Range [100 GeV]									
	Systematic Uncertainty [%]	[0.5,1]	[1,2]	[2,3]	[3,4]	[4,5]	[5,6]	[6,8]	[8,10]	[10,12]
Total Jet Energy Scale	+1.9	+1.5	+1.1	+1.1	+0.9	+1.0	+0.8	+0.7	+0.5	+0.5
Jet Energy Resolution	-1.7	-1.3	-1.1	-1.0	-0.8	-0.7	-0.8	-0.8	-0.5	-0.5
Charged Energy Loss	+1.3	+0.3	+0.1	+0.2	+0.3	+0.4	+0.2	+0.2	+0.2	+0.2
Other Tracking	-1.3	-0.3	-0.1	-0.2	-0.3	-0.4	-0.2	-0.2	-0.2	-0.2
Track Multiplicity	+0.0	+0.0	+0.0	+0.0	+0.2	+0.3	+0.3	+0.3	+0.4	+1.1
Correction Factors	-0.0	-0.0	-0.0	-0.0	-0.0	-0.0	-0.0	-0.0	-0.0	-0.0
Unfolding Procedure	+0.0	+0.1	+0.2	+0.3	+0.4	+0.5	+0.5	+0.5	+0.5	+0.4
Total Systematic	-0.3	-0.3	-0.4	-0.4	-0.5	-0.4	-0.5	-0.5	-0.4	-0.4
Data Statistics	+0.0	+0.0	+0.0	+0.0	+0.0	+0.1	+0.2	+0.2	+0.3	+0.2
Total Uncertainty	-0.2	-0.3	-0.2	-0.1	-0.0	-0.0	-0.0	-0.0	-0.0	-0.0
Measured Value [e]	+0.9	+0.1	+0.0	+0.1	+0.0	+0.1	+0.0	+0.0	+0.0	+0.0
	-0.9	-0.1	-0.0	-0.1	-0.0	-0.1	-0.0	-0.0	-0.0	-0.0
	+1.9	+0.4	+0.0	+0.1	+0.2	+0.0	+0.1	+0.3	+0.4	+1.7
	-1.9	-0.4	-0.0	-0.1	-0.2	-0.0	-0.1	-0.3	-0.4	-1.7
Total Systematic	+3.1	+1.6	+1.1	+1.2	+1.1	+1.2	+1.0	+1.0	+1.0	+2.1
Data Statistics	-3.0	-1.5	-1.2	-1.1	-1.0	-0.9	-0.9	-1.0	-0.8	-1.8
Total Uncertainty	0.9	0.3	0.1	0.1	0.0	0.1	0.1	0.3	0.6	1.0
Measured Value [e]	+3.2	+1.6	+1.1	+1.2	+1.1	+1.2	+1.0	+1.1	+1.2	+2.4
	-3.1	-1.5	-1.2	-1.1	-1.0	-0.9	-1.0	-1.0	-1.0	-2.1

the modeling of these processes in simulation. There is also a contribution from the response to single hadrons [79]. Additional sources of uncertainty are due to the modeling of the in-time and out-of-time pileup corrections to the jet energy scale as well as differences in the response due to the flavor of the jet. To assess the impact of each component of the jet energy scale uncertainty, the jet energies in simulation are shifted according to the p_T - and η -dependent $\pm 1\sigma$ variations. For a fixed variation, the response matrix, and fake and inefficiency factors are recomputed and the unfolding procedure is repeated. The resulting uncertainty on the jet charge distribution's mean and standard deviation is about 1% or less for jet p_T above 200 GeV. The jet energy resolution uncertainty is

derived using data-driven techniques in dijet events [80]. To assess the impact of a slightly larger jet energy resolution, jet energies are smeared according to p_T - and η -dependent factors and propagated through the entire unfolding procedure, as for the jet energy scale uncertainty. The jet energy resolution uncertainty is subdominant to the jet energy scale uncertainty.

B. Tracking uncertainties

Uncertainties on tracking are broken down into contributions related to (i) the efficiency of reconstructing tracks and (ii) measurements of those tracks that are successfully reconstructed. The uncertainty on the inclusive track

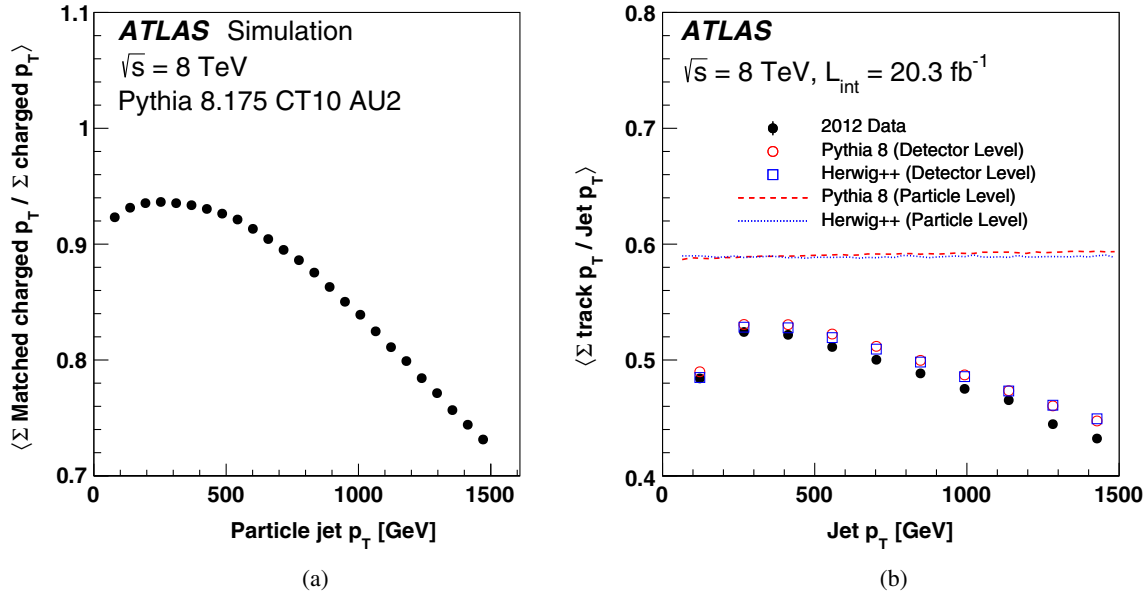


FIG. 7. (a): The average of the p_T -weighted ratio of charged particles that were matched to reconstructed tracks ($\Sigma \text{ Matched charged } p_T$) to all the charged particles ($\Sigma \text{ charged } p_T$) as a function of the particle-level jet p_T . (b): The average of the ratio of the sum of p_T from tracks to the calorimeter jet p_T ($\Sigma \text{ track } p_T / \text{Jet } p_T$) as a function of jet p_T in both data and simulation. The momentum ratio of charged particles to all particles is nearly $2/3$ due to the number of pion species (as indicated by the straight lines for HERWIG++ and PYTHIA predictions at particle level), but is not exactly $2/3$ due to the presence of photons and kaons in the jet.

reconstruction efficiency is dominated by the uncertainty in the material in the ID. The amount of material is known to within $\sim 5\%$ [81]. Simulated detector geometries with various levels of material in the ID within the measured uncertainties are used to estimate the track reconstruction efficiency uncertainty. These uncertainties are η - and p_T -dependent, ranging from $\lesssim 1\%$ for $|\eta| < 2.1$ to $\lesssim 4\%$ for $2.1 \leq |\eta| < 2.3$ and $\lesssim 7\%$ for $2.3 \leq |\eta| < 2.5$. The impact of the uncertainty is estimated by randomly removing tracks within the p_T - and η -dependent probabilities, leading to a $\lesssim 0.5\%$ uncertainty on the jet charge distribution's mean and standard deviation. An additional uncertainty accounts for the difference in efficiency between data and simulation due to the modeling of the track χ^2 per number of degrees of freedom (NDF) requirement. A requirement of $\chi^2 / \text{NDF} < 3$ is more than 99% efficient across jet and track p_T , but the efficiency is generally higher in simulation than in data. The difference in the efficiency between data and simulation is $\lesssim 10\%$ of the inefficiency. The impact of this mismodeling is evaluated by independently removing tracks with a probability that is 10% of the $\chi^2 / \text{NDF} < 3$ requirement inefficiency. As a result of this procedure, the jet charge distribution's mean and standard deviation change by $\lesssim 0.1\%$ in most p_T bins.

In addition to the loss of tracks due to the material in the ID, tracks can be lost due to the busy environment inside the cores of jets. This loss can be studied in simulation by comparing the reconstructed charged-particle momentum with the charged-particle momentum inside the corresponding particle-level jet. In order to remove the impact of the

tracking resolution and the contribution from fake tracks already accounted for separately, reconstructed tracks in the simulation are matched with charged particles. The matching is performed by considering the energy deposited in the various layers of the ID by charged particles due to material interactions modeled with GEANT4. Weights are assigned to charged particles based on the energy deposited in detector elements that were used to reconstruct a given track. A match is declared if the weight for one charged particle is sufficiently high. Figure 7(a) shows the ratio in simulation of the sum of the p_T of charged particles that were matched to reconstructed tracks to the sum of the p_T of all the charged particles as a function of the jet p_T . At low p_T , the ratio increases with p_T due to losses as a result of hadronic interactions with the material in the ID. Beyond about 200 GeV, the fraction monotonically decreases due to the loss of tracks in the core of the jet. A related quantity is $\langle \Sigma \text{ track } p_T / \text{Jet } p_T \rangle$, where the denominator is the reconstructed calorimeter jet p_T and the numerator is a sum over tracks associated with the jet. Since the particle-level charged-to-neutral fraction of the energy is independent of p_T , a degradation in this ratio can provide information about the loss of tracks inside the core of a jet in data. Figure 7(b) shows the distribution of $\langle \Sigma \text{ track } p_T / \text{Jet } p_T \rangle$ as a function of jet p_T . It exhibits trends very similar to those in Fig. 7(a), and in fact the relative loss (fraction with respect to the peak) is similar. The MC underestimates the loss by $\lesssim 1\%$. The impact of the charged-particle momentum loss inside the cores of jets is estimated by randomly removing tracks with a p_T -dependent probability such that the relative

loss in the simulation matches that in the data. This uncertainty is negligible for jets with $p_T < 400$ GeV, but is non-negligible for higher- p_T jets, resulting in a $\lesssim 4\%$ uncertainty on the average jet charge in the highest p_T bin.

The momentum resolution of isolated tracks has been well measured in $J/\psi \rightarrow \mu\mu$ and $Z \rightarrow \mu\mu$ events [82]. The scale and resolution of reconstructed muon candidates are shifted and smeared in the MC simulation to account for differences between the data and the simulation for $m_{\mu\mu}$. Generic tracks are not corrected in the same way as muon candidates reconstructed from the ID (and ignoring the muon spectrometer). Thus, the correction factors are taken here as the systematic uncertainty on the momentum resolution. The momentum resolution is parametrized as a sum in quadrature of a p_T^{-1} -dependent term, a constant term, and a term linear in the track p_T , with coefficients r_0 , r_1 , and r_2 , respectively. The first term accounts for fluctuations in the energy loss in the detector material, the second term captures effects due to multiple scattering, and the third term accounts for the intrinsic resolution caused by misalignment and the finite spatial resolution of ID hits. Unlike muon spectrometer tracks, ID tracks do not traverse a significant amount of material and so the energy-loss coefficient r_0 and its uncertainty are neglected. The uncertainties on r_1 , r_2 and the momentum scale s are estimated by randomly smearing the p_T of every track with $|\eta|$ -dependent factors that are $\lesssim 2\%$ for track $p_T < 100$ GeV and increase to 10–20% at 1 TeV depending on $|\eta|$. Propagating these variations through the unfolding procedure results in uncertainties that are subdominant to other uncertainties, but non-negligible ($\sim 2\%$) in the highest p_T bins for the average jet charge.

Aside from the track p_T , the other track parameter that is relevant for the jet charge is the track charge. Especially at high p_T when the tracks are very straight, the probability for misidentifying the track charge can become non-negligible. Simulated particles matched to generator-level information, as described above, are used to study the charge-flipping probability (charge misidentification rate) for nonfake tracks originating from charged particles inside jets (mostly pions). The rate predicted from the simulation is $< 0.1\%$ for track $p_T < 100$ GeV, 0.5% for $100 \text{ GeV} \leq p_T < 200$ GeV, 1% for $200 \text{ GeV} \leq p_T < 300$ GeV, 2% for $300 \text{ GeV} \leq p_T < 400$ GeV and 4% for $p_T \geq 400$ GeV. Dedicated studies of charge flipping in searches for same-sign leptons [83] suggest that the mismodeling of the charge-flipping rate is (much) less than 50%. Therefore, the impact of charge flipping on the jet charge measurement is conservatively estimated by randomly flipping the charge of tracks at 50% of the charge misidentification rate. The impact on the measured jet charge mean and standard deviation is negligible.

Random combinations of hits in the detector can be combined to form a reconstructed track. Tracks resulting in particular from multiparticle trajectories that have kinks can

result in very large reconstructed track p_T . The quality criteria are effective at mitigating the presence of fake tracks, which constitute less than $\lesssim 0.1\%$ of all reconstructed tracks. To determine the impact of fake tracks on the jet charge, fake tracks are randomly removed with a probability that is 50% of the rate in simulation. This results in a negligibly small uncertainty on the mean jet charge and a $\lesssim 0.5\%$ uncertainty on the standard deviation of the jet charge distribution.

The tracking uncertainties described so far take into account the resolution and efficiency of reconstruction of charged-particle momenta. One last source of systematic uncertainty is the number of charged particles. The unfolding procedure uncertainty takes into account the uncertainty on the prior due to the charged-particle multiplicity, but the jet charge resolution also changes with the charged-particle multiplicity. To assess the impact on the response matrix of the mismodeled charged-particle multiplicity, the distribution of n_{track} is reweighted in the simulation per p_T bin and the relative difference when unfolding the nominal PYTHIA distribution with the reweighted PYTHIA distribution is taken as a systematic uncertainty.⁷ This uncertainty is subdominant for the standard deviation across p_T and for the mean at low to moderate jet p_T . For the mean jet charge, the largest uncertainty is with the smallest κ and for large p_T , where it is 3–4% percent in the highest p_T bin for $\kappa = 0.3$ and $\kappa = 0.5$.

VIII. RESULTS

The data satisfying the event selection criteria described in Sec. IV are unfolded according to the procedure in Sec. VI and the average and standard deviation of the jet charge distribution are computed as a function of the jet p_T . These results, along with the systematic uncertainties detailed in Sec. VII, are discussed in Sec. VIII A. The PDF uncertainty and jet formation uncertainties in the theory predictions are compared to the unfolded data in Secs. VIII B and VIII C, respectively. Using PDF information as input, the average charge per jet flavor is extracted in Sec. VIII E and its p_T dependence is studied in Sec. VIII F.

A. Unfolded jet charge spectrum

The unfolded jet charge mean is shown as a function of the jet p_T in the top plots of Fig. 8 for $\kappa = 0.3, 0.5$ and 0.7 . The average charge increases with jet p_T due to the increase in up-flavor jets from PDF effects. The average charge increases from $0.01e$ at $p_T \sim 100$ GeV to $0.15e$ at $p_T \sim 1.5$ TeV. Systematic uncertainties are generally a few percent, except at low jet p_T where the fractional uncertainty is large because the average jet charge in the denominator is small, and at high p_T where the tracking

⁷Since the prior is also changed, this uncertainty at least partially includes the unfolding procedure uncertainty.

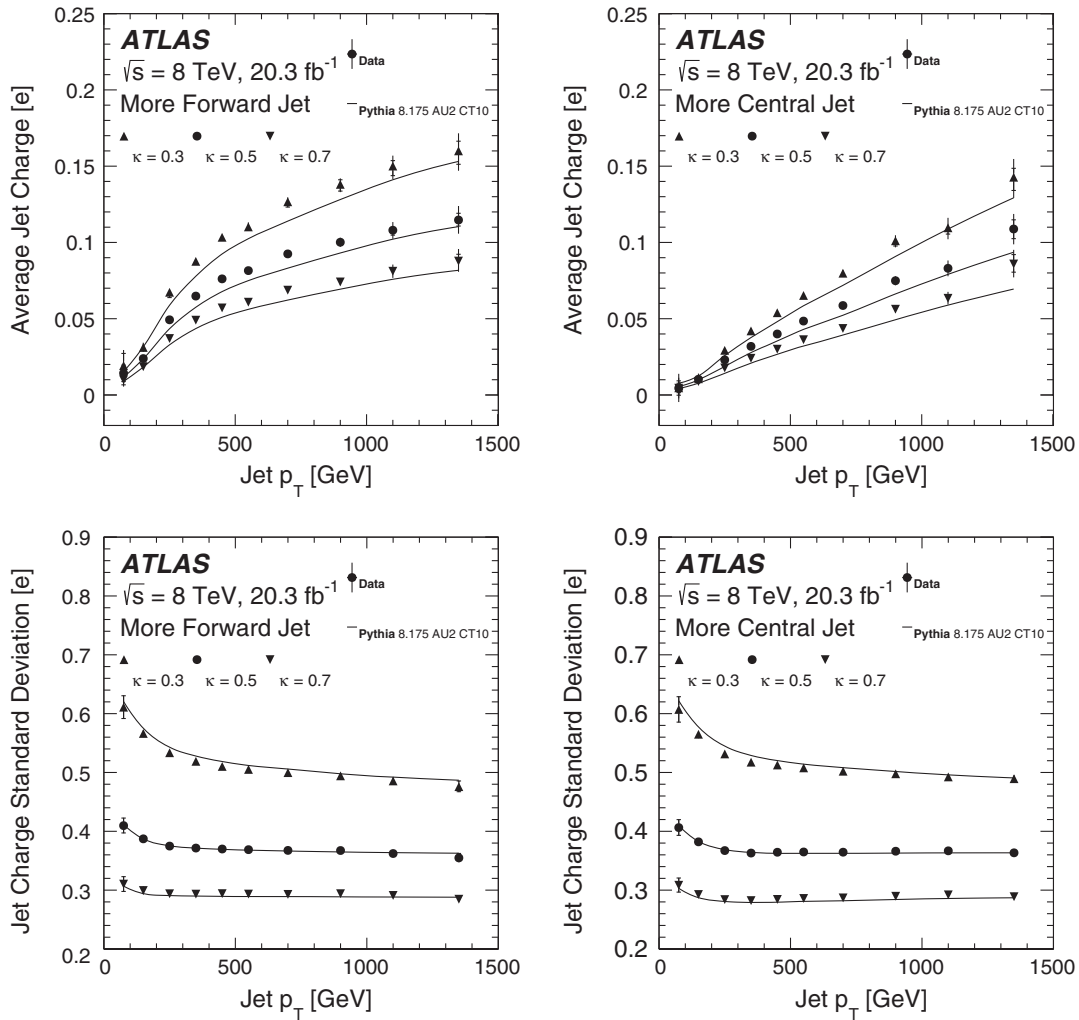


FIG. 8. The measured average (standard deviation) of the jet charge distribution on top (bottom) in units of the positron charge as a function of the jet p_T for $\kappa = 0.3, 0.5$, and 0.7 for the more forward jet (left) and the more central jet (right). The crossed lines in the bars on the data indicate the systematic uncertainty and the full extent of the bars is the sum in quadrature of the statistical and systematic uncertainties.

uncertainties are not negligible. The statistical uncertainty is estimated by repeating the measurement on an ensemble of bootstrapped data sets: each event is used in each pseudo-data set n times, where n is a random number distributed according to a Poisson distribution with mean one. The first bin suffers from large statistical uncertainties (up to 170%), but for the higher p_T bins the systematic uncertainty is dominant, except at the highest p_T bin where statistical and systematic uncertainties are of similar size (about 7%). The jet charge distributions of the more forward and more central jet differ in shape, in particular at low p_T , due to the different shape of the up-/down-flavor fractions in those bins as shown in Fig. 2(b).

Analogous results for the standard deviation of the jet charge distribution are shown in the bottom plots of Fig. 8. Even though the standard deviation of the reconstructed jet charge distribution increases with jet p_T (Fig. 6), the particle-level value decreases and approaches an asymptote for $p_T \gtrsim 300$ GeV.

B. Sensitivity of PDF modeling

Variations in the PDF set impact the relative flavor fractions and thus in turn change the jet charge distribution. Such changes do not vary much with κ , since the PDF impacts the jet charge distribution mostly through the flavor fractions. Figures 9 and 10 compare the unfolded distributions of the jet charge distribution's average and standard deviation with several PDF sets, with tuned predictions for PYTHIA for each PDF, and with the same AU2 family of tunes. The sampling of PDF sets results in a significant spread for the average jet charge, but has almost no effect on the standard deviation. CTEQ6L1 describes the data best, although the data/MC ratio has a stronger p_T dependence. In particular, the data/MC differences with CTEQ6L1 are up to 10% (15%) at moderate p_T for the more forward (central) jet. For high p_T , differences between data and simulation are less significant. NLO PDFs such as CT10 are consistently below the data by about 10–15%.

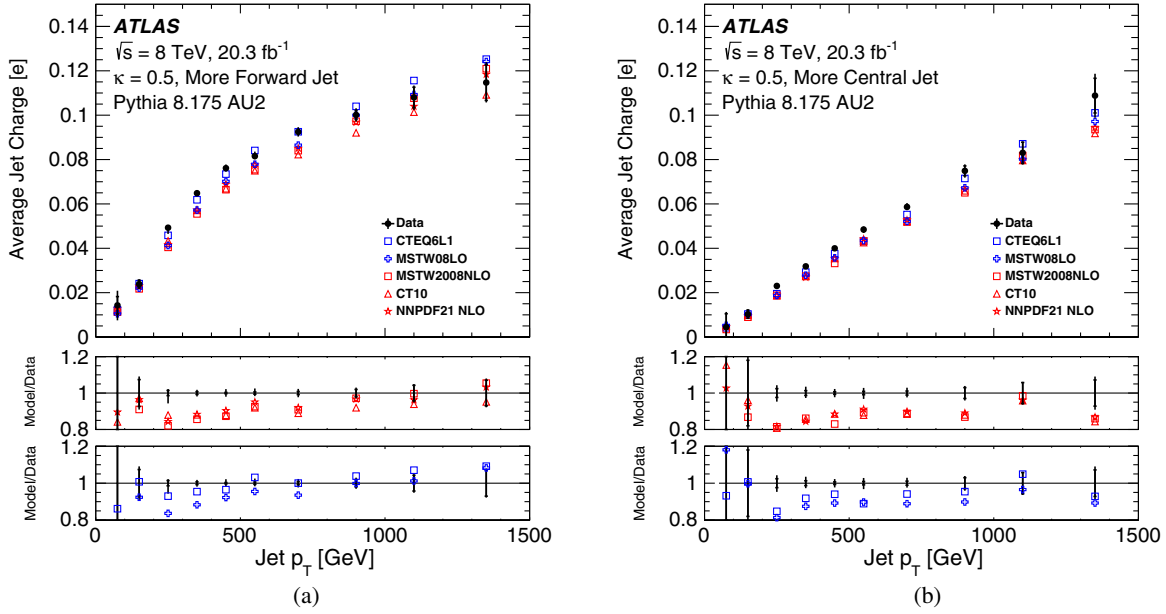


FIG. 9. The average jet charge ($\kappa = 0.5$) in units of the positron charge for (a) the more forward jet and (b) the more central jet compared with theory predictions due to various PDF sets. The crossed lines in the bars on the data indicate the statistical uncertainty and the full extent of the bars is the sum in quadrature of the statistical and systematic uncertainties.

C. Sensitivity of QCD models and tunes

The measurements presented in Sec. VIII A show that there are qualitative differences between the data and the MC simulations, and comparisons in Sec. VIII B suggest that variations in the PDF set cannot fully explain the differences. Differences in Sec. VIII A between PYTHIA and HERWIG++ suggest that some aspect of the modeling of fragmentation could lead to the observed differences

between the simulation and the data. One possible source is the hadronization modeling, which differs between PYTHIA (Lund-string fragmentation) and HERWIG++ (cluster fragmentation). The modeling of final-state radiation (FSR) is expected to have an impact on the jet charge distribution because variations in the radiation lead to different energy flow around the initial parton and hence different fragmentation of the jet. The plots in

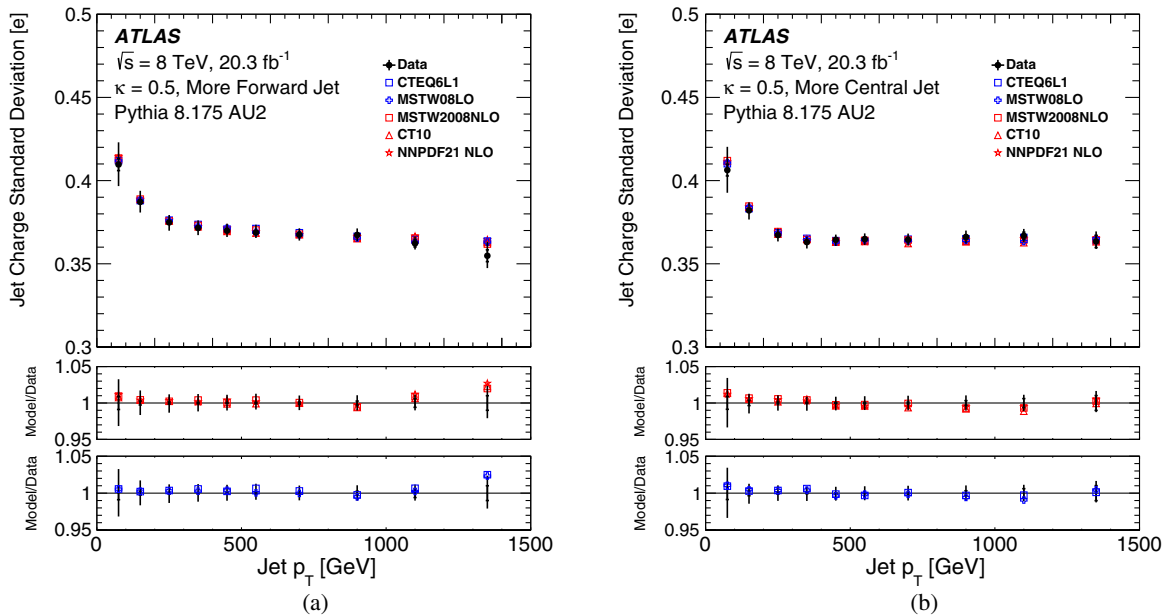


FIG. 10. The standard deviation of the jet charge ($\kappa = 0.5$) distribution in units of the positron charge for (a) the more forward jet and (b) the more central jet compared with theory predictions due to various PDF sets. The crossed lines in the bars on the data indicate the statistical uncertainty and the full extent of the bars is the sum in quadrature of the statistical and systematic uncertainties.

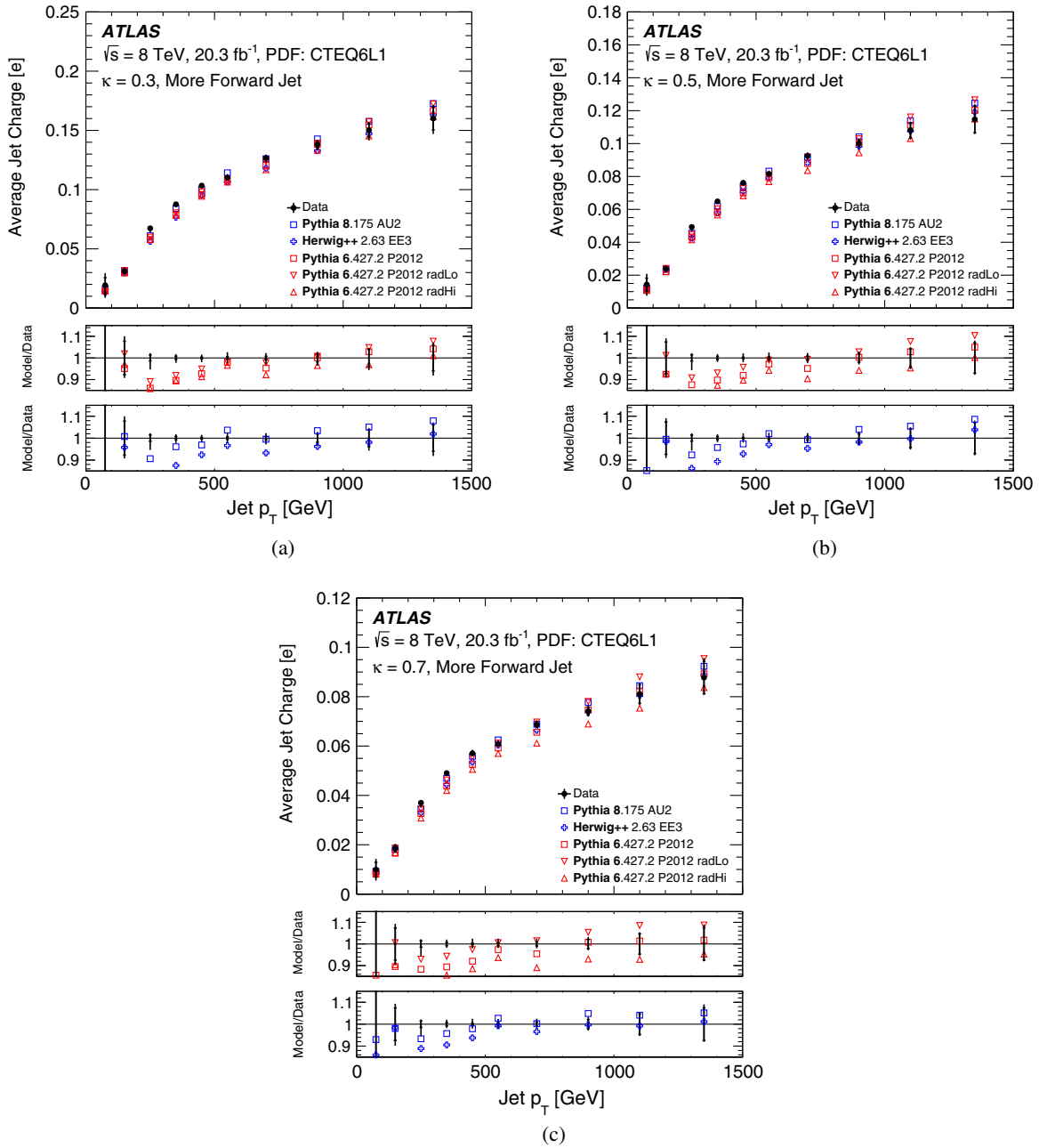


FIG. 11. The average of the jet charge distribution in units of the positron charge for (a) $\kappa = 0.3$, (b) 0.5, and (c) 0.7 comparing various QCD MC models and tunes for the more forward jet. The crossed lines in the bars on the data indicate the statistical uncertainty and the full extent of the bars is the sum in quadrature of the statistical and systematic uncertainties.

Figs. 11 and 12 show the measured average jet charge and the jet charge distribution's standard deviation, respectively, for $\kappa = 0.3$, 0.5, and 0.7, compared to various models for a fixed PDF set (CTEQ6L1). In addition to PYTHIA 8 and HERWIG++ model predictions, Figs. 11 and 12 contain the predictions from PYTHIA 6 using the Perugia 2012 tune [84] and the radHi and radLo Perugia 2012 tune variations. These Perugia tune variations test the sensitivity to higher/lower amounts of initial- and final-state radiation (via the scaling of α_s), although only variations of the FSR are important for the jet charge distribution. For the mean

jet charge, PYTHIA 6 with the P2012 radLo tune is very similar to PYTHIA 8 with the AU2 tune. The spread in the average jet charge due to the difference between the radHi and radLo tunes increases with κ , since suppression of soft radiation makes the jet charge distribution more sensitive to the modeling of the energy fraction of the leading emissions. For the jet charge distribution's standard deviation, the sensitivity to the α_s scaling is large at both high and low κ . However, the sensitivity is inverted: radHi gives a larger standard deviation for $\kappa = 0.3$, but a lower standard deviation for $\kappa = 0.7$. Other Perugia 2012 tunes have been

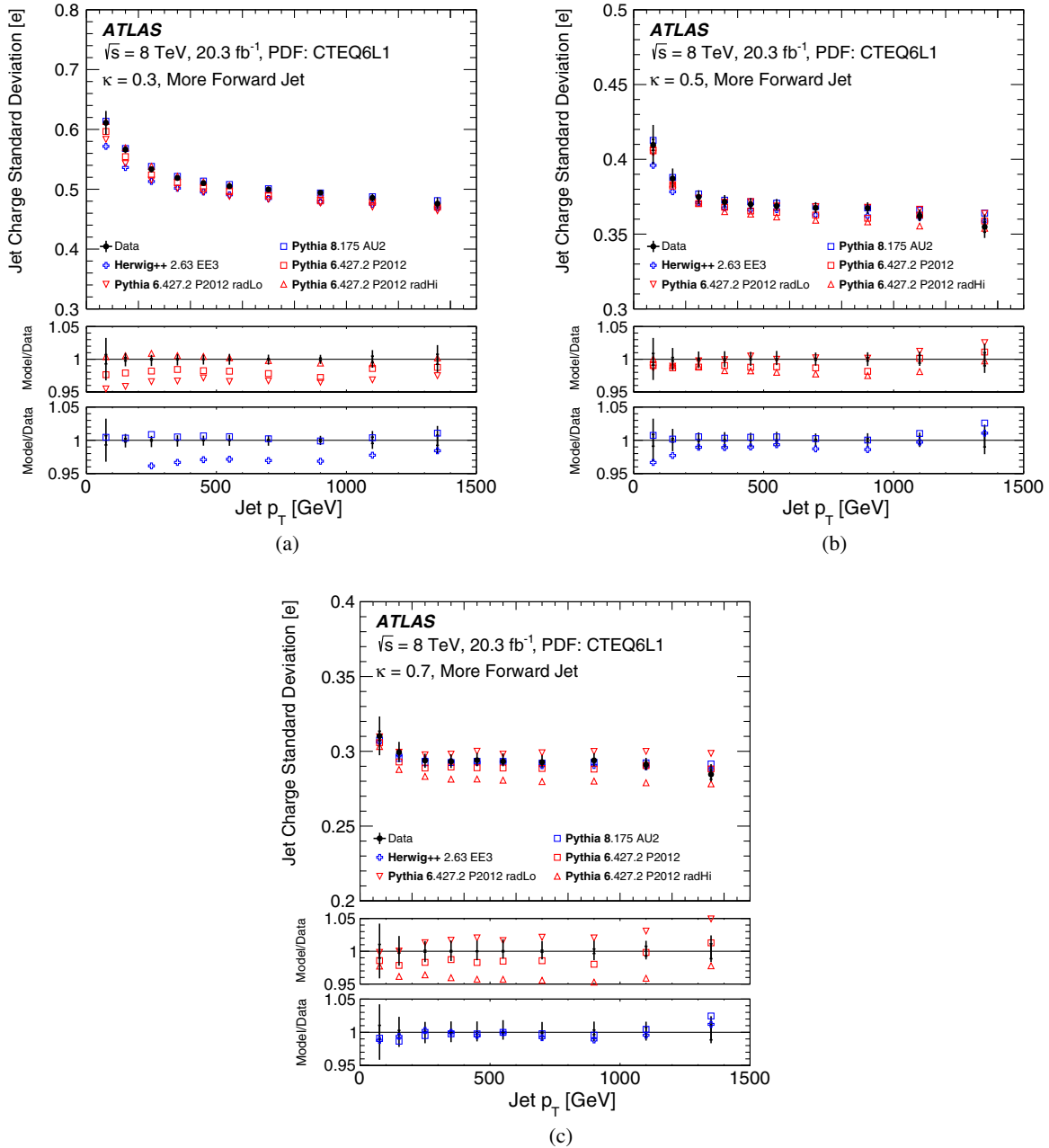


FIG. 12. The standard deviation of the jet charge distribution in units of the positron charge for (a) $\kappa = 0.3$, (b) 0.5, and (c) 0.7 comparing various QCD MC models and tunes for the more forward jet. The crossed lines in the bars on the data indicate the statistical uncertainty and the full extent of the bars is the sum in quadrature of the statistical and systematic uncertainties.

studied, testing the sensitivity to color reconnection and multiple parton interactions, but the differences in the jet charge distribution's mean and standard deviation are small. The Perugia 2012 tunes may not fully capture the spread in nonperturbative effects, which is also suggested by the increasing difference between PYTHIA 8 and HERWIG++ for decreasing κ .

D. Model comparison overview

Figures 13 and 14 show comparisons of the unfolded jet charge distribution's mean and standard deviation for

different QCD simulations using LO and NLO PDF sets. The predictions using the CT10 NLO PDF set as shown in Fig. 13 are generally about 10% below the data. Consistent with the expectation that the PDF and (nearly collinear) fragmentation are responsible for the jet charge distribution's mean and standard deviation, there does not seem to be an effect from the POWHEG NLO matrix element. For the jet charge distribution's standard deviation and $\kappa = 0.3$, the data falls between PYTHIA (larger standard deviation) and HERWIG++ (smaller standard deviation), but this trend is less evident for larger κ values, suggesting a difference due

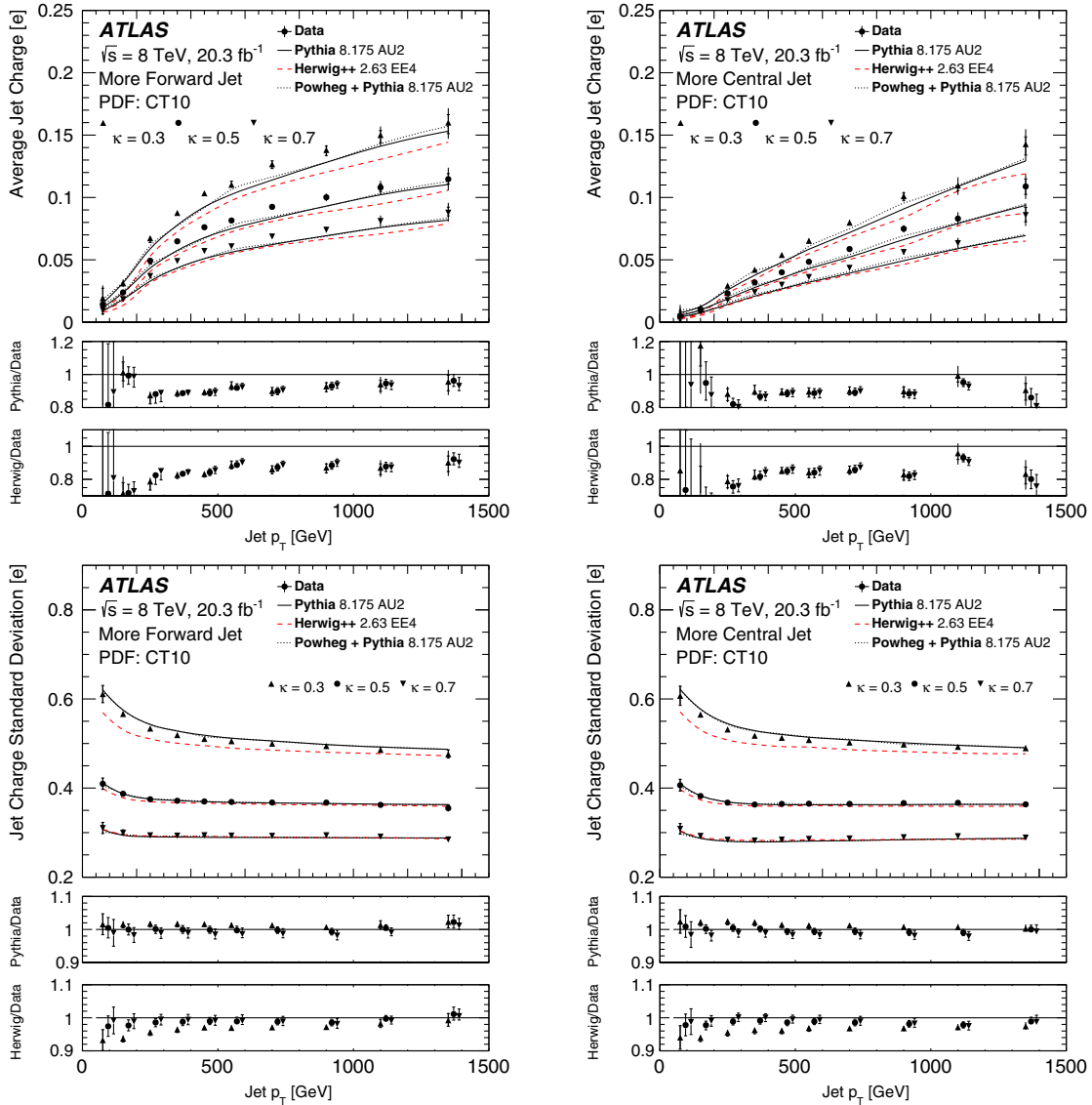


FIG. 13. The measured average of the jet charge distribution (top), and the standard deviation (bottom), in units of the positron charge as a function of the jet p_T for $\kappa = 0.3, 0.5$, and 0.7 for the more forward jet (left) and the more central jet (right) using CT10 as the PDF set. The markers in the lower panel are artificially displaced horizontally to make distinguishing the three κ values easier. The POWHEG + PYTHIA curves are nearly on top of the PYTHIA curves. The crossed lines in the bars on the data indicate the systematic uncertainty and the full extent of the bars is the sum in quadrature of the statistical and systematic uncertainties.

to soft tracks. As seen in Sec. VIII B, comparisons with CTEQ6L1 show it to be a better model for the p_T dependence of the mean jet charge than CT10. The analogous plots to Fig. 8 but using CTEQ6L1 instead of CT10 are shown in Fig. 14. Generally, there is agreement between the simulation and the data with only a $\lesssim 5\%$ difference in the lower p_T bins.

E. Extraction of the average up-quark and down-quark jet charges

In addition to understanding the trends in the jet charge distribution from PDFs, one can use PDFs to extract information about jets of a particular flavor. These

exclusive interpretations rely on flavor-fraction information in PDFs and matrix element calculations to extract the jet charge distribution for particular jet (anti)flavors in each p_T bin. The required nonperturbative information is summarized in Fig. 2(a). Jets with flavors other than up/down/anti-up/anti-down/gluon are not included in Fig. 2(a) and give a negligible contribution ($\lesssim 2\%$) in the highest p_T bins.

One way of extracting the up- and down-flavor average jet charges is to exploit the difference in flavor fractions shown in Fig. 2(a) between the more forward and the more central jets. Due to the p_T -balance requirement between the leading and subleading jet in the event selection, to a good approximation, the p_T spectrum is the same for the more forward and the more central jet. Assuming that the average

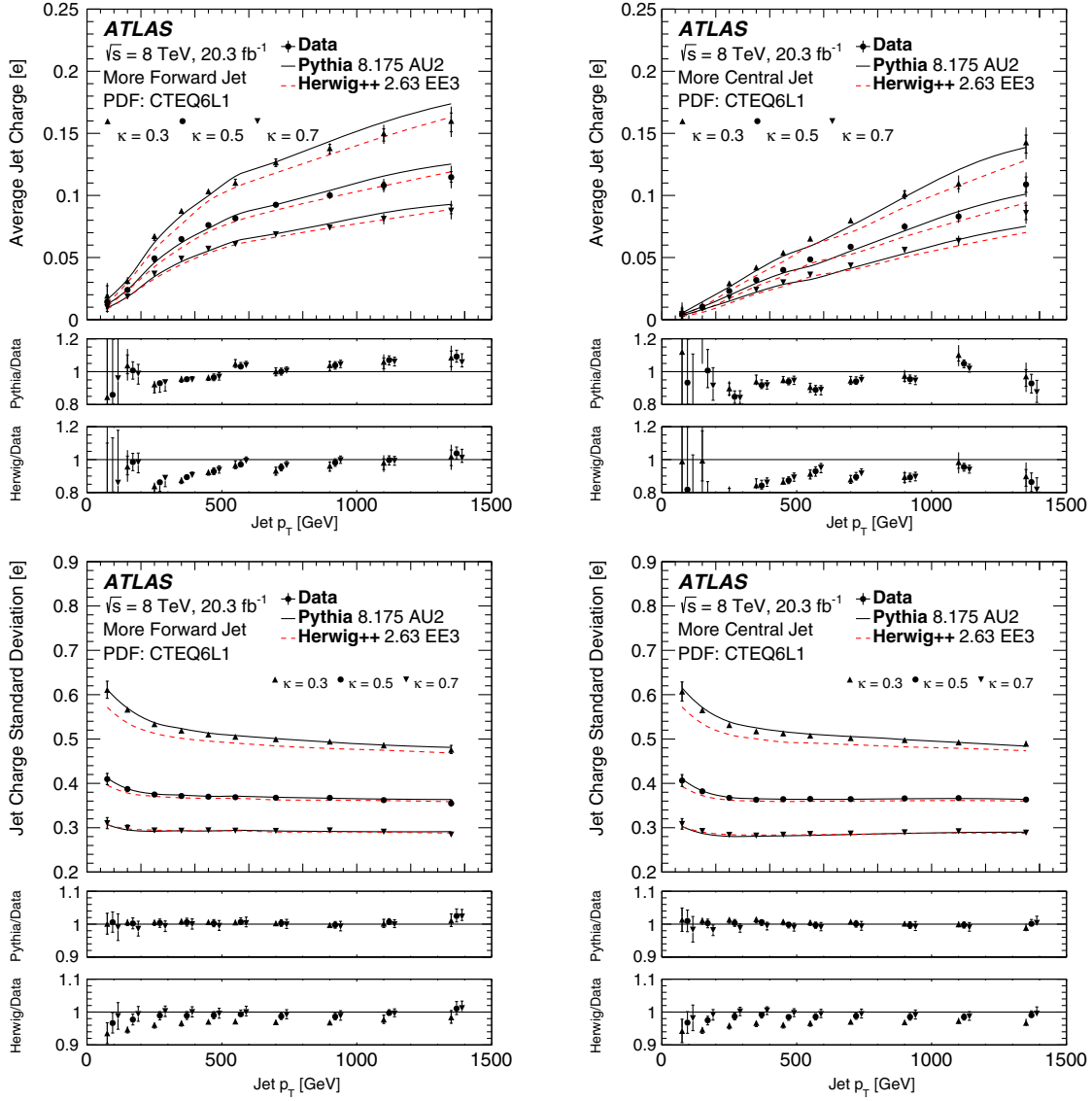


FIG. 14. The measured average of the jet charge distribution (top), and the standard deviation (bottom), in units of the positron charge as a function of the jet p_T for $\kappa = 0.3, 0.5$, and 0.7 for the more forward jet (left) and the more central jet (right) using CTEQ6L1 as the PDF set. The markers in the lower panel are artificially displaced horizontally to make distinguishing the three κ values easier. The crossed lines in the bars on the data indicate the systematic uncertainty and the full extent of the bars is the sum in quadrature of the statistical and systematic uncertainties.

jet charge of the sum of flavors that are not up/down/anti-up/anti-down is zero, in each bin i of p_T :

$$\begin{aligned}
 \langle Q_J^{\text{forward}} \rangle_i &= (f_{\text{up},i}^{\text{forward}} - f_{\text{anti-up},i}^{\text{forward}}) Q_i^{\text{up}} \\
 &\quad + (f_{\text{down},i}^{\text{forward}} - f_{\text{anti-down},i}^{\text{forward}}) Q_i^{\text{down}}, \\
 \langle Q_J^{\text{central}} \rangle_i &= (f_{\text{up},i}^{\text{central}} - f_{\text{anti-up},i}^{\text{central}}) Q_i^{\text{up}} \\
 &\quad + (f_{\text{down},i}^{\text{central}} - f_{\text{anti-down},i}^{\text{central}}) Q_i^{\text{down}}, \quad (2)
 \end{aligned}$$

where Q_J is the jet charge from Eq. (1), $f_{y,i}^x$ is the fraction of flavor y in p_T bin i for the jet $x \in \{\text{more forward, more central}\}$ and Q_i^y is the average jet

charge for such jets. The values $f_{y,i}^x$ are taken from simulation (PYTHIA with CT10 PDF and AU2 tune), which then allows an extraction of Q_i^y by solving the system of equations in Eq. (2). This extraction is performed separately in each p_T bin. Figure 15 shows the extracted up- and down-flavor jet charges in bins of jet p_T . At very high jet p_T , the absolute quark-flavor fractions are large (Fig. 2), but the difference between the more forward and more central jets is small and the statistical uncertainty is large. At low jet p_T , the difference between the more forward and more central jets is large (Fig. 2), but the absolute quark-flavor fraction is small and the statistical uncertainty is once again large because the mean jet charge is close to zero. In the limit that

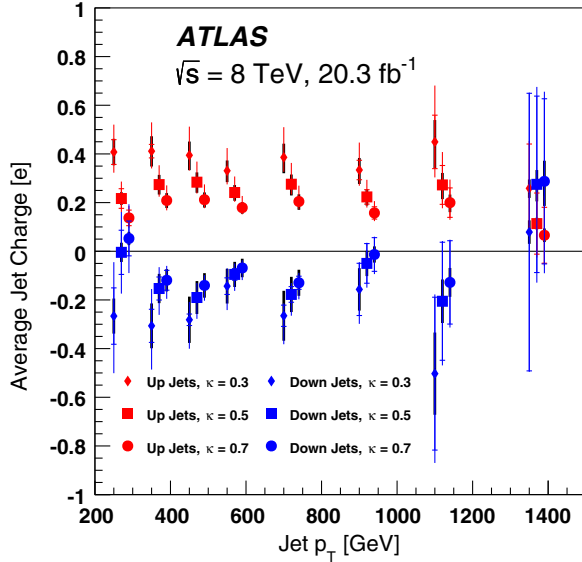


FIG. 15. The extracted value of up- and down-quark jet charges in units of the positron charge in bins of jet p_T for $\kappa = 0.3, 0.5,$ and 0.7 . The error bars include statistical, experimental systematic, and CT10 PDF uncertainties added in quadrature. The thick part of the error bar indicates the PDF contribution to the total uncertainty and the horizontal line on each error bar indicates the contribution from the statistical uncertainty. The first two p_T bins are excluded due to their very large uncertainties.

the flavor fractions are identical for the more forward and more central jet, the equations become degenerate and it is not possible to simultaneously extract the average up- and down-flavor jet charges. The uncertainties on the flavor fractions and on the measured average jet charges are propagated through the solutions of Eq. (2). Generally, the uncertainty is larger for the down-flavor jets because the fraction of these jets is smaller than the fraction of up-flavor jets.

F. Dependence of the up-quark and down-quark jet charge on p_T

Using the methods of Sec. VIII E, one can examine the residual p_T dependence of the average jet charge *after* accounting for PDF effects. The inclusive jet charge has been shown to increase with p_T due to a mixing of jet flavors and the following subsection investigates the p_T dependence of a fixed jet flavor. Section VIII F 1 describes the theory predictions and the extracted p_T dependence from the data is discussed in Sec. VIII F 2.

1. Theory prediction

Recent theoretical studies have shown that the energy dependence of jet charge moments is calculable perturbatively [34,35]. At leading power (treating $m_{\text{jet}}/E_{\text{jet}}$ as the expansion parameter), the charge defined with jet and track energies is equivalent to the one given in Eq. (1),

since the jet opening angle is small. For jets defined by a radius R at an energy E , the average jet charge $\langle Q_J \rangle$ is given by

$$\langle Q_J \rangle = [1 + \mathcal{O}(\alpha_s)] \sum_h Q_h \tilde{D}_q^h(\kappa, E \times R), \quad (3)$$

where Q_h is the charge of hadron h and the functions $\tilde{D}_q^h(\kappa, \mu)$ are the Mellin moments of the fragmentation functions

$$\tilde{D}_q^h(\kappa, \mu) = \int_0^1 dx x^\kappa D_q^h(x, \mu). \quad (4)$$

The fragmentation functions $D_q^h(x, \mu)$ describe the probability for a hadron h to carry a momentum fraction x of a quark q at the energy scale μ [85,86]. The $\mathcal{O}(\alpha_s)$ correction is small and is dominated by the uncertainty on the fragmentation functions [34]. Ratios of $\langle Q_J \rangle$ at different energies result in a cancellation of the leading corrections and associated uncertainties. Soft corrections to the average jet charge are small not only because of the additional suppression at $\kappa > 0$ compared to collinear radiation, but also because the leading soft emissions are made of gluons, which carry no electric charge. Although gluons can split into quark and antiquark pairs, the same number of quarks and antiquarks go into the jet so that on average the jet charge is unchanged.⁸

The leading energy dependence of the average jet charge is due to the derivative of the fragmentation functions with respect to E , which is determined by the renormalization group equations for $\tilde{D}_q^h(\kappa, \mu)$:

$$\frac{d}{d \ln \mu} \tilde{D}_q^h(\kappa, \mu) = \frac{\alpha_s}{\pi} \tilde{P}_{qq}(\kappa) \tilde{D}_q^h(\kappa, \mu) + \mathcal{O}(\alpha_s^2), \quad (5)$$

where $\tilde{P}_{qq}(\kappa)$ is the moment of the leading-order splitting function

$$\tilde{P}_{qq}(\kappa) = C_F \int_0^1 dz (z^\kappa - 1) \frac{1+z^2}{1-z}. \quad (6)$$

Recalling that E/p_T is constant at leading power for all particles in the jet, the prediction for the *scale violation* of a quark jet is given by

$$\frac{p_T}{\langle Q_\kappa \rangle} \frac{d}{dp_T} \langle Q_\kappa \rangle = \frac{\alpha_s}{\pi} \tilde{P}_{qq}(\kappa) \equiv c_\kappa \approx \begin{cases} -0.024 \pm 0.004 & \kappa = 0.3, \\ -0.038 \pm 0.006 & \kappa = 0.5, \\ -0.049 \pm 0.008 & \kappa = 0.7 \end{cases} \quad (7)$$

⁸This is not strictly true, as the soft radiation pattern depends on the partonic colors, which are correlated with electric charge, but these correlations are negligible compared to the other uncertainties.

where the last form consists of numerical approximations setting $\mu = E \times R$ equal to 50 and 500 GeV with their average giving the central value, and using $\alpha_s(50 \text{ GeV}) = 0.130$ and $\alpha_s(500 \text{ GeV}) = 0.094$. Experimentally, one measures combinations of quark and gluon jets with the fractions of different partonic flavors varying with energy. The next subsection discusses how the scaling violation parameter, defined in Eq. (7), can be extracted from the data.

2. Extraction from the data

Since $c_\kappa \ll 1$ from Eq. (7), one can approximate a linear dependence on c_κ :

$$\langle Q_J \rangle(p_T) = \bar{Q}(1 + c_\kappa \ln(p_T/\bar{p}_T)) + \mathcal{O}(c_\kappa^2), \quad (8)$$

where $\bar{Q} = \langle Q_J \rangle(\bar{p}_T)$ for some fixed (but arbitrary) transverse momentum, \bar{p}_T . Therefore, for a fixed p_T bin i , the measured charge is given as a superposition of the average jet charge for various jet flavors:

$$\langle Q_i \rangle \approx \sum_f \beta_{f,i} \bar{Q}_f (1 + c_\kappa \ln(p_{T,i}/\bar{p}_T)), \quad (9)$$

where $\beta_{f,i}$ is the fraction of flavor f in bin i , \bar{Q}_f is the average jet charge of flavor f and \bar{p}_T is a fixed transverse momentum. Fitting the model in Eq. (9) directly to the data to extract \bar{Q}_f is not practical because there are three parameters and only ten p_T bins, some of which have very little sensitivity due to low fractions β or large uncertainties on $\langle Q_J \rangle$. One way around this is to extract \bar{Q}_f in one fixed bin of transverse momentum (denoted \bar{p}_T) as described in Sec. VIII E. Then Eq. (9) is highly constrained, with only one parameter for which each other bin of p_T gives an estimate. The systematic uncertainties are propagated through the fit treated as fully correlated between bins and the statistical uncertainty is treated coherently by bootstrapping.⁹ A weighted average is performed across all p_T bins and for both the more forward and the more central jet. The procedure is summarized below:

- (1) In the bin $600 \text{ GeV} < p_T < 800 \text{ GeV}$, extract the values \bar{Q}_{up} and \bar{Q}_{down} . These values can be seen in the fifth p_T bin of Fig. 15.
- (2) With \bar{Q}_{up} and \bar{Q}_{down} fixed, extract the scale violation parameter estimate $c_{\kappa,i}$ in each p_T bin i by solving

⁹Pseudo-data sets are generated by adding each event in the nominal data set j times where j is a Poisson random variable with mean 1. Since events are coherently added, this respects the correlations in the statistical uncertainty for the more forward and central jet charges.

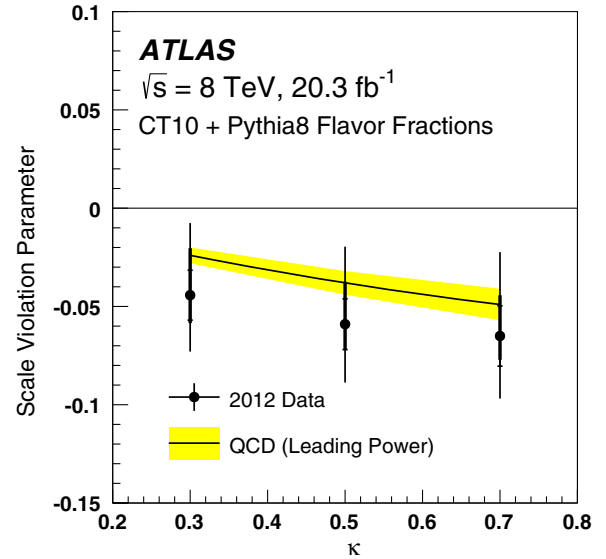


FIG. 16. The extracted values of the scale violation parameter c_κ from the data compared to theoretical calculations [34,35]. The error bars include statistical, experimental systematic, and PDF uncertainties added in quadrature. The thick part of the error bar indicates the PDF contribution to the total uncertainty and the horizontal line on each error bar indicates the contribution from the statistical uncertainty (each shown without adding in quadrature any other source of uncertainty).

$$\langle Q_i \rangle_{\text{measured}} = \sum_f \beta_{f,i} \bar{Q}_f (1 + c_{\kappa,i} \ln(p_{T,i}/\bar{p}_T)) \quad (10)$$

where $\bar{p}_T = 700 \text{ GeV}$ is the bin center from the previous step.

- (3) Repeat the above procedure for all systematic variations and for all bootstrap pseudo-data sets to arrive at estimates of the uncertainty $\sigma(c_{\kappa,i})$ for each p_T bin i .
- (4) The central value for the extracted scale violation parameter is $c_\kappa = (\sum_i c_{\kappa,i} / \sigma(c_{\kappa,i})) / \sum_i (1 / \sigma(c_{\kappa,i}))$.
- (5) The uncertainty $\sigma(c_\kappa)$ is determined by repeating step 3 with the nominal values $c_{\kappa,i}$ replaced by their systematic varied versions or the bootstrap pseudo-data values for the statistical uncertainty estimate.

The results are presented in Fig. 16. The data support the prediction that $c_\kappa < 0$ and $\partial c_\kappa / \partial \kappa < 0$. Linear correlations between κ values can be determined using the bootstrapped data sets: about 0.9 between $c_{0.3}$ and $c_{0.5}$ as well as between $c_{0.5}$ and $c_{0.7}$, while the correlation is about 0.7 between $c_{0.3}$ and $c_{0.7}$. Thus, the three points are quite correlated, but there is additional information from considering more than one κ value.

IX. SUMMARY

This paper presents a measurement of the particle-level p_T dependence of the jet charge distribution's mean and standard deviation in dijet events from 20.3 fb^{-1} of $\sqrt{s} =$

8 TeV pp collision data recorded by the ATLAS detector at the LHC. The measured jet charge distribution was unfolded to correct for the detector acceptance and resolution for direct comparison to particle-level models. Comparisons were made at particle level between the measured jet charge distribution and various PDF sets and models of jet formation. Simulations with PYTHIA 8 using the CTEQ6L1 PDF set describe the average jet charge of the more forward jet within about 5% and the more central jet within about 10%. The jet charge distribution's standard deviation is described within 2%. HERWIG++ shows a similarly good agreement for $p_T > 500$ GeV and $\kappa = 0.7$. However, the HERWIG++ predictions decrease systematically for both the average and the standard deviation for decreasing κ . Predictions with the CT10 NLO PDF are systematically below the data across jet p_T for the average jet charge and systematically above for the jet charge distribution's standard deviation. Taking the PDFs as inputs, the average up- and down-flavor jet charges were extracted as a function of p_T and were compared with predictions for scale violation. The data show that the average up- and down-quark jet charges decrease slightly with p_T and this decrease increases with κ , as predicted. The particle-level spectra are publicly available [87] for further interpretation and can serve as a benchmark for future measurements of the evolution of nonperturbative jet observables to validate QCD MC predictions and tune their free model parameters.

ACKNOWLEDGMENTS

We thank CERN for the very successful operation of the LHC, as well as the support staff from our institutions without whom ATLAS could not be operated efficiently. We acknowledge the support of ANPCyT, Argentina; YerPhI, Armenia; ARC, Australia; BMWFW and FWF, Austria; ANAS, Azerbaijan; SSTC, Belarus; CNPq and FAPESP,

Brazil; NSERC, NRC and CFI, Canada; CERN; CONICYT, Chile; CAS, MOST and NSFC, China; COLCIENCIAS, Colombia; MSMT CR, MPO CR and VSC CR, Czech Republic; DNRF, DNSRC and Lundbeck Foundation, Denmark; IN2P3-CNRS, CEA-DSM/IRFU, France; GNSF, Georgia; BMBF, HGF, and MPG, Germany; GSRT, Greece; RGC, Hong Kong SAR, China; ISF, I-CORE and Benoziyo Center, Israel; INFN, Italy; MEXT and JSPS, Japan; CNRST, Morocco; FOM and NWO, Netherlands; RCN, Norway; MNiSW and NCN, Poland; FCT, Portugal; MNE/IFA, Romania; MES of Russia and NRC KI, Russian Federation; JINR; MESTD, Serbia; MSSR, Slovakia; ARRS and MIZŠ, Slovenia; DST/NRF, South Africa; MINECO, Spain; SRC and Wallenberg Foundation, Sweden; SERI, SNSF and Cantons of Bern and Geneva, Switzerland; MOST, Taiwan; TAEK, Turkey; STFC, United Kingdom; DOE and NSF, United States of America. In addition, individual groups and members have received support from BCKDF, the Canada Council, CANARIE, CRC, Compute Canada, FQRNT, and the Ontario Innovation Trust, Canada; EPLANET, ERC, FP7, Horizon 2020 and Marie Skłodowska-Curie Actions, European Union; Investissements d'Avenir Labex and IDEX, ANR, Region Auvergne and Fondation Partager le Savoir, France; DFG and AvH Foundation, Germany; Herakleitos, Thales and Aristeia programmes co-financed by EU-ESF and the Greek NSRF; BSF, GIF and Minerva, Israel; BRF, Norway; the Royal Society and Leverhulme Trust, United Kingdom. The crucial computing support from all WLCG partners is acknowledged gratefully, in particular from CERN and the ATLAS Tier-1 facilities at TRIUMF (Canada), NDGF (Denmark, Norway, Sweden), CC-IN2P3 (France), KIT/GridKA (Germany), INFN-CNAF (Italy), NL-T1 (Netherlands), PIC (Spain), ASGC (Taiwan), RAL (UK) and BNL (USA) and in the Tier-2 facilities worldwide.

-
- [1] R. D. Field and R. P. Feynman, A parameterization of the properties of quark jets, *Nucl. Phys.* **B136**, 1 (1978).
 - [2] J. Berge *et al.*, Net charge in deep inelastic antineutrino-nucleon scattering, *Phys. Lett.* **91B**, 311 (1980).
 - [3] J. Berge *et al.*, Quark jets from antineutrino interactions (I). Net charge and factorization in the quark jets, *Nucl. Phys.* **B184**, 13 (1981).
 - [4] P. Allen *et al.*, Multiplicity distributions in neutrino-hydrogen interactions, *Nucl. Phys.* **B181**, 385 (1981).
 - [5] P. Allen *et al.*, Charge properties of the hadronic system in νp and $\bar{\nu} p$ interactions, *Phys. Lett.* **112B**, 88 (1982).
 - [6] J. Albanese *et al.*, Quark charge retention in final state hadrons from deep inelastic muon scattering, *Phys. Lett.* **144B**, 302 (1984).
 - [7] S. Barlag *et al.*, Charged hadron multiplicities in high energy $\bar{\nu}_\mu n$ and $\bar{\nu}_\mu p$ interactions, *Z. Phys.* **C 11**, 283 (1982).
 - [8] R. Erickson *et al.*, Charge retention in deep-inelastic electroproduction, *Phys. Rev. Lett.* **42**, 822 (1979).
 - [9] K. Abe *et al.* (SLD Collaboration), Measurement of the parity-violation parameter A_b from the left-right forward-backward asymmetry of b quark production in Z^0 decays using a momentum-weighted track-charge technique, *Phys. Rev. Lett.* **74**, 2890 (1995).
 - [10] W. Braunschweig *et al.* (TASSO Collaboration), Measurement of the asymmetry of b quark production in e^+e^- annihilation of $\sqrt{s} = 35$ GeV, *Z. Phys.* **C 48**, 433 (1990).
 - [11] P. Abreu, W. Adam, F. Adami, T. Adye, T. Akesson, G. D. Alekseev, P. Allen, S. Almeded, and S.J. Alvsvaag, A

- measurement of $\sin^2\theta(W)$ from the charge asymmetry of hadronic events at the Z^0 peak, *Phys. Lett. B* **277**, 371 (1992).
- [12] D. Decamp *et al.* (ALEPH Collaboration), Measurement of charge asymmetry in hadronic Z decays, *Phys. Lett. B* **259**, 377 (1991).
- [13] P. D. Acton *et al.* (OPAL Collaboration), A measurement of the forward-backward charge asymmetry in hadronic decays of the Z^0 , *Phys. Lett. B* **294**, 436 (1992).
- [14] R. Akers *et al.* (OPAL Collaboration), Measurement of the time dependence of $B_d^0 \leftrightarrow \bar{B}_d^0$ mixing using a jet charge technique, *Phys. Lett. B* **327**, 411 (1994).
- [15] P. Abreu *et al.* (DELPHI Collaboration), Measurement of the B_d^0 oscillation frequency using kaons, leptons and jet charge, *Z. Phys. C* **72**, 17 (1996).
- [16] F. Abe *et al.* (CDF Collaboration), Measurement of $B^0 - \bar{B}^0$ flavor oscillations using jet-charge and lepton flavor tagging in $p\bar{p}$ collisions at $\sqrt{s} = 1.8$ TeV, *Phys. Rev. D* **60**, 072003 (1999).
- [17] V. Abazov *et al.* (D0 Collaboration), Experimental discrimination between charge $2e/3$ top quark and charge $4e/3$ exotic quark production scenarios, *Phys. Rev. Lett.* **98**, 041801 (2007).
- [18] T. Aaltonen *et al.* (CDF Collaboration), Exclusion of exotic top-like quarks with $-4/3$ electric charge using jet-charge tagging in single-lepton $t\bar{t}$ events at CDF, *Phys. Rev. D* **88**, 032003 (2013).
- [19] ATLAS Collaboration, Measurement of the top quark charge in pp collisions at $\sqrt{s} = 7$ TeV with the ATLAS detector, *J. High Energy Phys.* **11** (2013) 031.
- [20] R. Barate *et al.* (ALEPH Collaboration), Measurement of triple gauge-boson couplings at 172 GeV, *Phys. Lett. B* **422**, 369 (1998).
- [21] P. Abreu *et al.* (DELPHI Collaboration), Measurement of trilinear gauge boson couplings WWV , ($V = Z, \gamma$) in $e^+ e^-$ collisions at 189 GeV, *Phys. Lett. B* **502**, 9 (2001).
- [22] M. Acciarri *et al.* (L3 Collaboration), Measurement of triple gauge boson couplings of the W boson at LEP, *Phys. Lett. B* **467**, 171 (1999).
- [23] G. Abbiendi *et al.* (OPAL Collaboration), Measurement of triple gauge boson couplings from W^+W^- production at LEP energies up to 189 GeV, *Eur. Phys. J. C* **19**, 1 (2001).
- [24] ATLAS Collaboration, Jet charge studies with the ATLAS detector using $\sqrt{s} = 8$ TeV proton-proton collision data, <https://cds.cern.ch/record/1572980>.
- [25] V. Khachatryan *et al.* (CMS Collaboration), Identification techniques for highly boosted W bosons that decay into hadrons, *J. High Energy Phys.* **12** (2014) 017.
- [26] ATLAS Collaboration, Light-quark and gluon jet discrimination in pp collisions at $\sqrt{s} = 7$ TeV with the ATLAS detector, *Eur. Phys. J. C* **74**, 3023 (2014).
- [27] P. D. Acton *et al.* (OPAL Collaboration), A study of the electric charge distributions of quark and gluon jets in hadronic Z^0 decays, *Phys. Lett. B* **302**, 523 (1993).
- [28] G. Arnison *et al.* (UA1 Collaboration), Analysis of the fragmentation properties of quark and gluon jets at the CERN SPS $p\bar{p}$ collider, *Nucl. Phys.* **B276**, 253 (1986).
- [29] G. Watt and R. Thorne, Study of Monte Carlo approach to experimental uncertainty propagation with MSTW 2008 PDFs, *J. High Energy Phys.* **08** (2012) 052.
- [30] L. A. Harland-Lang, A. D. Martin, P. Motylinski, and R. S. Thorne, Parton distributions in the LHC era: MMHT 2014 PDFs, *Eur. Phys. J. C* **75**, 204 (2015).
- [31] F. Aaron *et al.*, Combined measurement and QCD analysis of the inclusive $e^\pm p$ scattering cross sections at HERA, *J. High Energy Phys.* **01** (2010) 109.
- [32] H. Abramowicz *et al.* (H1 and ZEUS Collaborations), Combination of measurements of inclusive deep inelastic $e^\pm p$ scattering cross sections and QCD analysis of HERA data, *Eur. Phys. J. C* **75**, 580 (2015).
- [33] R. D. Ball *et al.*, Parton distributions for the LHC Run II, *J. High Energy Phys.* **04** (2015) 040.
- [34] W. J. Waalewijn, Calculating the charge of a jet, *Phys. Rev. D* **86**, 094030 (2012).
- [35] D. Krohn, T. Lin, M. D. Schwartz, and W. J. Waalewijn, Jet charge at the LHC, *Phys. Rev. Lett.* **110**, 212001 (2013).
- [36] C. W. Bauer, S. Fleming, and M. E. Luke, Summing Sudakov logarithms in $B \rightarrow X_s \gamma$ in effective field theory, *Phys. Rev. D* **63**, 014006 (2000).
- [37] C. W. Bauer, S. Fleming, D. Pirjol, and I. W. Stewart, An Effective field theory for collinear and soft gluons: Heavy to light decays, *Phys. Rev. D* **63**, 114020 (2001).
- [38] C. W. Bauer and I. W. Stewart, Invariant operators in collinear effective theory, *Phys. Lett. B* **516**, 134 (2001).
- [39] C. W. Bauer, D. Pirjol, and I. W. Stewart, Soft collinear factorization in effective field theory, *Phys. Rev. D* **65**, 054022 (2002).
- [40] G Aad *et al.* (ATLAS Collaboration), The ATLAS experiment at the CERN Large Hadron Collider, *J. Instrum.* **3**, S08003 (2008).
- [41] ATLAS Collaboration, Performance of the ATLAS trigger system in 2010, *Eur. Phys. J. C* **72**, 1849 (2012).
- [42] ATLAS Collaboration, Data-quality requirements and event cleaning for jets and missing transverse energy reconstruction with the ATLAS detector in proton-proton collisions at a center-of-mass energy of $\sqrt{s} = 7$ TeV, <https://cds.cern.ch/record/1277678>.
- [43] ATLAS Collaboration, Performance of primary vertex reconstruction in proton-proton collisions at $\sqrt{s} = 7$ TeV in the ATLAS experiment, <https://cds.cern.ch/record/1281344>.
- [44] T. Sjöstrand, S. Mrenna, and P. Z. Skands, A brief introduction to PYTHIA 8.1, *Comput. Phys. Commun.* **178**, 852 (2008).
- [45] ATLAS Collaboration, Summary of ATLAS PYTHIA 8 tunes, <https://cds.cern.ch/record/1474107>.
- [46] J. M. Campbell, J. Huston, and W. Stirling, Hard interactions of quarks and gluons: A primer for LHC physics, *Rep. Prog. Phys.* **70**, 89 (2007).
- [47] A. Sherstnev and R. Thorne, Parton distributions for LO generators, *Eur. Phys. J. C* **55**, 553 (2008).
- [48] H.-L. Lai, M. Guzzi, J. Huston, Z. Li, P. M. Nadolsky, J. Pumplin, and C.-P. Yuan, New parton distributions for collider physics, *Phys. Rev. D* **82**, 074024 (2010).
- [49] J. Gao, M. Guzzi, J. Huston, H.-L. Lai, Z. Li, P. Nadolsky, J. Pumplin, D. Stump, and C.-P. Yuan, The CT10 NNLO global analysis of QCD, *Phys. Rev. D* **89**, 033009 (2014).
- [50] M. Bähr *et al.*, HERWIG++ physics and manual, *Eur. Phys. J. C* **58**, 639 (2008).
- [51] K. Arnold *et al.*, HERWIG++ 2.6 release note, [arXiv:1205.4902](https://arxiv.org/abs/1205.4902).

- [52] S. Gieseke, C. Rohr, and A. Siodmok, Colour reconnections in HERWIG++, *Eur. Phys. J. C* **72**, 2225 (2012).
- [53] J. Pumplin, D. R. Stump, J. Huston, H.-L. Lai, P. Nadolsky, and W.-K. Tung, New generation of parton distributions with uncertainties from global QCD analysis, *J. High Energy Phys.* **07** (2002) 012.
- [54] T. Sjöstrand and P.Z. Skands, Transverse-momentum-ordered showers and interleaved multiple interactions, *Eur. Phys. J. C* **39**, 129 (2005).
- [55] S. Gieseke, P. Stephens, and B. Webber, New formalism for QCD parton showers, *J. High Energy Phys.* **12** (2003) 045.
- [56] T. Sjöstrand and P.Z. Skands, Multiple interactions and the structure of beam remnants, *J. High Energy Phys.* **03** (2004) 053.
- [57] M. Bähr, S. Gieseke, and M.H. Seymour, Simulation of multiple partonic interactions in HERWIG++, *J. High Energy Phys.* **07** (2008) 076.
- [58] B. Andersson, G. Gustafson, G. Ingelman, and T. Sjöstrand, Parton fragmentation and string dynamics, *Phys. Rep.* **97**, 31 (1983).
- [59] B. Webber, A QCD model for jet fragmentation including soft gluon interference, *Nucl. Phys.* **B238**, 492 (1984).
- [60] R. D. Ball, L. D. Debbio, S. Forte, A. Guffanti, J. I. Latorre, J. Rojo, and M. Ubiali, A first unbiased global NLO determination of parton distributions and their uncertainties, *Nucl. Phys.* **B838**, 136 (2010).
- [61] P. Nason, A New method for combining NLO QCD with shower Monte Carlo algorithms, *J. High Energy Phys.* **11** (2004) 040.
- [62] S. Frixione, P. Nason, and C. Oleari, Matching NLO QCD computations with parton shower simulations: the POWHEG method, *J. High Energy Phys.* **11** (2007) 070.
- [63] S. Alioli, P. Nason, C. Oleari, and E. Re, A general framework for implementing NLO calculations in shower Monte Carlo programs: the POWHEG BOX, *J. High Energy Phys.* **06** (2010) 043.
- [64] S. Frixione, P. Nason, and G. Ridolfi, A positive-weight next-to-leading-order Monte Carlo for heavy flavour hadroproduction, *J. High Energy Phys.* **09** (2007) 126.
- [65] ATLAS Collaboration, The ATLAS simulation infrastructure, *Eur. Phys. J. C* **70**, 823 (2010).
- [66] S. Agostinelli *et al.* (GEANT4 Collaboration), GEANT4: A simulation toolkit, *Nucl. Instrum. Methods Phys. Res., Sect. A* **506**, 250 (2003).
- [67] M. Cacciari, G.P. Salam, and G. Soyez, The anti- k_r jet clustering algorithm, *J. High Energy Phys.* **04** (2008) 063.
- [68] M. Cacciari, G. P. Salam, and G. Soyez, Fastjet user manual, *Eur. Phys. J. C* **72**, 1896 (2012).
- [69] W Lampl *et al.*, Calorimeter clustering algorithms: description and performance, <https://cds.cern.ch/record/1099735>.
- [70] C. Cojocaru *et al.*, Hadronic calibration of the ATLAS liquid argon end-cap calorimeter in the pseudorapidity region $1.6 < |\eta| < 1.8$ in beam tests, *Nucl. Instrum. Methods Phys. Res., Sect. A* **531**, 481 (2004).
- [71] ATLAS Collaboration, Local hadronic calibration, URL: <https://cds.cern.ch/record/1112035>.
- [72] ATLAS Collaboration, Pile-up subtraction and suppression for jets in ATLAS, Report No. ATLAS-CONF-2013-083, <https://cds.cern.ch/record/1570994>.
- [73] M. Cacciari, G. P. Salam, and G. Soyez, The catchment area of jets, *J. High Energy Phys.* **04** (2008) 005.
- [74] A. Banfi, G.P. Salam, and G. Zanderighi, Infrared safe definition of jet flavor, *Eur. Phys. J. C* **47**, 113 (2006).
- [75] G. D'Agostini, A multidimensional unfolding method based on Bayes theorem, *Nucl. Instrum. Methods Phys. Res., Sect. A* **362**, 487 (1995).
- [76] T. Adye, Unfolding algorithms and tests using rooufold, in *Proceedings of the PHYSTAT 2011 Workshop, CERN, Geneva, Switzerland, January, 2011*, edited by H. B. Prosper and L. Lyons (CERN, Geneva, 2011), p. 313.
- [77] B. Malaescu, An iterative, dynamically stabilized method of data unfolding, [arXiv:0907.3791](https://arxiv.org/abs/0907.3791).
- [78] ATLAS Collaboration, Jet energy measurement and its systematic uncertainty in proton-proton collisions at $\sqrt{s} = 7$ TeV with the ATLAS detector, *Eur. Phys. J. C* **75**, 17 (2015).
- [79] ATLAS Collaboration, Single hadron response measurement and calorimeter jet energy scale uncertainty with the ATLAS detector at the LHC, *Eur. Phys. J. C* **73**, 2305 (2013).
- [80] ATLAS Collaboration, Jet energy resolution in proton-proton collisions at $\sqrt{s} = 7$ TeV recorded in 2010 with the ATLAS detector, *Eur. Phys. J. C* **73**, 2306 (2013).
- [81] ATLAS Collaboration, A study of the material in the ATLAS inner detector using secondary hadronic interactions, *J. Instrum.* **7**, P01013 (2012).
- [82] ATLAS Collaboration, Measurement of the muon reconstruction performance of the ATLAS detector using 2011 and 2012 LHC proton-proton collision data, *Eur. Phys. J. C* **74**, 3130 (2014).
- [83] ATLAS Collaboration, Search for anomalous production of prompt same-sign lepton pairs and pair-produced doubly charged Higgs bosons with $\sqrt{s} = 8$ TeV pp collisions using the ATLAS detector, *J. High Energy Phys.* **03** (2015) 041.
- [84] P.Z. Skands, Tuning Monte Carlo generators: the Perugia tunes, *Phys. Rev. D* **82**, 074018 (2010).
- [85] J. C. Collins and D. E. Soper, Parton distribution and decay functions, *Nucl. Phys.* **B194**, 445 (1982).
- [86] J. C. Collins and D. E. Soper, Back-to-back jets in QCD, *Nucl. Phys.* **B193**, 381 (1981).
- [87] <http://hepdata.cedar.ac.uk/>.

G. Aad,⁸⁵ B. Abbott,¹¹³ J. Abdallah,¹⁵¹ O. Abidinov,¹¹ R. Aben,¹⁰⁷ M. Abolins,⁹⁰ O. S. AbouZeid,¹⁵⁸ H. Abramowicz,¹⁵³ H. Abreu,¹⁵² R. Abreu,¹¹⁶ Y. Abulaiti,^{146a,146b} B. S. Acharya,^{164a,164b,a} L. Adamczyk,^{38a} D. L. Adams,²⁵ J. Adelman,¹⁰⁸ S. Adomeit,¹⁰⁰ T. Adye,¹³¹ A. A. Affolder,⁷⁴ T. Agatonovic-Jovin,¹³ J. Agricola,⁵⁴ J. A. Aguilar-Saavedra,^{126a,126f}

S. P. Ahlen,²² F. Ahmadov,^{65,b} G. Aielli,^{133a,133b} H. Akerstedt,^{146a,146b} T. P. A. Åkesson,⁸¹ A. V. Akimov,⁹⁶
G. L. Alberghi,^{20a,20b} J. Albert,¹⁶⁹ S. Albrand,⁵⁵ M. J. Alconada Verzini,⁷¹ M. Aleksa,³⁰ I. N. Aleksandrov,⁶⁵ C. Alexa,^{26b}
G. Alexander,¹⁵³ T. Alexopoulos,¹⁰ M. Alhroob,¹¹³ G. Alimonti,^{91a} L. Alio,⁸⁵ J. Alison,³¹ S. P. Alkire,³⁵
B. M. M. Allbrooke,¹⁴⁹ P. P. Allport,¹⁸ A. Aloisio,^{104a,104b} A. Alonso,³⁶ F. Alonso,⁷¹ C. Alpigiani,¹³⁸ A. Altheimer,³⁵
B. Alvarez Gonzalez,³⁰ D. Álvarez Piqueras,¹⁶⁷ M. G. Alviggi,^{104a,104b} B. T. Amadio,¹⁵ K. Amako,⁶⁶ Y. Amaral Coutinho,^{24a}
C. Amelung,²³ D. Amidei,⁸⁹ S. P. Amor Dos Santos,^{126a,126c} A. Amorim,^{126a,126b} S. Amoroso,⁴⁸ N. Amram,¹⁵³
G. Amundsen,²³ C. Anastopoulos,¹³⁹ L. S. Ancu,⁴⁹ N. Andari,¹⁰⁸ T. Andeen,³⁵ C. F. Anders,^{58b} G. Anders,³⁰ J. K. Anders,⁷⁴
K. J. Anderson,³¹ A. Andreazza,^{91a,91b} V. Andrei,^{58a} S. Angelidakis,⁹ I. Angelozzi,¹⁰⁷ P. Anger,⁴⁴ A. Angerami,³⁵
F. Anghinolfi,³⁰ A. V. Anisenkov,^{109,c} N. Anjos,¹² A. Annovi,^{124a,124b} M. Antonelli,⁴⁷ A. Antonov,⁹⁸ J. Antos,^{144b}
F. Anulli,^{132a} M. Aoki,⁶⁶ L. Aperio Bella,¹⁸ G. Arabidze,⁹⁰ Y. Arai,⁶⁶ J. P. Araque,^{126a} A. T. H. Arce,⁴⁵ F. A. Arduh,⁷¹
J.-F. Arguin,⁹⁵ S. Argyropoulos,⁶³ M. Arik,^{19a} A. J. Armbruster,³⁰ O. Arnaez,³⁰ H. Arnold,⁴⁸ M. Arratia,²⁸ O. Arslan,²¹
A. Artamonov,⁹⁷ G. Artoni,²³ S. Asai,¹⁵⁵ N. Asbah,⁴² A. Ashkenazi,¹⁵³ B. Åsman,^{146a,146b} L. Asquith,¹⁴⁹ K. Assamagan,²⁵
R. Astalos,^{144a} M. Atkinson,¹⁶⁵ N. B. Atlay,¹⁴¹ K. Augsten,¹²⁸ M. Aourousseau,^{145b} G. Avolio,³⁰ B. Axen,¹⁵ M. K. Ayoub,¹¹⁷
G. Azuelos,^{95,d} M. A. Baak,³⁰ A. E. Baas,^{58a} M. J. Baca,¹⁸ C. Bacci,^{134a,134b} H. Bachacou,¹³⁶ K. Bachas,¹⁵⁴ M. Backes,³⁰
M. Backhaus,³⁰ P. Bagiacchi,^{132a,132b} P. Bagnaia,^{132a,132b} Y. Bai,^{33a} T. Bain,³⁵ J. T. Baines,¹³¹ O. K. Baker,¹⁷⁶
E. M. Baldin,^{109,c} P. Balek,¹²⁹ T. Balestri,¹⁴⁸ F. Balli,⁸⁴ W. K. Balunas,¹²² E. Banas,³⁹ Sw. Banerjee,¹⁷³ A. A. E. Bannoura,¹⁷⁵
L. Barak,³⁰ E. L. Barberio,⁸⁸ D. Barberis,^{50a,50b} M. Barbero,⁸⁵ T. Barillari,¹⁰¹ M. Barisonzi,^{164a,164b} T. Barklow,¹⁴³
N. Barlow,²⁸ S. L. Barnes,⁸⁴ B. M. Barnett,¹³¹ R. M. Barnett,¹⁵ Z. Barnovska,⁵ A. Baroncelli,^{134a} G. Barone,²³ A. J. Barr,¹²⁰
F. Barreiro,⁸² J. Barreiro Guimarães da Costa,⁵⁷ R. Bartoldus,¹⁴³ A. E. Barton,⁷² P. Bartos,^{144a} A. Basalaeu,¹²³ A. Bassalat,¹¹⁷
A. Basye,¹⁶⁵ R. L. Bates,⁵³ S. J. Batista,¹⁵⁸ J. R. Batley,²⁸ M. Battaglia,¹³⁷ M. Bause,^{132a,132b} F. Bauer,¹³⁶ H. S. Bawa,^{143,e}
J. B. Beacham,¹¹¹ M. D. Beattie,⁷² T. Beau,⁸⁰ P. H. Beauchemin,¹⁶¹ R. Beccherle,^{124a,124b} P. Bechtel,²¹ H. P. Beck,^{17,f}
K. Becker,¹²⁰ M. Becker,⁸³ M. Beckingham,¹⁷⁰ C. Becot,¹¹⁷ A. J. Beddall,^{19b} A. Beddall,^{19b} V. A. Bednyakov,⁶⁵ C. P. Bee,¹⁴⁸
L. J. Beemster,¹⁰⁷ T. A. Beermann,³⁰ M. Begel,²⁵ J. K. Behr,¹²⁰ C. Belanger-Champagne,⁸⁷ W. H. Bell,⁴⁹ G. Bella,¹⁵³
L. Bellagamba,^{20a} A. Bellerive,²⁹ M. Bellomo,⁸⁶ K. Belotskiy,⁹⁸ O. Beltramello,³⁰ O. Benary,¹⁵³ D. Benchekroun,^{135a}
M. Bender,¹⁰⁰ K. Bendtz,^{146a,146b} N. Benekos,¹⁰ Y. Benhammou,¹⁵³ E. Benhar Nocchioli,⁴⁹ J. A. Benitez Garcia,^{159b}
D. P. Benjamin,⁴⁵ J. R. Bensinger,²³ S. Bentvelsen,¹⁰⁷ L. Beresford,¹²⁰ M. Beretta,⁴⁷ D. Berge,¹⁰⁷ E. Bergeaas Kuutmann,¹⁶⁶
N. Berger,⁵ F. Berghaus,¹⁶⁹ J. Beringer,¹⁵ C. Bernard,²² N. R. Bernard,⁸⁶ C. Bernius,¹¹⁰ F. U. Bernlochner,²¹ T. Berry,⁷⁷
P. Berta,¹²⁹ C. Bertella,⁸³ G. Bertoli,^{146a,146b} F. Bertolucci,^{124a,124b} C. Bertsche,¹¹³ D. Bertsche,¹¹³ M. I. Besana,^{91a}
G. J. Besjes,³⁶ O. Bessidskaia Bylund,^{146a,146b} M. Bessner,⁴² N. Besson,¹³⁶ C. Betancourt,⁴⁸ S. Bethke,¹⁰¹ A. J. Bevan,⁷⁶
W. Bhimji,¹⁵ R. M. Bianchi,¹²⁵ L. Bianchini,²³ M. Bianco,³⁰ O. Biebel,¹⁰⁰ D. Biedermann,¹⁶ S. P. Bieniek,⁷⁸
N. V. Biesuz,^{124a,124b} M. Biglietti,^{134a} J. Bilbao De Mendizabal,⁴⁹ H. Bilokon,⁴⁷ M. Bindi,⁵⁴ S. Binet,¹¹⁷ A. Bingul,^{19b}
C. Bini,^{132a,132b} S. Biondi,^{20a,20b} D. M. Bjergaard,⁴⁵ C. W. Black,¹⁵⁰ J. E. Black,¹⁴³ K. M. Black,²² D. Blackburn,¹³⁸
R. E. Blair,⁶ J.-B. Blanchard,¹³⁶ J. E. Blanco,⁷⁷ T. Blazek,^{144a} I. Bloch,⁴² C. Blocker,²³ W. Blum,^{83,†} U. Blumenschein,⁵⁴
S. Blunier,^{32a} G. J. Bobbink,¹⁰⁷ V. S. Bobrovnikov,^{109,c} S. S. Bocchetta,⁸¹ A. Bocci,⁴⁵ C. Bock,¹⁰⁰ M. Boehler,⁴⁸
J. A. Bogaerts,³⁰ D. Bogavac,¹³ A. G. Bogdanchikov,¹⁰⁹ C. Bohm,^{146a} V. Boisvert,⁷⁷ T. Bold,^{38a} V. Boldea,^{26b}
A. S. Boldyrev,⁹⁹ M. Bomben,⁸⁰ M. Bona,⁷⁶ M. Boonekamp,¹³⁶ A. Borisov,¹³⁰ G. Borissov,⁷² S. Borroni,⁴² J. Bortfeldt,¹⁰⁰
V. Bortolotto,^{60a,60b,60c} K. Bos,¹⁰⁷ D. Boscherini,^{20a} M. Bosman,¹² J. Boudreau,¹²⁵ J. Bouffard,² E. V. Bouhova-Thacker,⁷²
D. Boumediene,³⁴ C. Bourdarios,¹¹⁷ N. Bousson,¹¹⁴ S. K. Boutle,⁵³ A. Boveia,³⁰ J. Boyd,³⁰ I. R. Boyko,⁶⁵ I. Bozic,¹³
J. Bracinik,¹⁸ A. Brandt,⁸ G. Brandt,⁵⁴ O. Brandt,^{58a} U. Bratzler,¹⁵⁶ B. Brau,⁸⁶ J. E. Brau,¹¹⁶ H. M. Braun,^{175†}
W. D. Breaden Madden,⁵³ K. Brendlinger,¹²² A. J. Brennan,⁸⁸ L. Brenner,¹⁰⁷ R. Brenner,¹⁶⁶ S. Bressler,¹⁷² K. Bristow,^{145c}
T. M. Bristow,⁴⁶ D. Britton,⁵³ D. Britzger,⁴² F. M. Brochu,²⁸ I. Brock,²¹ R. Brock,⁹⁰ J. Bronner,¹⁰¹ G. Brooijmans,³⁵
T. Brooks,⁷⁷ W. K. Brooks,^{32b} J. Brosamer,¹⁵ E. Brost,¹¹⁶ P. A. Bruckman de Renstrom,³⁹ D. Bruncko,^{144b} R. Bruneliere,⁴⁸
A. Bruni,^{20a} G. Bruni,^{20a} M. Bruschi,^{20a} N. Brusino,²¹ L. Bryngemark,⁸¹ T. Buanes,¹⁴ Q. Buat,¹⁴² P. Buchholz,¹⁴¹
A. G. Buckley,⁵³ S. I. Buda,^{26b} I. A. Budagov,⁶⁵ F. Buehrer,⁴⁸ L. Bugge,¹¹⁹ M. K. Bugge,¹¹⁹ O. Bulekov,⁹⁸ D. Bullock,⁸
H. Burckhart,³⁰ S. Burdin,⁷⁴ C. D. Burgard,⁴⁸ B. Burghgrave,¹⁰⁸ S. Burke,¹³¹ I. Burmeister,⁴³ E. Busato,³⁴ D. Büscher,⁴⁸
V. Büscher,⁸³ P. Bussey,⁵³ J. M. Butler,²² A. I. Butt,³ C. M. Buttar,⁵³ J. M. Butterworth,⁷⁸ P. Butti,¹⁰⁷ W. Buttinger,²⁵
A. Buzatu,⁵³ A. R. Buzykaev,^{109,c} S. Cabrera Urbán,¹⁶⁷ D. Caforio,¹²⁸ V. M. Cairo,^{37a,37b} O. Cakir,^{4a} N. Calace,⁴⁹
P. Calafiura,¹⁵ A. Calandri,¹³⁶ G. Calderini,⁸⁰ P. Calfayan,¹⁰⁰ L. P. Caloba,^{24a} D. Calvet,³⁴ S. Calvet,³⁴ R. Camacho Toro,³¹
S. Camarda,⁴² P. Camarri,^{133a,133b} D. Cameron,¹¹⁹ R. Caminal Armadans,¹⁶⁵ S. Campana,³⁰ M. Campanelli,⁷⁸

A. Campoverde,¹⁴⁸ V. Canale,^{104a,104b} A. Canepa,^{159a} M. Cano Bret,^{33e} J. Cantero,⁸² R. Cantrill,^{126a} T. Cao,⁴⁰ M. D. M. Capeans Garrido,³⁰ I. Caprini,^{26b} M. Caprini,^{26b} M. Capua,^{37a,37b} R. Caputo,⁸³ R. M. Carbone,³⁵ R. Cardarelli,^{133a} F. Cardillo,⁴⁸ T. Carli,³⁰ G. Carlino,^{104a} L. Carminati,^{91a,91b} S. Caron,¹⁰⁶ E. Carquin,^{32a} G. D. Carrillo-Montoya,³⁰ J. R. Carter,²⁸ J. Carvalho,^{126a,126c} D. Casadei,⁷⁸ M. P. Casado,¹² M. Casolino,¹² E. Castaneda-Miranda,^{145a} A. Castelli,¹⁰⁷ V. Castillo Gimenez,¹⁶⁷ N. F. Castro,^{126a,g} P. Catastini,⁵⁷ A. Catinaccio,³⁰ J. R. Catmore,¹¹⁹ A. Cattai,³⁰ J. Caudron,⁸³ V. Cavaliere,¹⁶⁵ D. Cavalli,^{91a} M. Cavalli-Sforza,¹² V. Cavasinni,^{124a,124b} F. Ceradini,^{134a,134b} B. C. Cerio,⁴⁵ K. Cerny,¹²⁹ A. S. Cerqueira,^{24b} A. Cerri,¹⁴⁹ L. Cerrito,⁷⁶ F. Cerutti,¹⁵ M. Cerv,³⁰ A. Cervelli,¹⁷ S. A. Cetin,^{19c} A. Chafaq,^{135a} D. Chakraborty,¹⁰⁸ I. Chalupkova,¹²⁹ P. Chang,¹⁶⁵ J. D. Chapman,²⁸ D. G. Charlton,¹⁸ C. C. Chau,¹⁵⁸ C. A. Chavez Barajas,¹⁴⁹ S. Cheatham,¹⁵² A. Chegwiddden,⁹⁰ S. Chekanov,⁶ S. V. Chekulaev,^{159a} G. A. Chelkov,^{65,h} M. A. Chelstowska,⁸⁹ C. Chen,⁶⁴ H. Chen,²⁵ K. Chen,¹⁴⁸ L. Chen,^{33d,i} S. Chen,^{33c} S. Chen,¹⁵⁵ X. Chen,^{33f} Y. Chen,⁶⁷ H. C. Cheng,⁸⁹ Y. Cheng,³¹ A. Cheplakov,⁶⁵ E. Cheremushkina,¹³⁰ R. Cherkaoui El Moursli,^{135e} V. Chernyatin,^{25†} E. Cheu,⁷ L. Chevalier,¹³⁶ V. Chiarella,⁴⁷ G. Chiarelli,^{124a,124b} G. Chiodini,^{73a} A. S. Chisholm,¹⁸ R. T. Chislett,⁷⁸ A. Chitan,^{26b} M. V. Chizhov,⁶⁵ K. Choi,⁶¹ S. Chouridou,⁹ B. K. B. Chow,¹⁰⁰ V. Christodoulou,⁷⁸ D. Chromek-Burckhart,³⁰ J. Chudoba,¹²⁷ A. J. Chuinard,⁸⁷ J. J. Chwastowski,³⁹ L. Chytka,¹¹⁵ G. Ciapetti,^{132a,132b} A. K. Ciftci,^{4a} D. Cinca,⁵³ V. Cindro,⁷⁵ I. A. Cioara,²¹ A. Ciocio,¹⁵ F. Ciroto,^{104a,104b} Z. H. Citron,¹⁷² M. Ciubancan,^{26b} A. Clark,⁴⁹ B. L. Clark,⁵⁷ P. J. Clark,⁴⁶ R. N. Clarke,¹⁵ C. Clement,^{146a,146b} Y. Coadou,⁸⁵ M. Cobal,^{164a,164c} A. Coccaro,⁴⁹ J. Cochran,⁶⁴ L. Coffey,²³ J. G. Cogan,¹⁴³ L. Colasurdo,¹⁰⁶ B. Cole,³⁵ S. Cole,¹⁰⁸ A. P. Colijn,¹⁰⁷ J. Collot,⁵⁵ T. Colombo,^{58c} G. Compostella,¹⁰¹ P. Conde Muno,^{126a,126b} E. Coniavitis,⁴⁸ S. H. Connell,^{145b} I. A. Connelly,⁷⁷ V. Consorti,⁴⁸ S. Constantinescu,^{26b} C. Conta,^{121a,121b} G. Conti,³⁰ F. Conventi,^{104a,j} M. Cooke,¹⁵ B. D. Cooper,⁷⁸ A. M. Cooper-Sarkar,¹²⁰ T. Cornelissen,¹⁷⁵ M. Corradi,^{20a} F. Corriveau,^{87,k} A. Corso-Radu,¹⁶³ A. Cortes-Gonzalez,¹² G. Cortiana,¹⁰¹ G. Costa,^{91a} M. J. Costa,¹⁶⁷ D. Costanzo,¹³⁹ D. Cote,⁸ G. Cottin,²⁸ G. Cowan,⁷⁷ B. E. Cox,⁸⁴ K. Cranmer,¹¹⁰ G. Cree,²⁹ S. Crepe-Renaudin,⁵⁵ F. Crescioli,⁸⁰ W. A. Cribbs,^{146a,146b} M. Crispin Ortuzar,¹²⁰ M. Cristinziani,²¹ V. Croft,¹⁰⁶ G. Crosetti,^{37a,37b} T. Cuhadar Donszelmann,¹³⁹ J. Cummings,¹⁷⁶ M. Curatolo,⁴⁷ J. Cuth,⁸³ C. Cuthbert,¹⁵⁰ H. Czirr,¹⁴¹ P. Czodrowski,³ S. D'Auria,⁵³ M. D'Onofrio,⁷⁴ M. J. Da Cunha Sargedas De Sousa,^{126a,126b} C. Da Via,⁸⁴ W. Dabrowski,^{38a} A. Dafinca,¹²⁰ T. Dai,⁸⁹ O. Dale,¹⁴ F. Dallaire,⁹⁵ C. Dallapiccola,⁸⁶ M. Dam,³⁶ J. R. Dandoy,³¹ N. P. Dang,⁴⁸ A. C. Daniells,¹⁸ M. Danninger,¹⁶⁸ M. Dano Hoffmann,¹³⁶ V. Dao,⁴⁸ G. Darbo,^{50a} S. Darmora,⁸ J. Dassoulas,³ A. Dattagupta,⁶¹ W. Davey,²¹ C. David,¹⁶⁹ T. Davidek,¹²⁹ E. Davies,^{120,l} M. Davies,¹⁵³ P. Davison,⁷⁸ Y. Davygora,^{58a} E. Dawe,⁸⁸ I. Dawson,¹³⁹ R. K. Daya-Ishmukhametova,⁸⁶ K. De,⁸ R. de Asmundis,^{104a} A. De Benedetti,¹¹³ S. De Castro,^{20a,20b} S. De Cecco,⁸⁰ N. De Groot,¹⁰⁶ P. de Jong,¹⁰⁷ H. De la Torre,⁸² F. De Lorenzi,⁶⁴ D. De Pedis,^{132a} A. De Salvo,^{132a} U. De Sanctis,¹⁴⁹ A. De Santo,¹⁴⁹ J. B. De Vivie De Regie,¹¹⁷ W. J. Dearnaley,⁷² R. Debbes,²⁵ C. Debenedetti,¹³⁷ D. V. Dedovich,⁶⁵ I. Deigaard,¹⁰⁷ J. Del Peso,⁸² T. Del Prete,^{124a,124b} D. Delgove,¹¹⁷ F. Deliot,¹³⁶ C. M. Delitzsch,⁴⁹ M. Deliyergiyev,⁷⁵ A. Dell'Acqua,³⁰ L. Dell'Asta,²² M. Dell'Orso,^{124a,124b} M. Della Pietra,^{104a,j} D. della Volpe,⁴⁹ M. Delmastro,⁵ P. A. Delsart,⁵⁵ C. Deluca,¹⁰⁷ D. A. DeMarco,¹⁵⁸ S. Demers,¹⁷⁶ M. Demichev,⁶⁵ A. Demilly,⁸⁰ S. P. Denisov,¹³⁰ D. Derendarz,³⁹ J. E. Derkaoui,^{135d} F. Derue,⁸⁰ P. Dervan,⁷⁴ K. Desch,²¹ C. Deterre,⁴² P. O. Deviveiros,³⁰ A. Dewhurst,¹³¹ S. Dhaliwal,²³ A. Di Ciaccio,^{133a,133b} L. Di Ciaccio,⁵ A. Di Domenico,^{132a,132b} C. Di Donato,^{104a,104b} A. Di Girolamo,³⁰ B. Di Girolamo,³⁰ A. Di Mattia,¹⁵² B. Di Micco,^{134a,134b} R. Di Nardo,⁴⁷ A. Di Simone,⁴⁸ R. Di Sipio,¹⁵⁸ D. Di Valentino,²⁹ C. Diaconu,⁸⁵ M. Diamond,¹⁵⁸ F. A. Dias,⁴⁶ M. A. Diaz,^{32a} E. B. Diehl,⁸⁹ J. Dietrich,¹⁶ S. Diglio,⁸⁵ A. Dimitrievska,¹³ J. Dingfelder,²¹ P. Dita,^{26b} S. Dita,^{26b} F. Dittus,³⁰ F. Djama,⁸⁵ T. Djobava,^{51b} J. I. Djuvsland,^{58a} M. A. B. do Vale,^{24c} D. Dobos,³⁰ M. Dobre,^{26b} C. Doglioni,⁸¹ T. Dohmae,¹⁵⁵ J. Dolejsi,¹²⁹ Z. Dolezal,¹²⁹ B. A. Dolgoshein,^{98†} M. Donadelli,^{24d} S. Donati,^{124a,124b} P. Dondero,^{121a,121b} J. Donini,³⁴ J. Dopke,¹³¹ A. Doria,^{104a} M. T. Dova,⁷¹ A. T. Doyle,⁵³ E. Drechsler,⁵⁴ M. Dris,¹⁰ E. Dubreuil,³⁴ E. Duchovni,¹⁷² G. Duckeck,¹⁰⁰ O. A. Ducu,^{26b,85} D. Duda,¹⁰⁷ A. Dudarev,³⁰ L. Duflot,¹¹⁷ L. Duguid,⁷⁷ M. Duhrssen,³⁰ M. Dunford,^{58a} H. Duran Yildiz,^{4a} M. Duren,⁵² A. Durglishvili,^{51b} D. Duschinger,⁴⁴ B. Dutta,⁴² M. Dyndal,^{38a} C. Eckardt,⁴² K. M. Ecker,¹⁰¹ R. C. Edgar,⁸⁹ W. Edson,² N. C. Edwards,⁴⁶ W. Ehrenfeld,²¹ T. Eifert,³⁰ G. Eigen,¹⁴ K. Einsweiler,¹⁵ T. Ekelof,¹⁶⁶ M. El Kacimi,^{135c} M. Ellert,¹⁶⁶ S. Elles,⁵ F. Ellinghaus,¹⁷⁵ A. A. Elliot,¹⁶⁹ N. Ellis,³⁰ J. Elmsheuser,¹⁰⁰ M. Elsing,³⁰ D. Emeliyanov,¹³¹ Y. Enari,¹⁵⁵ O. C. Endner,⁸³ M. Endo,¹¹⁸ J. Erdmann,⁴³ A. Ereditato,¹⁷ G. Ernis,¹⁷⁵ J. Ernst,² M. Ernst,²⁵ S. Errede,¹⁶⁵ E. Ertel,⁸³ M. Escalier,¹¹⁷ H. Esch,⁴³ C. Escobar,¹²⁵ B. Esposito,⁴⁷ A. I. Etienvre,¹³⁶ E. Etzion,¹⁵³ H. Evans,⁶¹ A. Ezhilov,¹²³ L. Fabbri,^{20a,20b} G. Facini,³¹ R. M. Fakhruddinov,¹³⁰ S. Falciano,^{132a} R. J. Falla,⁷⁸ J. Faltova,¹²⁹ Y. Fang,^{33a} M. Fanti,^{91a,91b} A. Farbin,⁸ A. Farilla,^{134a} T. Farooque,¹² S. Farrell,¹⁵ S. M. Farrington,¹⁷⁰ P. Farthouat,³⁰ F. Fassi,^{135e} P. Fassnacht,³⁰ D. Fassouliotis,⁹ M. Fauci Giannelli,⁷⁷ A. Favareto,^{50a,50b}

L. Fayard,¹¹⁷ O. L. Fedin,^{123,m} W. Fedorko,¹⁶⁸ S. Feigl,³⁰ L. Feligioni,⁸⁵ C. Feng,^{33d} E. J. Feng,³⁰ H. Feng,⁸⁹ A. B. Fenyuk,¹³⁰ L. Feremenga,⁸ P. Fernandez Martinez,¹⁶⁷ S. Fernandez Perez,³⁰ J. Ferrando,⁵³ A. Ferrari,¹⁶⁶ P. Ferrari,¹⁰⁷ R. Ferrari,^{121a} D. E. Ferreira de Lima,⁵³ A. Ferrer,¹⁶⁷ D. Ferrere,⁴⁹ C. Ferretti,⁸⁹ A. Ferretto Parodi,^{50a,50b} M. Fiascaris,³¹ F. Fiedler,⁸³ A. Filipčič,⁷⁵ M. Filipuzzi,⁴² F. Filthaut,¹⁰⁶ M. Fincke-Keeler,¹⁶⁹ K. D. Finelli,¹⁵⁰ M. C. N. Fiolhais,^{126a,126c} L. Fiorini,¹⁶⁷ A. Firan,⁴⁰ A. Fischer,² C. Fischer,¹² J. Fischer,¹⁷⁵ W. C. Fisher,⁹⁰ N. Flaschel,⁴² I. Fleck,¹⁴¹ P. Fleischmann,⁸⁹ G. T. Fletcher,¹³⁹ G. Fletcher,⁷⁶ R. R. M. Fletcher,¹²² T. Flick,¹⁷⁵ A. Floderus,⁸¹ L. R. Flores Castillo,^{60a} M. J. Flowerdew,¹⁰¹ A. Formica,¹³⁶ A. Forti,⁸⁴ D. Fournier,¹¹⁷ H. Fox,⁷² S. Fracchia,¹² P. Francavilla,⁸⁰ M. Franchini,^{20a,20b} D. Francis,³⁰ L. Franconi,¹¹⁹ M. Franklin,⁵⁷ M. Frate,¹⁶³ M. Fraternali,^{121a,121b} D. Freeborn,⁷⁸ S. T. French,²⁸ F. Friedrich,⁴⁴ D. Froidevaux,³⁰ J. A. Frost,¹²⁰ C. Fukunaga,¹⁵⁶ E. Fullana Torregrosa,⁸³ B. G. Fulsom,¹⁴³ T. Fusayasu,¹⁰² J. Fuster,¹⁶⁷ C. Gabaldon,⁵⁵ O. Gabizon,¹⁷⁵ A. Gabrielli,^{20a,20b} A. Gabrielli,¹⁵ G. P. Gach,¹⁸ S. Gadatsch,³⁰ S. Gadomski,⁴⁹ G. Gagliardi,^{50a,50b} P. Gagnon,⁶¹ C. Galea,¹⁰⁶ B. Galhardo,^{126a,126c} E. J. Gallas,¹²⁰ B. J. Gallop,¹³¹ P. Gallus,¹²⁸ G. Galster,³⁶ K. K. Gan,¹¹¹ J. Gao,^{33b,85} Y. Gao,⁴⁶ Y. S. Gao,^{143,e} F. M. Garay Walls,⁴⁶ F. Garberson,¹⁷⁶ C. García,¹⁶⁷ J. E. García Navarro,¹⁶⁷ M. Garcia-Sciveres,¹⁵ R. W. Gardner,³¹ N. Garelli,¹⁴³ V. Garonne,¹¹⁹ C. Gatti,⁴⁷ A. Gaudiello,^{50a,50b} G. Gaudio,^{121a} B. Gaur,¹⁴¹ L. Gauthier,⁹⁵ P. Gauzzi,^{132a,132b} I. L. Gavrilenko,⁹⁶ C. Gay,¹⁶⁸ G. Gaycken,²¹ E. N. Gazis,¹⁰ P. Ge,^{33d} Z. Gecse,¹⁶⁸ C. N. P. Gee,¹³¹ Ch. Geich-Gimbel,²¹ M. P. Geisler,^{58a} C. Gemme,^{50a} M. H. Genest,⁵⁵ S. Gentile,^{132a,132b} M. George,⁵⁴ S. George,⁷⁷ D. Gerbaudo,¹⁶³ A. Gershon,¹⁵³ S. Ghasemi,¹⁴¹ H. Ghazlane,^{135b} B. Giacobbe,^{20a} S. Giagu,^{132a,132b} V. Giangiobbe,¹² P. Giannetti,^{124a,124b} B. Gibbard,²⁵ S. M. Gibson,⁷⁷ M. Gignac,¹⁶⁸ M. Gilchriese,¹⁵ T. P. S. Gillam,²⁸ D. Gillberg,³⁰ G. Gilles,³⁴ D. M. Gingrich,^{3,d} N. Giokaris,⁹ M. P. Giordani,^{164a,164c} F. M. Giorgi,^{20a} F. M. Giorgi,¹⁶ P. F. Giraud,¹³⁶ P. Giromini,⁴⁷ D. Giugni,^{91a} C. Giuliani,⁴⁸ M. Giulini,^{58b} B. K. Gjelsten,¹¹⁹ S. Gkaitatzis,¹⁵⁴ I. Gkialas,¹⁵⁴ E. L. Gkougkousis,¹¹⁷ L. K. Gladilin,⁹⁹ C. Glasman,⁸² J. Glatzer,³⁰ P. C. F. Glaysher,⁴⁶ A. Glazov,⁴² M. Goblirsch-Kolb,¹⁰¹ J. R. Goddard,⁷⁶ J. Godlewski,³⁹ S. Goldfarb,⁸⁹ T. Golling,⁴⁹ D. Golubkov,¹³⁰ A. Gomes,^{126a,126b,126d} R. Gonçalves,^{126a} J. Goncalves Pinto Firmino Da Costa,¹³⁶ L. Gonella,²¹ S. González de la Hoz,¹⁶⁷ G. Gonzalez Parra,¹² S. Gonzalez-Sevilla,⁴⁹ L. Goossens,³⁰ P. A. Gorbounov,⁹⁷ H. A. Gordon,²⁵ I. Gorelov,¹⁰⁵ B. Gorini,³⁰ E. Gorini,^{73a,73b} A. Gorišek,⁷⁵ E. Gornicki,³⁹ A. T. Goshaw,⁴⁵ C. Gössling,⁴³ M. I. Gostkin,⁶⁵ D. Goujdami,^{135c} A. G. Goussiou,¹³⁸ N. Govender,^{145b} E. Gozani,¹⁵² H. M. X. Grabas,¹³⁷ L. Graber,⁵⁴ I. Grabowska-Bold,^{38a} P. O. J. Gradin,¹⁶⁶ P. Grafström,^{20a,20b} K.-J. Grahn,⁴² J. Gramling,⁴⁹ E. Gramstad,¹¹⁹ S. Grancagnolo,¹⁶ V. Gratchev,¹²³ H. M. Gray,³⁰ E. Graziani,^{134a} Z. D. Greenwood,^{79,n} C. Grefe,²¹ K. Gregersen,⁷⁸ I. M. Gregor,⁴² P. Grenier,¹⁴³ J. Griffiths,⁸ A. A. Grillo,¹³⁷ K. Grimm,⁷² S. Grinstein,^{12,o} Ph. Gris,³⁴ J.-F. Grivaz,¹¹⁷ J. P. Grohs,⁴⁴ A. Grohsjean,⁴² E. Gross,¹⁷² J. Grosse-Knetter,⁵⁴ G. C. Grossi,⁷⁹ Z. J. Grout,¹⁴⁹ L. Guan,⁸⁹ J. Guenther,¹²⁸ F. Guescini,⁴⁹ D. Guest,¹⁷⁶ O. Gueta,¹⁵³ E. Guido,^{50a,50b} T. Guillemin,¹¹⁷ S. Guindon,² U. Gul,⁵³ C. Gumpert,⁴⁴ J. Guo,^{33e} Y. Guo,^{33b,p} S. Gupta,¹²⁰ G. Gustavino,^{132a,132b} P. Gutierrez,¹¹³ N. G. Gutierrez Ortiz,⁷⁸ C. Gutsche,⁴⁴ C. Guyot,¹³⁶ C. Gwenlan,¹²⁰ C. B. Gwilliam,⁷⁴ A. Haas,¹¹⁰ C. Haber,¹⁵ H. K. Hadavand,⁸ N. Haddad,^{135e} P. Haefner,²¹ S. Hageböck,²¹ Z. Hajduk,³⁹ H. Hakobyan,¹⁷⁷ M. Haleem,⁴² J. Haley,¹¹⁴ D. Hall,¹²⁰ G. Halladjian,⁹⁰ G. D. Hallewell,⁸⁵ K. Hamacher,¹⁷⁵ P. Hamal,¹¹⁵ K. Hamano,¹⁶⁹ A. Hamilton,^{145a} G. N. Hamity,¹³⁹ P. G. Hamnett,⁴² L. Han,^{33b} K. Hanagaki,^{66,q} K. Hanawa,¹⁵⁵ M. Hance,¹³⁷ B. Haney,¹²² P. Hanke,^{58a} R. Hanna,¹³⁶ J. B. Hansen,³⁶ J. D. Hansen,³⁶ M. C. Hansen,²¹ P. H. Hansen,³⁶ K. Hara,¹⁶⁰ A. S. Hard,¹⁷³ T. Harenberg,¹⁷⁵ F. Hariri,¹¹⁷ S. Harkusha,⁹² R. D. Harrington,⁴⁶ P. F. Harrison,¹⁷⁰ F. Hartjes,¹⁰⁷ M. Hasegawa,⁶⁷ Y. Hasegawa,¹⁴⁰ A. Hasib,¹¹³ S. Hassani,¹³⁶ S. Haug,¹⁷ R. Hauser,⁹⁰ L. Hauswald,⁴⁴ M. Havranek,¹²⁷ C. M. Hawkes,¹⁸ R. J. Hawkings,³⁰ A. D. Hawkins,⁸¹ T. Hayashi,¹⁶⁰ D. Hayden,⁹⁰ C. P. Hays,¹²⁰ J. M. Hays,⁷⁶ H. S. Hayward,⁷⁴ S. J. Haywood,¹³¹ S. J. Head,¹⁸ T. Heck,⁸³ V. Hedberg,⁸¹ L. Heelan,⁸ S. Heim,¹²² T. Heim,¹⁷⁵ B. Heinemann,¹⁵ L. Heinrich,¹¹⁰ J. Hejbal,¹²⁷ L. Helary,²² S. Hellman,^{146a,146b} D. Hellmich,²¹ C. Hensens,¹² J. Henderson,¹²⁰ R. C. W. Henderson,⁷² Y. Heng,¹⁷³ C. Hengler,⁴² S. Henkelmann,¹⁶⁸ A. Henrichs,¹⁷⁶ A. M. Henriques Correia,³⁰ S. Henrot-Versille,¹¹⁷ G. H. Herbert,¹⁶ Y. Hernández Jiménez,¹⁶⁷ G. Herten,⁴⁸ R. Hertenberger,¹⁰⁰ L. Hervas,³⁰ G. G. Hesketh,⁷⁸ N. P. Hessey,¹⁰⁷ J. W. Hetherly,⁴⁰ R. Hickling,⁷⁶ E. Higón-Rodríguez,¹⁶⁷ E. Hill,¹⁶⁹ J. C. Hill,²⁸ K. H. Hiller,⁴² S. J. Hillier,¹⁸ I. Hinchliffe,¹⁵ E. Hines,¹²² R. R. Hinman,¹⁵ M. Hirose,¹⁵⁷ D. Hirschbuehl,¹⁷⁵ J. Hobbs,¹⁴⁸ N. Hod,¹⁰⁷ M. C. Hodgkinson,¹³⁹ P. Hodgson,¹³⁹ A. Hoecker,³⁰ M. R. Hoferkamp,¹⁰⁵ F. Hoenig,¹⁰⁰ M. Hohlfeld,⁸³ D. Hohn,²¹ T. R. Holmes,¹⁵ M. Homann,⁴³ T. M. Hong,¹²⁵ W. H. Hopkins,¹¹⁶ Y. Horii,¹⁰³ A. J. Horton,¹⁴² J.-Y. Hostachy,⁵⁵ S. Hou,¹⁵¹ A. Hoummada,^{135a} J. Howard,¹²⁰ J. Howarth,⁴² M. Hrabovsky,¹¹⁵ I. Hristova,¹⁶ J. Hrivnac,¹¹⁷ T. Hryn'ova,⁵ A. Hrynevich,⁹³ C. Hsu,^{145c} P. J. Hsu,^{151,r} S.-C. Hsu,¹³⁸ D. Hu,³⁵ Q. Hu,^{33b} X. Hu,⁸⁹ Y. Huang,⁴² Z. Hubacek,¹²⁸ F. Hubaut,⁸⁵ F. Huegging,²¹ T. B. Huffman,¹²⁰ E. W. Hughes,³⁵ G. Hughes,⁷² M. Huhtinen,³⁰ T. A. Hülsing,⁸³ N. Huseynov,^{65,b}

J. Huston,⁹⁰ J. Huth,⁵⁷ G. Iacobucci,⁴⁹ G. Iakovidis,²⁵ I. Ibragimov,¹⁴¹ L. Iconomidou-Fayard,¹¹⁷ E. Ideal,¹⁷⁶ Z. Idrissi,^{135e} P. Iengo,³⁰ O. Igonkina,¹⁰⁷ T. Iizawa,¹⁷¹ Y. Ikegami,⁶⁶ K. Ikematsu,¹⁴¹ M. Ikeno,⁶⁶ Y. Ilchenko,^{31,s} D. Iliadis,¹⁵⁴ N. Ilic,¹⁴³ T. Ince,¹⁰¹ G. Introzzi,^{121a,121b} P. Ioannou,⁹ M. Iodice,^{134a} K. Iordanidou,³⁵ V. Ippolito,⁵⁷ A. Irlles Quiles,¹⁶⁷ C. Isaksson,¹⁶⁶ M. Ishino,⁶⁸ M. Ishitsuka,¹⁵⁷ R. Ishmukhametov,¹¹¹ C. Issever,¹²⁰ S. Istin,^{19a} J. M. Iturbe Ponce,⁸⁴ R. Iuppa,^{133a,133b} J. Ivarsson,⁸¹ W. Iwanski,³⁹ H. Iwasaki,⁶⁶ J. M. Izen,⁴¹ V. Izzo,^{104a} S. Jabbar,³ B. Jackson,¹²² M. Jackson,⁷⁴ P. Jackson,¹ M. R. Jaekel,³⁰ V. Jain,² K. Jakobs,⁴⁸ S. Jakobsen,³⁰ T. Jakoubek,¹²⁷ J. Jakubek,¹²⁸ D. O. Jamin,¹¹⁴ D. K. Jana,⁷⁹ E. Jansen,⁷⁸ R. Jansky,⁶² J. Janssen,²¹ M. Janus,⁵⁴ G. Jarlskog,⁸¹ N. Javadov,^{65,b} T. Javůrek,⁴⁸ L. Jeanty,¹⁵ J. Jejelava,^{51a,t} G.-Y. Jeng,¹⁵⁰ D. Jennens,⁸⁸ P. Jenni,^{48,u} J. Jentzsch,⁴³ C. Jeske,¹⁷⁰ S. Jézéquel,⁵ H. Ji,¹⁷³ J. Jia,¹⁴⁸ Y. Jiang,^{33b} S. Jiggins,⁷⁸ J. Jimenez Pena,¹⁶⁷ S. Jin,^{33a} A. Jinaru,^{26b} O. Jinnouchi,¹⁵⁷ M. D. Joergensen,³⁶ P. Johansson,¹³⁹ K. A. Johns,⁷ W. J. Johnson,¹³⁸ K. Jon-And,^{146a,146b} G. Jones,¹⁷⁰ R. W. L. Jones,⁷² T. J. Jones,⁷⁴ J. Jongmanns,^{58a} P. M. Jorge,^{126a,126b} K. D. Joshi,⁸⁴ J. Jovicevic,^{159a} X. Ju,¹⁷³ P. Jussel,⁶² A. Juste Rozas,^{12,o} M. Kaci,¹⁶⁷ A. Kaczmarek,³⁹ M. Kado,¹¹⁷ H. Kagan,¹¹¹ M. Kagan,¹⁴³ S. J. Kahn,⁸⁵ E. Kajomovitz,⁴⁵ C. W. Kalderon,¹²⁰ S. Kama,⁴⁰ A. Kamenshchikov,¹³⁰ N. Kanaya,¹⁵⁵ S. Kaneti,²⁸ V. A. Kantserov,⁹⁸ J. Kanzaki,⁶⁶ B. Kaplan,¹¹⁰ L. S. Kaplan,¹⁷³ A. Kapliy,³¹ D. Kar,^{145c} K. Karakostas,¹⁰ A. Karamaoun,³ N. Karastathis,^{10,107} M. J. Kareem,⁵⁴ E. Karentzos,¹⁰ M. Karnevskiy,⁸³ S. N. Karpov,⁶⁵ Z. M. Karpova,⁶⁵ K. Karthik,¹¹⁰ V. Kartvelishvili,⁷² A. N. Karyukhin,¹³⁰ K. Kasahara,¹⁶⁰ L. Kashif,¹⁷³ R. D. Kass,¹¹¹ A. Kastanas,¹⁴ Y. Kataoka,¹⁵⁵ C. Kato,¹⁵⁵ A. Katre,⁴⁹ J. Katzy,⁴² K. Kawade,¹⁰³ K. Kawagoe,⁷⁰ T. Kawamoto,¹⁵⁵ G. Kawamura,⁵⁴ S. Kazama,¹⁵⁵ V. F. Kazanin,^{109,c} R. Keeler,¹⁶⁹ R. Kehoe,⁴⁰ J. S. Keller,⁴² J. J. Kempster,⁷⁷ H. Keoshkerian,⁸⁴ O. Kepka,¹²⁷ B. P. Kerševan,⁷⁵ S. Kersten,¹⁷⁵ R. A. Keyes,⁸⁷ F. Khalil-zada,¹¹ H. Khandanyan,^{146a,146b} A. Khanov,¹¹⁴ A. G. Kharlamov,^{109,c} T. J. Khoo,²⁸ V. Khovanskiy,⁹⁷ E. Khramov,⁶⁵ J. Khubua,^{51b,v} S. Kido,⁶⁷ H. Y. Kim,⁸ S. H. Kim,¹⁶⁰ Y. K. Kim,³¹ N. Kimura,¹⁵⁴ O. M. Kind,¹⁶ B. T. King,⁷⁴ M. King,¹⁶⁷ S. B. King,¹⁶⁸ J. Kirk,¹³¹ A. E. Kiryunin,¹⁰¹ T. Kishimoto,⁶⁷ D. Kisielewska,^{38a} F. Kiss,⁴⁸ K. Kiuchi,¹⁶⁰ O. Kivernyk,¹³⁶ E. Kladiva,^{144b} M. H. Klein,³⁵ M. Klein,⁷⁴ U. Klein,⁷⁴ K. Kleinknecht,⁸³ P. Klimek,^{146a,146b} A. Klimentov,²⁵ R. Klingenberg,⁴³ J. A. Klinger,¹³⁹ T. Klioutchnikova,³⁰ E.-E. Kluge,^{58a} P. Kluit,¹⁰⁷ S. Kluth,¹⁰¹ J. Knapik,³⁹ E. Kneringer,⁶² E. B. F. G. Knoops,⁸⁵ A. Knue,⁵³ A. Kobayashi,¹⁵⁵ D. Kobayashi,¹⁵⁷ T. Kobayashi,¹⁵⁵ M. Kobel,⁴⁴ M. Kocian,¹⁴³ P. Kodys,¹²⁹ T. Koffas,²⁹ E. Koffeman,¹⁰⁷ L. A. Kogan,¹²⁰ S. Kohlmann,¹⁷⁵ Z. Kohout,¹²⁸ T. Kohriki,⁶⁶ T. Koi,¹⁴³ H. Kolanoski,¹⁶ M. Kolb,^{58b} I. Koletsou,⁵ A. A. Komar,^{96†} Y. Komori,¹⁵⁵ T. Kondo,⁶⁶ N. Kondrashova,⁴² K. Köneke,⁴⁸ A. C. König,¹⁰⁶ T. Kono,⁶⁶ R. Konoplich,^{110,w} N. Konstantinidis,⁷⁸ R. Kopeliansky,¹⁵² S. Koperny,^{38a} L. Köpke,⁸³ A. K. Kopp,⁴⁸ K. Korcyl,³⁹ K. Kordas,¹⁵⁴ A. Korn,⁷⁸ A. A. Korol,^{109,c} I. Korolkov,¹² E. V. Korolkova,¹³⁹ O. Kortner,¹⁰¹ S. Kortner,¹⁰¹ T. Kosek,¹²⁹ V. V. Kostyukhin,²¹ V. M. Kotov,⁶⁵ A. Kotwal,⁴⁵ A. Kourkoumeli-Charalampidi,¹⁵⁴ C. Kourkoumelis,⁹ V. Kouskoura,²⁵ A. Koutsman,^{159a} R. Kowalewski,¹⁶⁹ T. Z. Kowalski,^{38a} W. Kozanecki,¹³⁶ A. S. Kozhin,¹³⁰ V. A. Kramarenko,⁹⁹ G. Kramberger,⁷⁵ D. Krasnopevtsev,⁹⁸ M. W. Krasny,⁸⁰ A. Krasznahorkay,³⁰ J. K. Kraus,²¹ A. Kravchenko,²⁵ S. Kreiss,¹¹⁰ M. Kretz,^{58c} J. Kretzschmar,⁷⁴ K. Kreutzfeldt,⁵² P. Krieger,¹⁵⁸ K. Krizka,³¹ K. Kroeninger,⁴³ H. Kroha,¹⁰¹ J. Kroll,¹²² J. Kroseberg,²¹ J. Krstic,¹³ U. Kruchonak,⁶⁵ H. Krüger,²¹ N. Krumnack,⁶⁴ A. Kruse,¹⁷³ M. C. Kruse,⁴⁵ M. Kruskal,²² T. Kubota,⁸⁸ H. Kucuk,⁷⁸ S. Kudah,^{4b} S. Kuehn,⁴⁸ A. Kugel,^{58c} F. Kuger,¹⁷⁴ A. Kuhl,¹³⁷ T. Kuhl,⁴² V. Kukhtin,⁶⁵ R. Kukla,¹³⁶ Y. Kulchitsky,⁹² S. Kuleshov,^{32b} M. Kuna,^{132a,132b} T. Kunigo,⁶⁸ A. Kupco,¹²⁷ H. Kurashige,⁶⁷ Y. A. Kurochkin,⁹² V. Kus,¹²⁷ E. S. Kuwertz,¹⁶⁹ M. Kuze,¹⁵⁷ J. Kvita,¹¹⁵ T. Kwan,¹⁶⁹ D. Kyriazopoulos,¹³⁹ A. La Rosa,¹³⁷ J. L. La Rosa Navarro,^{24d} L. La Rotonda,^{37a,37b} C. Lacasta,¹⁶⁷ F. Lacava,^{132a,132b} J. Lacey,²⁹ H. Lacker,¹⁶ D. Lacour,⁸⁰ V. R. Lacuesta,¹⁶⁷ E. Ladygin,⁶⁵ R. Lafaye,⁵ B. Laforge,⁸⁰ T. Lagouri,¹⁷⁶ S. Lai,⁵⁴ L. Lambourne,⁷⁸ S. Lammers,⁶¹ C. L. Lampen,⁷ W. Lampl,⁷ E. Lançon,¹³⁶ U. Landgraf,⁴⁸ M. P. J. Landon,⁷⁶ V. S. Lang,^{58a} J. C. Lange,¹² A. J. Lankford,¹⁶³ F. Lanni,²⁵ K. Lantzsch,²¹ A. Lanza,^{121a} S. Laplace,⁸⁰ C. Lapoire,³⁰ J. F. Laporte,¹³⁶ T. Lari,^{91a} F. Lasagni Manghi,^{20a,20b} M. Lassnig,³⁰ P. Laurelli,⁴⁷ W. Lavrijsen,¹⁵ A. T. Law,¹³⁷ P. Laycock,⁷⁴ T. Lazovich,⁵⁷ O. Le Dortz,⁸⁰ E. Le Guirriec,⁸⁵ E. Le Menedeu,¹² M. LeBlanc,¹⁶⁹ T. LeCompte,⁶ F. Ledroit-Guillon,⁵⁵ C. A. Lee,^{145a} S. C. Lee,¹⁵¹ L. Lee,¹ G. Lefebvre,⁸⁰ M. Lefebvre,¹⁶⁹ F. Legger,¹⁰⁰ C. Leggett,¹⁵ A. Lehan,⁷⁴ G. Lehmann Miotto,³⁰ X. Lei,⁷ W. A. Leight,²⁹ A. Leisos,^{154,x} A. G. Leister,¹⁷⁶ M. A. L. Leite,^{24d} R. Leitner,¹²⁹ D. Lellouch,¹⁷² B. Lemmer,⁵⁴ K. J. C. Leney,⁷⁸ T. Lenz,²¹ B. Lenzi,³⁰ R. Leone,⁷ S. Leone,^{124a,124b} C. Leonidopoulos,⁴⁶ S. Leontsinis,¹⁰ C. Leroy,⁹⁵ C. G. Lester,²⁸ M. Levchenko,¹²³ J. Levêque,⁵ D. Levin,⁸⁹ L. J. Levinson,¹⁷² M. Levy,¹⁸ A. Lewis,¹²⁰ A. M. Leyko,²¹ M. Leyton,⁴¹ B. Li,^{33b,y} H. Li,¹⁴⁸ H. L. Li,³¹ L. Li,⁴⁵ L. Li,^{33e} S. Li,⁴⁵ X. Li,⁸⁴ Y. Li,^{33c,z} Z. Liang,¹³⁷ H. Liao,³⁴ B. Liberti,^{133a} A. Liblong,¹⁵⁸ P. Lichard,³⁰ K. Lie,¹⁶⁵ J. Liebal,²¹ W. Liebig,¹⁴ C. Limbach,²¹ A. Limosani,¹⁵⁰ S. C. Lin,^{151,aa} T. H. Lin,⁸³ F. Linde,¹⁰⁷ B. E. Lindquist,¹⁴⁸ J. T. Linnemann,⁹⁰ E. Lipeles,¹²² A. Lipniacka,¹⁴ M. Lisovsky,^{58b} T. M. Liss,¹⁶⁵ D. Lissauer,²⁵ A. Lister,¹⁶⁸ A. M. Litke,¹³⁷ B. Liu,^{151,bb} D. Liu,¹⁵¹ H. Liu,⁸⁹ J. Liu,⁸⁵ J. B. Liu,^{33b}

K. Liu,⁸⁵ L. Liu,¹⁶⁵ M. Liu,⁴⁵ M. Liu,^{33b} Y. Liu,^{33b} M. Livan,^{121a,121b} A. Lleres,⁵⁵ J. Llorente Merino,⁸² S. L. Lloyd,⁷⁶
 F. Lo Sterzo,¹⁵¹ E. Lobodzinska,⁴² P. Loch,⁷ W. S. Lockman,¹³⁷ F. K. Loebinger,⁸⁴ A. E. Loevschall-Jensen,³⁶ K. M. Loew,²³
 A. Loginov,¹⁷⁶ T. Lohse,¹⁶ K. Lohwasser,⁴² M. Lokajicek,¹²⁷ B. A. Long,²² J. D. Long,¹⁶⁵ R. E. Long,⁷² K. A.Looper,¹¹¹
 L. Lopes,^{126a} D. Lopez Mateos,⁵⁷ B. Lopez Paredes,¹³⁹ I. Lopez Paz,¹² J. Lorenz,¹⁰⁰ N. Lorenzo Martinez,⁶¹ M. Losada,¹⁶²
 P. J. Lösel,¹⁰⁰ X. Lou,^{33a} A. Lounis,¹¹⁷ J. Love,⁶ P. A. Love,⁷² N. Lu,⁸⁹ H. J. Lubatti,¹³⁸ C. Luci,^{132a,132b} A. Lucotte,⁵⁵
 C. Luedtke,⁴⁸ F. Luehring,⁶¹ W. Lukas,⁶² L. Luminari,^{132a} O. Lundberg,^{146a,146b} B. Lund-Jensen,¹⁴⁷ D. Lynn,²⁵ R. Lysak,¹²⁷
 E. Lytken,⁸¹ H. Ma,²⁵ L. L. Ma,^{33d} G. Maccarrone,⁴⁷ A. Macchiolo,¹⁰¹ C. M. Macdonald,¹³⁹ B. Maček,⁷⁵
 J. Machado Miguens,^{122,126b} D. Macina,³⁰ D. Madaffari,⁸⁵ R. Madar,³⁴ H. J. Maddocks,⁷² W. F. Mader,⁴⁴ A. Madsen,¹⁶⁶
 J. Maeda,⁶⁷ S. Maeland,¹⁴ T. Maeno,²⁵ A. Maevskiy,⁹⁹ E. Magradze,⁵⁴ K. Mahboubi,⁴⁸ J. Mahlstedt,¹⁰⁷ C. Maiani,¹³⁶
 C. Maidantchik,^{24a} A. A. Maier,¹⁰¹ T. Maier,¹⁰⁰ A. Maio,^{126a,126b,126d} S. Majewski,¹¹⁶ Y. Makida,⁶⁶ N. Makovec,¹¹⁷
 B. Malaescu,⁸⁰ Pa. Malecki,³⁹ V. P. Maleev,¹²³ F. Malek,⁵⁵ U. Mallik,⁶³ D. Malon,⁶ C. Malone,¹⁴³ S. Maltezos,¹⁰
 V. M. Malyshev,¹⁰⁹ S. Malyukov,³⁰ J. Mamuzic,⁴² G. Mancini,⁴⁷ B. Mandelli,³⁰ L. Mandelli,^{91a} I. Mandić,⁷⁵ R. Mandrysch,⁶³
 J. Maneira,^{126a,126b} A. Manfredini,¹⁰¹ L. Manhaes de Andrade Filho,^{24b} J. Manjarres Ramos,^{159b} A. Mann,¹⁰⁰
 A. Manousakis-Katsikakis,⁹ B. Mansoulie,¹³⁶ R. Mantifel,⁸⁷ M. Mantoani,⁵⁴ L. Mapelli,³⁰ L. March,^{145c} G. Marchiori,⁸⁰
 M. Marcisovsky,¹²⁷ C. P. Marino,¹⁶⁹ M. Marjanovic,¹³ D. E. Marley,⁸⁹ F. Marroquim,^{24a} S. P. Marsden,⁸⁴ Z. Marshall,¹⁵
 L. F. Marti,¹⁷ S. Marti-Garcia,¹⁶⁷ B. Martin,⁹⁰ T. A. Martin,¹⁷⁰ V. J. Martin,⁴⁶ B. Martin dit Latour,¹⁴ M. Martinez,^{12,o}
 S. Martin-Haugh,¹³¹ V. S. Martoiu,^{26b} A. C. Martyniuk,⁷⁸ M. Marx,¹³⁸ F. Marzano,^{132a} A. Marzin,³⁰ L. Masetti,⁸³
 T. Mashimo,¹⁵⁵ R. Mashinistov,⁹⁶ J. Masik,⁸⁴ A. L. Maslennikov,^{109,c} I. Massa,^{20a,20b} L. Massa,^{20a,20b} P. Mastrandrea,⁵
 A. Mastroberardino,^{37a,37b} T. Masubuchi,¹⁵⁵ P. Mättig,¹⁷⁵ J. Mattmann,⁸³ J. Maurer,^{26b} S. J. Maxfield,⁷⁴ D. A. Maximov,^{109,c}
 R. Mazini,¹⁵¹ S. M. Mazza,^{91a,91b} G. Mc Goldrick,¹⁵⁸ S. P. Mc Kee,⁸⁹ A. McCarn,⁸⁹ R. L. McCarthy,¹⁴⁸ T. G. McCarthy,²⁹
 N. A. McCubbin,¹³¹ K. W. McFarlane,^{56†} J. A. Mcfayden,⁷⁸ G. Mchedlidze,⁵⁴ S. J. McMahon,¹³¹ R. A. McPherson,^{169,k}
 M. Medinnis,⁴² S. Meehan,^{145a} S. Mehlhase,¹⁰⁰ A. Mehta,⁷⁴ K. Meier,^{58a} C. Meineck,¹⁰⁰ B. Meirose,⁴¹
 B. R. Mellado Garcia,^{145c} F. Meloni,¹⁷ A. Mengarelli,^{20a,20b} S. Menke,¹⁰¹ E. Meoni,¹⁶¹ K. M. Mercurio,⁵⁷ S. Mergelmeyer,²¹
 P. Mermod,⁴⁹ L. Merola,^{104a,104b} C. Meroni,^{91a} F. S. Merritt,³¹ A. Messina,^{132a,132b} J. Metcalfe,²⁵ A. S. Mete,¹⁶³ C. Meyer,⁸³
 C. Meyer,¹²² J-P. Meyer,¹³⁶ J. Meyer,¹⁰⁷ H. Meyer Zu Theenhausen,^{58a} R. P. Middleton,¹³¹ S. Miglioranza,^{164a,164c}
 L. Mijović,²¹ G. Mikenberg,¹⁷² M. Mikestikova,¹²⁷ M. Mikuž,⁷⁵ M. Milesi,⁸⁸ A. Milic,³⁰ D. W. Miller,³¹ C. Mills,⁴⁶
 A. Milov,¹⁷² D. A. Milstead,^{146a,146b} A. A. Minaenko,¹³⁰ Y. Minami,¹⁵⁵ I. A. Minashvili,⁶⁵ A. I. Mincer,¹¹⁰ B. Mindur,^{38a}
 M. Mineev,⁶⁵ Y. Ming,¹⁷³ L. M. Mir,¹² K. P. Mistry,¹²² T. Mitani,¹⁷¹ J. Mitrevski,¹⁰⁰ V. A. Mitsou,¹⁶⁷ A. Miucci,⁴⁹
 P. S. Miyagawa,¹³⁹ J. U. Mjörnmark,⁸¹ T. Moa,^{146a,146b} K. Mochizuki,⁸⁵ S. Mohapatra,³⁵ W. Mohr,⁴⁸ S. Molander,^{146a,146b}
 R. Moles-Valls,²¹ R. Monden,⁶⁸ K. Mönig,⁴² C. Monini,⁵⁵ J. Monk,³⁶ E. Monnier,⁸⁵ A. Montalbano,¹⁴⁸
 J. Montejo Berlingen,¹² F. Monticelli,⁷¹ S. Monzani,^{132a,132b} R. W. Moore,³ N. Morange,¹¹⁷ D. Moreno,¹⁶²
 M. Moreno Llácer,⁵⁴ P. Morettini,^{50a} D. Mori,¹⁴² T. Mori,¹⁵⁵ M. Morii,⁵⁷ M. Morinaga,¹⁵⁵ V. Morisbak,¹¹⁹ S. Moritz,⁸³
 A. K. Morley,¹⁵⁰ G. Mornacchi,³⁰ J. D. Morris,⁷⁶ S. S. Mortensen,³⁶ A. Morton,⁵³ L. Morvaj,¹⁰³ M. Mosidze,^{51b} J. Moss,¹⁴³
 K. Motohashi,¹⁵⁷ R. Mount,¹⁴³ E. Mountricha,²⁵ S. V. Mouraviev,^{96†} E. J. W. Moyses,⁸⁶ S. Muanza,⁸⁵ R. D. Mudd,¹⁸
 F. Mueller,¹⁰¹ J. Mueller,¹²⁵ R. S. P. Mueller,¹⁰⁰ T. Mueller,²⁸ D. Muenstermann,⁴⁹ P. Mullen,⁵³ G. A. Mullier,¹⁷
 J. A. Murillo Quijada,¹⁸ W. J. Murray,^{170,131} H. Musheghyan,⁵⁴ E. Musto,¹⁵² A. G. Myagkov,^{130,cc} M. Myska,¹²⁸
 B. P. Nachman,¹⁴³ O. Nackenhorst,⁵⁴ J. Nadal,⁵⁴ K. Nagai,¹²⁰ R. Nagai,¹⁵⁷ Y. Nagai,⁸⁵ K. Nagano,⁶⁶ A. Nagarkar,¹¹¹
 Y. Nagasaka,⁵⁹ K. Nagata,¹⁶⁰ M. Nagel,¹⁰¹ E. Nagy,⁸⁵ A. M. Nairz,³⁰ Y. Nakahama,³⁰ K. Nakamura,⁶⁶ T. Nakamura,¹⁵⁵
 I. Nakano,¹¹² H. Namasivayam,⁴¹ R. F. Naranjo Garcia,⁴² R. Narayan,³¹ D. I. Narrias Villar,^{58a} T. Naumann,⁴² G. Navarro,¹⁶²
 R. Nayyar,⁷ H. A. Neal,⁸⁹ P. Yu. Nechaeva,⁹⁶ T. J. Neep,⁸⁴ P. D. Nef,¹⁴³ A. Negri,^{121a,121b} M. Negrini,^{20a} S. Nektarijevic,¹⁰⁶
 C. Nellist,¹¹⁷ A. Nelson,¹⁶³ S. Nemecek,¹²⁷ P. Nemethy,¹¹⁰ A. A. Nepomuceno,^{24a} M. Nessi,^{30,dd} M. S. Neubauer,¹⁶⁵
 M. Neumann,¹⁷⁵ R. M. Neves,¹¹⁰ P. Nevski,²⁵ P. R. Newman,¹⁸ D. H. Nguyen,⁶ R. B. Nickerson,¹²⁰ R. Nicolaidou,¹³⁶
 B. Nicquevert,³⁰ J. Nielsen,¹³⁷ N. Nikiforou,³⁵ A. Nikiforov,¹⁶ V. Nikolaenko,^{130,cc} I. Nikolic-Audit,⁸⁰ K. Nikolopoulos,¹⁸
 J. K. Nilsen,¹¹⁹ P. Nilsson,²⁵ Y. Ninomiya,¹⁵⁵ A. Nisati,^{132a} R. Nisius,¹⁰¹ T. Nobe,¹⁵⁵ M. Nomachi,¹¹⁸ I. Nomidis,²⁹
 T. Nooney,⁷⁶ S. Norberg,¹¹³ M. Nordberg,³⁰ O. Novgorodova,⁴⁴ S. Nowak,¹⁰¹ M. Nozaki,⁶⁶ L. Nozka,¹¹⁵ K. Ntekas,¹⁰
 G. Nunes Hanninger,⁸⁸ T. Nunnemann,¹⁰⁰ E. Nurse,⁷⁸ F. Nuti,⁸⁸ B. J. O'Brien,⁴⁶ F. O'grady,⁷ D. C. O'Neil,¹⁴² V. O'Shea,⁵³
 F. G. Oakham,^{29,d} H. Oberlack,¹⁰¹ T. Obermann,²¹ J. Ocariz,⁸⁰ A. Ochi,⁶⁷ I. Ochoa,³⁵ J. P. Ochoa-Ricoux,^{32a} S. Oda,⁷⁰
 S. Odaka,⁶⁶ H. Ogren,⁶¹ A. Oh,⁸⁴ S. H. Oh,⁴⁵ C. C. Ohm,¹⁵ H. Ohman,¹⁶⁶ H. Oide,³⁰ W. Okamura,¹¹⁸ H. Okawa,¹⁶⁰
 Y. Okumura,³¹ T. Okuyama,⁶⁶ A. Olariu,^{26b} S. A. Olivares Pino,⁴⁶ D. Oliveira Damazio,²⁵ A. Olszewski,³⁹ J. Olszowska,³⁹

A. Onofre,^{126a,126e} K. Onogi,¹⁰³ P. U. E. Onyisi,^{31,s} C. J. Oram,^{159a} M. J. Oreglia,³¹ Y. Oren,¹⁵³ D. Orestano,^{134a,134b}
N. Orlando,¹⁵⁴ C. Oropeza Barrera,⁵³ R. S. Orr,¹⁵⁸ B. Osculati,^{50a,50b} R. Ospanov,⁸⁴ G. Otero y Garzon,²⁷ H. Otono,⁷⁰
M. Ouchrif,^{135d} F. Ould-Saada,¹¹⁹ A. Ouraou,¹³⁶ K. P. Oussoren,¹⁰⁷ Q. Ouyang,^{33a} A. Ovcharova,¹⁵ M. Owen,⁵³
R. E. Owen,¹⁸ V. E. Ozcan,^{19a} N. Ozturk,⁸ K. Pachal,¹⁴² A. Pacheco Pages,¹² C. Padilla Aranda,¹² M. Pagáčová,⁴⁸
S. Pagan Griso,¹⁵ E. Paganis,¹³⁹ F. Paige,²⁵ P. Pais,⁸⁶ K. Pajchel,¹¹⁹ G. Palacino,^{159b} S. Palestini,³⁰ M. Palka,^{38b} D. Pallin,³⁴
A. Palma,^{126a,126b} Y. B. Pan,¹⁷³ E. Panagiotopoulou,¹⁰ C. E. Pandini,⁸⁰ J. G. Panduro Vazquez,⁷⁷ P. Pani,^{146a,146b} S. Panitkin,²⁵
D. Pantea,^{26b} L. Paolozzi,⁴⁹ Th.D. Papadopoulou,¹⁰ K. Papageorgiou,¹⁵⁴ A. Paramonov,⁶ D. Paredes Hernandez,¹⁵⁴
M. A. Parker,²⁸ K. A. Parker,¹³⁹ F. Parodi,^{50a,50b} J. A. Parsons,³⁵ U. Parzefall,⁴⁸ E. Pasqualucci,^{132a} S. Passaggio,^{50a}
F. Pastore,^{134a,134b†} Fr. Pastore,⁷⁷ G. Pásztor,²⁹ S. Patariaia,¹⁷⁵ N. D. Patel,¹⁵⁰ J. R. Pater,⁸⁴ T. Pauly,³⁰ J. Pearce,¹⁶⁹
B. Pearson,¹¹³ L. E. Pedersen,³⁶ M. Pedersen,¹¹⁹ S. Pedraza Lopez,¹⁶⁷ R. Pedro,^{126a,126b} S. V. Peleganchuk,^{109,c} D. Pelikan,¹⁶⁶
O. Penc,¹²⁷ C. Peng,^{33a} H. Peng,^{33b} B. Penning,³¹ J. Penwell,⁶¹ D. V. Perepelitsa,²⁵ E. Perez Codina,^{159a}
M. T. Pérez García-Estañ,¹⁶⁷ L. Perini,^{91a,91b} H. Pernegger,³⁰ S. Perrella,^{104a,104b} R. Peschke,⁴² V. D. Peshekhonov,⁶⁵
K. Peters,³⁰ R. F. Y. Peters,⁸⁴ B. A. Petersen,³⁰ T. C. Petersen,³⁶ E. Petit,⁴² A. Petridis,¹ C. Petridou,¹⁵⁴ P. Petroff,¹¹⁷
E. Petrolo,^{132a} F. Petrucci,^{134a,134b} N. E. Pettersson,¹⁵⁷ R. Pezoa,^{32b} P. W. Phillips,¹³¹ G. Piacquadio,¹⁴³ E. Pianori,¹⁷⁰
A. Picazio,⁴⁹ E. Piccaro,⁷⁶ M. Piccinini,^{20a,20b} M. A. Pickering,¹²⁰ R. Piegai,²⁷ D. T. Pignotti,¹¹¹ J. E. Pilcher,³¹
A. D. Pilkington,⁸⁴ A. W. J. Pin,⁸⁴ J. Pina,^{126a,126b,126d} M. Pinamonti,^{164a,164c,ee} J. L. Pinfold,³ A. Pingel,³⁶ S. Pires,⁸⁰
H. Pirumov,⁴² M. Pitt,¹⁷² C. Pizio,^{91a,91b} L. Plazak,^{144a} M.-A. Pleier,²⁵ V. Pleskot,¹²⁹ E. Plotnikova,⁶⁵ P. Plucinski,^{146a,146b}
D. Pluth,⁶⁴ R. Poettgen,^{146a,146b} L. Poggioli,¹¹⁷ D. Pohl,²¹ G. Polesello,^{121a} A. Poley,⁴² A. Policicchio,^{37a,37b} R. Polifka,¹⁵⁸
A. Polini,^{20a} C. S. Pollard,⁵³ V. Polychronakos,²⁵ K. Pommès,³⁰ L. Pontecorvo,^{132a} B. G. Pope,⁹⁰ G. A. Popeneciu,^{26c}
D. S. Popovic,¹³ A. Poppleton,³⁰ S. Pospisil,¹²⁸ K. Potamianos,¹⁵ I. N. Potrap,⁶⁵ C. J. Potter,¹⁴⁹ C. T. Potter,¹¹⁶ G. Poulard,³⁰
J. Poveda,³⁰ V. Pozdnyakov,⁶⁵ P. Pralavorio,⁸⁵ A. Pranko,¹⁵ S. Prasad,³⁰ S. Prell,⁶⁴ D. Price,⁸⁴ L. E. Price,⁶ M. Primavera,^{73a}
S. Prince,⁸⁷ M. Proissl,⁴⁶ K. Prokofiev,^{60c} F. Prokoshin,^{32b} E. Protopapadaki,¹³⁶ S. Protopopescu,²⁵ J. Proudfoot,⁶
M. Przybycien,^{38a} E. Ptacek,¹¹⁶ D. Puddu,^{134a,134b} E. Pueschel,⁸⁶ D. Poldon,¹⁴⁸ M. Purohit,^{25,ff} P. Puzo,¹¹⁷ J. Qian,⁸⁹ G. Qin,⁵³
Y. Qin,⁸⁴ A. Quadt,⁵⁴ D. R. Quarrie,¹⁵ W. B. Quayle,^{164a,164b} M. Queitsch-Maitland,⁸⁴ D. Quilty,⁵³ S. Raddum,¹¹⁹
V. Radeka,²⁵ V. Radescu,⁴² S. K. Radhakrishnan,¹⁴⁸ P. Radloff,¹¹⁶ P. Rados,⁸⁸ F. Ragusa,^{91a,91b} G. Rahal,¹⁷⁸ S. Rajagopalan,²⁵
M. Rammensee,³⁰ C. Rangel-Smith,¹⁶⁶ F. Rauscher,¹⁰⁰ S. Rave,⁸³ T. Ravenscroft,⁵³ M. Raymond,³⁰ A. L. Read,¹¹⁹
N. P. Readioff,⁷⁴ D. M. Rebuffi,^{121a,121b} A. Redelbach,¹⁷⁴ G. Redlinger,²⁵ R. Reece,¹³⁷ K. Reeves,⁴¹ L. Rehnisch,¹⁶
J. Reichert,¹²² H. Reisin,²⁷ C. Rembser,³⁰ H. Ren,^{33a} A. Renaud,¹¹⁷ M. Rescigno,^{132a} S. Resconi,^{91a} O. L. Rezanova,^{109,c}
P. Reznicek,¹²⁹ R. Rezvani,⁹⁵ R. Richter,¹⁰¹ S. Richter,⁷⁸ E. Richter-Was,^{38b} O. Ricken,²¹ M. Ridel,⁸⁰ P. Rieck,¹⁶
C. J. Riegel,¹⁷⁵ J. Rieger,⁵⁴ O. Rifki,¹¹³ M. Rijssenbeek,¹⁴⁸ A. Rimoldi,^{121a,121b} L. Rinaldi,^{20a} B. Ristić,⁴⁹ E. Ritsch,³⁰ I. Riu,¹²
F. Rizatdinova,¹¹⁴ E. Rizvi,⁷⁶ S. H. Robertson,^{87,k} A. Robichaud-Veronneau,⁸⁷ D. Robinson,²⁸ J. E. M. Robinson,⁴²
A. Robson,⁵³ C. Roda,^{124a,124b} S. Roe,³⁰ O. Røhne,¹¹⁹ S. Rolli,¹⁶¹ A. Romaniouk,⁹⁸ M. Romano,^{20a,20b} S. M. Romano Saez,³⁴
E. Romero Adam,¹⁶⁷ N. Rompotis,¹³⁸ M. Ronzani,⁴⁸ L. Roos,⁸⁰ E. Ros,¹⁶⁷ S. Rosati,^{132a} K. Rosbach,⁴⁸ P. Rose,¹³⁷
P. L. Rosendahl,¹⁴ O. Rosenthal,¹⁴¹ V. Rossetti,^{146a,146b} E. Rossi,^{104a,104b} L. P. Rossi,^{50a} J. H. N. Rosten,²⁸ R. Rosten,¹³⁸
M. Rotaru,^{26b} I. Roth,¹⁷² J. Rothberg,¹³⁸ D. Rousseau,¹¹⁷ C. R. Royon,¹³⁶ A. Rozanov,⁸⁵ Y. Rozen,¹⁵² X. Ruan,^{145c}
F. Rubbo,¹⁴³ I. Rubinskiy,⁴² V. I. Rud,⁹⁹ C. Rudolph,⁴⁴ M. S. Rudolph,¹⁵⁸ F. Rühr,⁴⁸ A. Ruiz-Martinez,³⁰ Z. Rurikova,⁴⁸
N. A. Rusakovich,⁶⁵ A. Ruschke,¹⁰⁰ H. L. Russell,¹³⁸ J. P. Rutherford,⁷ N. Ruthmann,³⁰ Y. F. Ryabov,¹²³ M. Rybar,¹⁶⁵
G. Rybkin,¹¹⁷ N. C. Ryder,¹²⁰ A. F. Saavedra,¹⁵⁰ G. Sabato,¹⁰⁷ S. Sacerdoti,²⁷ A. Saddique,³ H.F.-W. Sadrozinski,¹³⁷
R. Sadykov,⁶⁵ F. Safai Tehrani,^{132a} P. Saha,¹⁰⁸ M. Sahinsoy,^{58a} M. Saimpert,¹³⁶ T. Saito,¹⁵⁵ H. Sakamoto,¹⁵⁵ Y. Sakurai,¹⁷¹
G. Salamanna,^{134a,134b} A. Salamon,^{133a} J. E. Salazar Loyola,^{32b} M. Saleem,¹¹³ D. Salek,¹⁰⁷ P. H. Sales De Bruin,¹³⁸
D. Salihagic,¹⁰¹ A. Salnikov,¹⁴³ J. Salt,¹⁶⁷ D. Salvatore,^{37a,37b} F. Salvatore,¹⁴⁹ A. Salvucci,^{60a} A. Salzburger,³⁰ D. Sammel,⁴⁸
D. Sampsonidis,¹⁵⁴ A. Sanchez,^{104a,104b} J. Sánchez,¹⁶⁷ V. Sanchez Martinez,¹⁶⁷ H. Sandaker,¹¹⁹ R. L. Sandbach,⁷⁶
H. G. Sander,⁸³ M. P. Sanders,¹⁰⁰ M. Sandhoff,¹⁷⁵ C. Sandoval,¹⁶² R. Sandstroem,¹⁰¹ D. P. C. Sankey,¹³¹ M. Sannino,^{50a,50b}
A. Sansoni,⁴⁷ C. Santoni,³⁴ R. Santonico,^{133a,133b} H. Santos,^{126a} I. Santoyo Castillo,¹⁴⁹ K. Sapp,¹²⁵ A. Saponov,⁶⁵
J. G. Saraiva,^{126a,126d} B. Sarrazin,²¹ O. Sasaki,⁶⁶ Y. Sasaki,¹⁵⁵ K. Sato,¹⁶⁰ G. Sauvage,^{5†} E. Sauvan,⁵ G. Savage,⁷⁷
P. Savard,^{158,d} C. Sawyer,¹³¹ L. Sawyer,^{79,n} J. Saxon,³¹ C. Sbarra,^{20a} A. Sbrizzi,^{20a,20b} T. Scanlon,⁷⁸ D. A. Scannicchio,¹⁶³
M. Scarcella,¹⁵⁰ V. Scarfone,^{37a,37b} J. Schaarschmidt,¹⁷² P. Schacht,¹⁰¹ D. Schaefer,³⁰ R. Schaefer,⁴² J. Schaeffer,⁸³
S. Schaepe,²¹ S. Schaezel,^{58b} U. Schäfer,⁸³ A. C. Schaffer,¹¹⁷ D. Schaile,¹⁰⁰ R. D. Schamberger,¹⁴⁸ V. Scharf,^{58a}
V. A. Schegelsky,¹²³ D. Scheirich,¹²⁹ M. Schernau,¹⁶³ C. Schiavi,^{50a,50b} C. Schillo,⁴⁸ M. Schioppa,^{37a,37b} S. Schlenker,³⁰

K. Schmieden,³⁰ C. Schmitt,⁸³ S. Schmitt,^{58b} S. Schmitt,⁴² B. Schneider,^{159a} Y. J. Schnellbach,⁷⁴ U. Schnoor,⁴⁴ L. Schoeffel,¹³⁶ A. Schoening,^{58b} B. D. Schoenrock,⁹⁰ E. Schopf,²¹ A. L. S. Schorlemmer,⁵⁴ M. Schott,⁸³ D. Schouten,^{159a} J. Schovancova,⁸ S. Schramm,⁴⁹ M. Schreyer,¹⁷⁴ N. Schuh,⁸³ M. J. Schultens,²¹ H.-C. Schultz-Coulon,^{58a} H. Schulz,¹⁶ M. Schumacher,⁴⁸ B. A. Schumm,¹³⁷ Ph. Schune,¹³⁶ C. Schwanenberger,⁸⁴ M. Schwartz,⁵⁷ A. Schwartzman,¹⁴³ T. A. Schwarz,⁸⁹ Ph. Schwegler,¹⁰¹ H. Schweiger,⁸⁴ Ph. Schwemling,¹³⁶ R. Schwienhorst,⁹⁰ J. Schwindling,¹³⁶ T. Schwindt,²¹ F. G. Sciacca,¹⁷ E. Scifo,¹¹⁷ G. Sciolla,²³ F. Scuri,^{124a,124b} F. Scutti,²¹ J. Searcy,⁸⁹ G. Sedov,⁴² E. Sedykh,¹²³ P. Seema,²¹ S. C. Seidel,¹⁰⁵ A. Seiden,¹³⁷ F. Seifert,¹²⁸ J. M. Seixas,^{24a} G. Sekhniaidze,^{104a} K. Sekhon,⁸⁹ S. J. Sekula,⁴⁰ D. M. Seliverstov,^{123†} N. Semprini-Cesari,^{20a,20b} C. Serfon,³⁰ L. Serin,¹¹⁷ L. Serkin,^{164a,164b} T. Serre,⁸⁵ M. Sessa,^{134a,134b} R. Seuster,^{159a} H. Severini,¹¹³ T. Sfiligoj,⁷⁵ F. Sforza,³⁰ A. Sfyrta,³⁰ E. Shabalina,⁵⁴ M. Shamim,¹¹⁶ L. Y. Shan,^{33a} R. Shang,¹⁶⁵ J. T. Shank,²² M. Shapiro,¹⁵ P. B. Shatalov,⁹⁷ K. Shaw,^{164a,164b} S. M. Shaw,⁸⁴ A. Shcherbakova,^{146a,146b} C. Y. Shehu,¹⁴⁹ P. Sherwood,⁷⁸ L. Shi,^{151,gg} S. Shimizu,⁶⁷ C. O. Shimmin,¹⁶³ M. Shimojima,¹⁰² M. Shiyakova,⁶⁵ A. Shmeleva,⁹⁶ D. Shoaleh Saadi,⁹⁵ M. J. Shochet,³¹ S. Shojaii,^{91a,91b} S. Shrestha,¹¹¹ E. Shulga,⁹⁸ M. A. Shupe,⁷ S. Shushkevich,⁴² P. Sicho,¹²⁷ P. E. Sidebo,¹⁴⁷ O. Sidiropoulou,¹⁷⁴ D. Sidorov,¹¹⁴ A. Sidoti,^{20a,20b} F. Siegert,⁴⁴ Dj. Sijacki,¹³ J. Silva,^{126a,126d} Y. Silver,¹⁵³ S. B. Silverstein,^{146a} V. Simak,¹²⁸ O. Simard,⁵ Lj. Simic,¹³ S. Simion,¹¹⁷ E. Simioni,⁸³ B. Simmons,⁷⁸ D. Simon,³⁴ P. Sinervo,¹⁵⁸ N. B. Sinev,¹¹⁶ M. Sioli,^{20a,20b} G. Siragusa,¹⁷⁴ A. N. Sisakyan,^{65†} S. Yu. Sivoklov,⁹⁹ J. Sjölin,^{146a,146b} T. B. Sjursen,¹⁴ M. B. Skinner,⁷² H. P. Skottowe,⁵⁷ P. Skubic,¹¹³ M. Slater,¹⁸ T. Slavicek,¹²⁸ M. Slawinska,¹⁰⁷ K. Sliwa,¹⁶¹ V. Smakhtin,¹⁷² B. H. Smart,⁴⁶ L. Smestad,¹⁴ S. Yu. Smirnov,⁹⁸ Y. Smirnov,⁹⁸ L. N. Smirnova,^{99,hh} O. Smirnova,⁸¹ M. N. K. Smith,³⁵ R. W. Smith,³⁵ M. Smizanska,⁷² K. Smolek,¹²⁸ A. A. Snesarev,⁹⁶ G. Snidero,⁷⁶ S. Snyder,²⁵ R. Sobie,^{169,k} F. Socher,⁴⁴ A. Soffer,¹⁵³ D. A. Soh,^{151,gg} G. Sokhrannyi,⁷⁵ C. A. Solans,³⁰ M. Solar,¹²⁸ J. Solc,¹²⁸ E. Yu. Soldatov,⁹⁸ U. Soldevila,¹⁶⁷ A. A. Solodkov,¹³⁰ A. Soloshenko,⁶⁵ O. V. Solovyanov,¹³⁰ V. Solovyev,¹²³ P. Sommer,⁴⁸ H. Y. Song,^{33b,y} N. Soni,¹ A. Sood,¹⁵ A. Sopczak,¹²⁸ B. Sopko,¹²⁸ V. Sopko,¹²⁸ V. Sorin,¹² D. Sosa,^{58b} M. Sosebee,⁸ C. L. Sotiropoulou,^{124a,124b} R. Soualah,^{164a,164c} A. M. Soukharev,^{109,c} D. South,⁴² B. C. Sowden,⁷⁷ S. Spagnolo,^{73a,73b} M. Spalla,^{124a,124b} M. Spangenberg,¹⁷⁰ F. Spanò,⁷⁷ W. R. Spearman,⁵⁷ D. Sperlich,¹⁶ F. Spettel,¹⁰¹ R. Spighi,^{20a} G. Spigo,³⁰ L. A. Spiller,⁸⁸ M. Spousta,¹²⁹ R. D. St. Denis,^{53†} A. Stabile,^{91a} S. Staerz,⁴⁴ J. Stahlman,¹²² R. Stamen,^{58a} S. Stamm,¹⁶ E. Stanecka,³⁹ C. Stanescu,^{134a} M. Stanescu-Bellu,⁴² M. M. Stanitzki,⁴² S. Stapnes,¹¹⁹ E. A. Starchenko,¹³⁰ J. Stark,⁵⁵ P. Staroba,¹²⁷ P. Starovoitov,^{58a} R. Staszewski,³⁹ P. Steinberg,²⁵ B. Stelzer,¹⁴² H. J. Stelzer,³⁰ O. Stelzer-Chilton,^{159a} H. Stenzel,⁵² G. A. Stewart,⁵³ J. A. Stillings,²¹ M. C. Stockton,⁸⁷ M. Stoebe,⁸⁷ G. Stoica,^{26b} P. Stolte,⁵⁴ S. Stonjek,¹⁰¹ A. R. Stradling,⁸ A. Straessner,⁴⁴ M. E. Stramaglia,¹⁷ J. Strandberg,¹⁴⁷ S. Strandberg,^{146a,146b} A. Strandlie,¹¹⁹ E. Strauss,¹⁴³ M. Strauss,¹¹³ P. Strizenec,^{144b} R. Ströhmer,¹⁷⁴ D. M. Strom,¹¹⁶ R. Stroynowski,⁴⁰ A. Strubig,¹⁰⁶ S. A. Stucci,¹⁷ B. Stugu,¹⁴ N. A. Styles,⁴² D. Su,¹⁴³ J. Su,¹²⁵ R. Subramaniam,⁷⁹ A. Succurro,¹² Y. Sugaya,¹¹⁸ M. Suk,¹²⁸ V. V. Sulin,⁹⁶ S. Sultansoy,^{4c} T. Sumida,⁶⁸ S. Sun,⁵⁷ X. Sun,^{33a} J. E. Sundermann,⁴⁸ K. Suruliz,¹⁴⁹ G. Susinno,^{37a,37b} M. R. Sutton,¹⁴⁹ S. Suzuki,⁶⁶ M. Svatos,¹²⁷ M. Swiatlowski,¹⁴³ I. Sykora,^{144a} T. Sykora,¹²⁹ D. Ta,⁴⁸ C. Taccini,^{134a,134b} K. Tackmann,⁴² J. Taenzer,¹⁵⁸ A. Taffard,¹⁶³ R. Tahirout,^{159a} N. Taiblum,¹⁵³ H. Takai,²⁵ R. Takashima,⁶⁹ H. Takeda,⁶⁷ T. Takeshita,¹⁴⁰ Y. Takubo,⁶⁶ M. Talby,⁸⁵ A. A. Talyshev,^{109,c} J. Y. C. Tam,¹⁷⁴ K. G. Tan,⁸⁸ J. Tanaka,¹⁵⁵ R. Tanaka,¹¹⁷ S. Tanaka,⁶⁶ B. B. Tannenwald,¹¹¹ N. Tannoury,²¹ S. Tapia Araya,^{32b} S. Tapprogge,⁸³ S. Tarem,¹⁵² F. Tarrade,²⁹ G. F. Tartarelli,^{91a} P. Tas,¹²⁹ M. Tasevsky,¹²⁷ T. Tashiro,⁶⁸ E. Tassi,^{37a,37b} A. Tavares Delgado,^{126a,126b} Y. Tayalati,^{135d} F. E. Taylor,⁹⁴ G. N. Taylor,⁸⁸ P. T. E. Taylor,⁸⁸ W. Taylor,^{159b} F. A. Teischinger,³⁰ M. Teixeira Dias Castanheira,⁷⁶ P. Teixeira-Dias,⁷⁷ K. K. Temming,⁴⁸ D. Temple,¹⁴² H. Ten Kate,³⁰ P. K. Teng,¹⁵¹ J. J. Teoh,¹¹⁸ F. Tepel,¹⁷⁵ S. Terada,⁶⁶ K. Terashi,¹⁵⁵ J. Terron,⁸² S. Terzo,¹⁰¹ M. Testa,⁴⁷ R. J. Teuscher,^{158,k} T. Theveneaux-Pelzer,³⁴ J. P. Thomas,¹⁸ J. Thomas-Wilsker,⁷⁷ E. N. Thompson,³⁵ P. D. Thompson,¹⁸ R. J. Thompson,⁸⁴ A. S. Thompson,⁵³ L. A. Thomsen,¹⁷⁶ E. Thomson,¹²² M. Thomson,²⁸ R. P. Thun,^{89†} M. J. Tibbetts,¹⁵ R. E. Ticse Torres,⁸⁵ V. O. Tikhomirov,^{96,ii} Yu. A. Tikhonov,^{109,c} S. Timoshenko,⁹⁸ E. Tiouchichine,⁸⁵ P. Tipton,¹⁷⁶ S. Tisserant,⁸⁵ K. Todome,¹⁵⁷ T. Todorov,^{5†} S. Todorova-Nova,¹²⁹ J. Tojo,⁷⁰ S. Tokár,^{144a} K. Tokushuku,⁶⁶ K. Tollefson,⁹⁰ E. Tolley,⁵⁷ L. Tomlinson,⁸⁴ M. Tomoto,¹⁰³ L. Tompkins,^{143,jj} K. Toms,¹⁰⁵ E. Torrence,¹¹⁶ H. Torres,¹⁴² E. Torró Pastor,¹³⁸ J. Toth,^{85,kk} F. Touchard,⁸⁵ D. R. Tovey,¹³⁹ T. Trefzger,¹⁷⁴ L. Tremblet,³⁰ A. Tricoli,³⁰ I. M. Trigger,^{159a} S. Trincaz-Duvoid,⁸⁰ M. F. Tripiana,¹² W. Trischuk,¹⁵⁸ B. Trocmé,⁵⁵ C. Troncon,^{91a} M. Trotter-McDonald,¹⁵ M. Trovatelli,¹⁶⁹ L. Truong,^{164a,164c} M. Trzebinski,³⁹ A. Trzupek,³⁹ C. Tsarouchas,³⁰ J. C.-L. Tseng,¹²⁰ P. V. Tsiarehshka,⁹² D. Tsionou,¹⁵⁴ G. Tsipolitis,¹⁰ N. Tsirintanis,⁹ S. Tsiskaridze,¹² V. Tsiskaridze,⁴⁸ E. G. Tskhadadze,^{51a} I. I. Tsukerman,⁹⁷ V. Tsulaia,¹⁵ S. Tsuno,⁶⁶ D. Tsybychev,¹⁴⁸ A. Tudorache,^{26b} V. Tudorache,^{26b} A. N. Tuna,⁵⁷ S. A. Tupputi,^{20a,20b} S. Turchikhin,^{99,hh} D. Turecek,¹²⁸ R. Turra,^{91a,91b} A. J. Turvey,⁴⁰

P. M. Tuts,³⁵ A. Tykhonov,⁴⁹ M. Tylmad,^{146a,146b} M. Tyndel,¹³¹ I. Ueda,¹⁵⁵ R. Ueno,²⁹ M. Ughetto,^{146a,146b} M. Ugland,¹⁴ F. Ukegawa,¹⁶⁰ G. Unal,³⁰ A. Undrus,²⁵ G. Unel,¹⁶³ F. C. Ungaro,⁴⁸ Y. Unno,⁶⁶ C. Unverdorben,¹⁰⁰ J. Urban,^{144b} P. Urquijo,⁸⁸ P. Urrejola,⁸³ G. Usai,⁸ A. Usanova,⁶² L. Vacavant,⁸⁵ V. Vacek,¹²⁸ B. Vachon,⁸⁷ C. Valderanis,⁸³ N. Valencic,¹⁰⁷ S. Valentini,^{20a,20b} A. Valero,¹⁶⁷ L. Valery,¹² S. Valkar,¹²⁹ S. Vallecorsa,⁴⁹ J. A. Valls Ferrer,¹⁶⁷ W. Van Den Wollenberg,¹⁰⁷ P. C. Van Der Deijl,¹⁰⁷ R. van der Geer,¹⁰⁷ H. van der Graaf,¹⁰⁷ N. van Eldik,¹⁵² P. van Gemmeren,⁶ J. Van Nieuwkoop,¹⁴² I. van Vulpen,¹⁰⁷ M. C. van Woerden,³⁰ M. Vanadia,^{132a,132b} W. Vandelli,³⁰ R. Vanguri,¹²² A. Vaniachine,⁶ F. Vannucci,⁸⁰ G. Vardanyan,¹⁷⁷ R. Vari,^{132a} E. W. Varnes,⁷ T. Varol,⁴⁰ D. Varouchas,⁸⁰ A. Vartapetian,⁸ K. E. Varvell,¹⁵⁰ F. Vazeille,³⁴ T. Vazquez Schroeder,⁸⁷ J. Veatch,⁷ L. M. Veloce,¹⁵⁸ F. Veloso,^{126a,126c} T. Velz,²¹ S. Veneziano,^{132a} A. Ventura,^{73a,73b} D. Ventura,⁸⁶ M. Venturi,¹⁶⁹ N. Venturi,¹⁵⁸ A. Venturini,²³ V. Vercesi,^{121a} M. Verducci,^{132a,132b} W. Verkerke,¹⁰⁷ J. C. Vermeulen,¹⁰⁷ A. Vest,⁴⁴ M. C. Vetterli,^{142,d} O. Viazlo,⁸¹ I. Vichou,¹⁶⁵ T. Vickey,¹³⁹ O. E. Vickey Boeriu,¹³⁹ G. H. A. Viehhauser,¹²⁰ S. Viel,¹⁵ R. Vigne,⁶² M. Villa,^{20a,20b} M. Villaplana Perez,^{91a,91b} E. Vilucchi,⁴⁷ M. G. Vincker,²⁹ V. B. Vinogradov,⁶⁵ I. Vivarelli,¹⁴⁹ F. Vives Vaque,³ S. Vlachos,¹⁰ D. Vladoiu,¹⁰⁰ M. Vlasak,¹²⁸ M. Vogel,^{32a} P. Vokac,¹²⁸ G. Volpi,^{124a,124b} M. Volpi,⁸⁸ H. von der Schmitt,¹⁰¹ H. von Radziewski,⁴⁸ E. von Toerne,²¹ V. Vorobel,¹²⁹ K. Vorobev,⁹⁸ M. Vos,¹⁶⁷ R. Voss,³⁰ J. H. Vosseveld,⁷⁴ N. Vranjes,¹³ M. Vranjes Milosavljevic,¹³ V. Vrba,¹²⁷ M. Vreeswijk,¹⁰⁷ R. Vuillemet,³⁰ I. Vukotic,³¹ Z. Vykydal,¹²⁸ P. Wagner,²¹ W. Wagner,¹⁷⁵ H. Wahlberg,⁷¹ S. Wahrmund,⁴⁴ J. Wakabayashi,¹⁰³ J. Walder,⁷² R. Walker,¹⁰⁰ W. Walkowiak,¹⁴¹ C. Wang,¹⁵¹ F. Wang,¹⁷³ H. Wang,¹⁵ H. Wang,⁴⁰ J. Wang,⁴² J. Wang,¹⁵⁰ K. Wang,⁸⁷ R. Wang,⁶ S. M. Wang,¹⁵¹ T. Wang,²¹ T. Wang,³⁵ X. Wang,¹⁷⁶ C. Wanotayaroj,¹¹⁶ A. Warburton,⁸⁷ C. P. Ward,²⁸ D. R. Wardrope,⁷⁸ A. Washbrook,⁴⁶ C. Wasicki,⁴² P. M. Watkins,¹⁸ A. T. Watson,¹⁸ I. J. Watson,¹⁵⁰ M. F. Watson,¹⁸ G. Watts,¹³⁸ S. Watts,⁸⁴ B. M. Waugh,⁷⁸ S. Webb,⁸⁴ M. S. Weber,¹⁷ S. W. Weber,¹⁷⁴ J. S. Webster,³¹ A. R. Weidberg,¹²⁰ B. Weinert,⁶¹ J. Weingarten,⁵⁴ C. Weiser,⁴⁸ H. Weits,¹⁰⁷ P. S. Wells,³⁰ T. Wenaus,²⁵ T. Wengler,³⁰ S. Wenig,³⁰ N. Wermes,²¹ M. Werner,⁴⁸ P. Werner,³⁰ M. Wessels,^{58a} J. Wetter,¹⁶¹ K. Whalen,¹¹⁶ A. M. Wharton,⁷² A. White,⁸ M. J. White,¹ R. White,^{32b} S. White,^{124a,124b} D. Whiteson,¹⁶³ F. J. Wickens,¹³¹ W. Wiedenmann,¹⁷³ M. Wielers,¹³¹ P. Wienemann,²¹ C. Wiglesworth,³⁶ L. A. M. Wiik-Fuchs,²¹ A. Wildauer,¹⁰¹ H. G. Wilkens,³⁰ H. H. Williams,¹²² S. Williams,¹⁰⁷ C. Willis,⁹⁰ S. Willocq,⁸⁶ A. Wilson,⁸⁹ J. A. Wilson,¹⁸ I. Wingerter-Seez,⁵ F. Winklmeier,¹¹⁶ B. T. Winter,²¹ M. Wittgen,¹⁴³ J. Wittkowski,¹⁰⁰ S. J. Wollstadt,⁸³ M. W. Wolter,³⁹ H. Wolters,^{126a,126c} B. K. Wosiek,³⁹ J. Wotschack,³⁰ M. J. Woudstra,⁸⁴ K. W. Wozniak,³⁹ M. Wu,⁵⁵ M. Wu,³¹ S. L. Wu,¹⁷³ X. Wu,⁴⁹ Y. Wu,⁸⁹ T. R. Wyatt,⁸⁴ B. M. Wynne,⁴⁶ S. Xella,³⁶ D. Xu,^{33a} L. Xu,²⁵ B. Yabsley,¹⁵⁰ S. Yacoob,^{145a} R. Yakabe,⁶⁷ M. Yamada,⁶⁶ D. Yamaguchi,¹⁵⁷ Y. Yamaguchi,¹¹⁸ A. Yamamoto,⁶⁶ S. Yamamoto,¹⁵⁵ T. Yamanaka,¹⁵⁵ K. Yamauchi,¹⁰³ Y. Yamazaki,⁶⁷ Z. Yan,²² H. Yang,^{33e} H. Yang,¹⁷³ Y. Yang,¹⁵¹ W-M. Yao,¹⁵ Y. Yasu,⁶⁶ E. Yatsenko,⁵ K. H. Yau Wong,²¹ J. Ye,⁴⁰ S. Ye,²⁵ I. Yeletsikh,⁶⁵ A. L. Yen,⁵⁷ E. Yildirim,⁴² K. Yorita,¹⁷¹ R. Yoshida,⁶ K. Yoshihara,¹²² C. Young,¹⁴³ C. J. S. Young,³⁰ S. Youssef,²² D. R. Yu,¹⁵ J. Yu,⁸ J. M. Yu,⁸⁹ J. Yu,¹¹⁴ L. Yuan,⁶⁷ S. P. Y. Yuen,²¹ A. Yurkewicz,¹⁰⁸ I. Yusuff,^{28,11} B. Zabinski,³⁹ R. Zaidan,⁶³ A. M. Zaitsev,^{130,cc} J. Zalieckas,¹⁴ A. Zaman,¹⁴⁸ S. Zambito,⁵⁷ L. Zanello,^{132a,132b} D. Zanzi,⁸⁸ C. Zeitnitz,¹⁷⁵ M. Zeman,¹²⁸ A. Zemla,^{38a} Q. Zeng,¹⁴³ K. Zengel,²³ O. Zenin,¹³⁰ T. Ženiš,^{144a} D. Zerwas,¹¹⁷ D. Zhang,⁸⁹ F. Zhang,¹⁷³ G. Zhang,^{33b} H. Zhang,^{33c} J. Zhang,⁶ L. Zhang,⁴⁸ R. Zhang,^{33b,i} X. Zhang,^{33d} Z. Zhang,¹¹⁷ X. Zhao,⁴⁰ Y. Zhao,^{33d,117} Z. Zhao,^{33b} A. Zhemchugov,⁶⁵ J. Zhong,¹²⁰ B. Zhou,⁸⁹ C. Zhou,⁴⁵ L. Zhou,³⁵ L. Zhou,⁴⁰ M. Zhou,¹⁴⁸ N. Zhou,^{33f} C. G. Zhu,^{33d} H. Zhu,^{33a} J. Zhu,⁸⁹ Y. Zhu,^{33b} X. Zhuang,^{33a} K. Zhukov,⁹⁶ A. Zibell,¹⁷⁴ D. Zieminska,⁶¹ N. I. Zimine,⁶⁵ C. Zimmermann,⁸³ S. Zimmermann,⁴⁸ Z. Zinonos,⁵⁴ M. Zinser,⁸³ M. Ziolkowski,¹⁴¹ L. Živković,¹³ G. Zobernig,¹⁷³ A. Zoccoli,^{20a,20b} M. zur Nedden,¹⁶ G. Zurzolo,^{104a,104b} and L. Zwalinski³⁰

(ATLAS Collaboration)

¹*Department of Physics, University of Adelaide, Adelaide, Australia*²*Physics Department, SUNY Albany, Albany NY, United States of America*³*Department of Physics, University of Alberta, Edmonton AB, Canada*^{4a}*Department of Physics, Ankara University, Ankara, Turkey*^{4b}*Istanbul Aydin University, Istanbul, Turkey*^{4c}*Division of Physics, TOBB University of Economics and Technology, Ankara, Turkey*⁵*LAPP, CNRS/IN2P3 and Université Savoie Mont Blanc, Annecy-le-Vieux, France*⁶*High Energy Physics Division, Argonne National Laboratory, Argonne IL, United States of America*⁷*Department of Physics, University of Arizona, Tucson AZ, United States of America*⁸*Department of Physics, The University of Texas at Arlington, Arlington TX, United States of America*

- ⁹*Physics Department, University of Athens, Athens, Greece*
- ¹⁰*Physics Department, National Technical University of Athens, Zografou, Greece*
- ¹¹*Institute of Physics, Azerbaijan Academy of Sciences, Baku, Azerbaijan*
- ¹²*Institut de Física d'Altes Energies and Departament de Física de la Universitat Autònoma de Barcelona, Barcelona, Spain*
- ¹³*Institute of Physics, University of Belgrade, Belgrade, Serbia*
- ¹⁴*Department for Physics and Technology, University of Bergen, Bergen, Norway*
- ¹⁵*Physics Division, Lawrence Berkeley National Laboratory and University of California, Berkeley CA, United States of America*
- ¹⁶*Department of Physics, Humboldt University, Berlin, Germany*
- ¹⁷*Albert Einstein Center for Fundamental Physics and Laboratory for High Energy Physics, University of Bern, Bern, Switzerland*
- ¹⁸*School of Physics and Astronomy, University of Birmingham, Birmingham, United Kingdom*
- ^{19a}*Department of Physics, Bogazici University, Istanbul, Turkey*
- ^{19b}*Department of Physics Engineering, Gaziantep University, Gaziantep, Turkey*
- ^{19c}*Department of Physics, Dogus University, Istanbul, Turkey*
- ^{20a}*INFN Sezione di Bologna, Italy*
- ^{20b}*Dipartimento di Fisica e Astronomia, Università di Bologna, Bologna, Italy*
- ²¹*Physikalisches Institut, University of Bonn, Bonn, Germany*
- ²²*Department of Physics, Boston University, Boston MA, United States of America*
- ²³*Department of Physics, Brandeis University, Waltham MA, United States of America*
- ^{24a}*Universidade Federal do Rio De Janeiro COPPE/EE/IF, Rio de Janeiro, Brazil*
- ^{24b}*Electrical Circuits Department, Federal University of Juiz de Fora (UFJF), Juiz de Fora, Brazil*
- ^{24c}*Federal University of Sao Joao del Rei (UFSJ), Sao Joao del Rei, Brazil*
- ^{24d}*Instituto de Física, Universidade de Sao Paulo, Sao Paulo, Brazil*
- ²⁵*Physics Department, Brookhaven National Laboratory, Upton NY, United States of America*
- ^{26a}*Transilvania University of Brasov, Brasov, Romania, Romania*
- ^{26b}*National Institute of Physics and Nuclear Engineering, Bucharest, Romania*
- ^{26c}*National Institute for Research and Development of Isotopic and Molecular Technologies, Physics Department, Cluj Napoca, Romania*
- ^{26d}*University Politehnica Bucharest, Bucharest, Romania*
- ^{26e}*West University in Timisoara, Timisoara, Romania*
- ²⁷*Departamento de Física, Universidad de Buenos Aires, Buenos Aires, Argentina*
- ²⁸*Cavendish Laboratory, University of Cambridge, Cambridge, United Kingdom*
- ²⁹*Department of Physics, Carleton University, Ottawa ON, Canada*
- ³⁰*CERN, Geneva, Switzerland*
- ³¹*Enrico Fermi Institute, University of Chicago, Chicago IL, United States of America*
- ^{32a}*Departamento de Física, Pontificia Universidad Católica de Chile, Santiago, Chile*
- ^{32b}*Departamento de Física, Universidad Técnica Federico Santa María, Valparaíso, Chile*
- ^{33a}*Institute of High Energy Physics, Chinese Academy of Sciences, Beijing, China*
- ^{33b}*Department of Modern Physics, University of Science and Technology of China, Anhui, China*
- ^{33c}*Department of Physics, Nanjing University, Jiangsu, China*
- ^{33d}*School of Physics, Shandong University, Shandong, China*
- ^{33e}*Department of Physics and Astronomy, Shanghai Key Laboratory for Particle Physics and Cosmology, Shanghai Jiao Tong University, Shanghai, China*
- ^{33f}*Physics Department, Tsinghua University, Beijing 100084, China*
- ³⁴*Laboratoire de Physique Corpusculaire, Clermont Université and Université Blaise Pascal and CNRS/IN2P3, Clermont-Ferrand, France*
- ³⁵*Nevis Laboratory, Columbia University, Irvington NY, United States of America*
- ³⁶*Niels Bohr Institute, University of Copenhagen, Kobenhavn, Denmark*
- ^{37a}*INFN Gruppo Collegato di Cosenza, Laboratori Nazionali di Frascati, Italy*
- ^{37b}*Dipartimento di Fisica, Università della Calabria, Rende, Italy*
- ^{38a}*AGH University of Science and Technology, Faculty of Physics and Applied Computer Science, Krakow, Poland*
- ^{38b}*Marian Smoluchowski Institute of Physics, Jagiellonian University, Krakow, Poland*
- ³⁹*Institute of Nuclear Physics Polish Academy of Sciences, Krakow, Poland*
- ⁴⁰*Physics Department, Southern Methodist University, Dallas TX, United States of America*
- ⁴¹*Physics Department, University of Texas at Dallas, Richardson TX, United States of America*
- ⁴²*DESY, Hamburg and Zeuthen, Germany*
- ⁴³*Institut für Experimentelle Physik IV, Technische Universität Dortmund, Dortmund, Germany*

- ⁴⁴*Institut für Kern- und Teilchenphysik, Technische Universität Dresden, Dresden, Germany*
- ⁴⁵*Department of Physics, Duke University, Durham NC, United States of America*
- ⁴⁶*SUPA—School of Physics and Astronomy, University of Edinburgh, Edinburgh, United Kingdom*
- ⁴⁷*INFN Laboratori Nazionali di Frascati, Frascati, Italy*
- ⁴⁸*Fakultät für Mathematik und Physik, Albert-Ludwigs-Universität, Freiburg, Germany*
- ⁴⁹*Section de Physique, Université de Genève, Geneva, Switzerland*
- ^{50a}*INFN Sezione di Genova, Italy*
- ^{50b}*Dipartimento di Fisica, Università di Genova, Genova, Italy*
- ^{51a}*E. Andronikashvili Institute of Physics, Iv. Javakishvili Tbilisi State University, Tbilisi, Georgia*
- ^{51b}*High Energy Physics Institute, Tbilisi State University, Tbilisi, Georgia*
- ⁵²*II Physikalisches Institut, Justus-Liebig-Universität Giessen, Giessen, Germany*
- ⁵³*SUPA—School of Physics and Astronomy, University of Glasgow, Glasgow, United Kingdom*
- ⁵⁴*II Physikalisches Institut, Georg-August-Universität, Göttingen, Germany*
- ⁵⁵*Laboratoire de Physique Subatomique et de Cosmologie, Université Grenoble-Alpes, CNRS/IN2P3, Grenoble, France*
- ⁵⁶*Department of Physics, Hampton University, Hampton VA, United States of America*
- ⁵⁷*Laboratory for Particle Physics and Cosmology, Harvard University, Cambridge MA, United States of America*
- ^{58a}*Kirchhoff-Institut für Physik, Ruprecht-Karls-Universität Heidelberg, Heidelberg, Germany*
- ^{58b}*Physikalisches Institut, Ruprecht-Karls-Universität Heidelberg, Heidelberg, Germany*
- ^{58c}*ZITI Institut für technische Informatik, Ruprecht-Karls-Universität Heidelberg, Mannheim, Germany*
- ⁵⁹*Faculty of Applied Information Science, Hiroshima Institute of Technology, Hiroshima, Japan*
- ^{60a}*Department of Physics, The Chinese University of Hong Kong, Shatin, N.T., Hong Kong, China*
- ^{60b}*Department of Physics, The University of Hong Kong, Hong Kong, China*
- ^{60c}*Department of Physics, The Hong Kong University of Science and Technology, Clear Water Bay, Kowloon, Hong Kong, China*
- ⁶¹*Department of Physics, Indiana University, Bloomington IN, United States of America*
- ⁶²*Institut für Astro- und Teilchenphysik, Leopold-Franzens-Universität, Innsbruck, Austria*
- ⁶³*University of Iowa, Iowa City IA, United States of America*
- ⁶⁴*Department of Physics and Astronomy, Iowa State University, Ames IA, United States of America*
- ⁶⁵*Joint Institute for Nuclear Research, JINR Dubna, Dubna, Russia*
- ⁶⁶*KEK, High Energy Accelerator Research Organization, Tsukuba, Japan*
- ⁶⁷*Graduate School of Science, Kobe University, Kobe, Japan*
- ⁶⁸*Faculty of Science, Kyoto University, Kyoto, Japan*
- ⁶⁹*Kyoto University of Education, Kyoto, Japan*
- ⁷⁰*Department of Physics, Kyushu University, Fukuoka, Japan*
- ⁷¹*Instituto de Física La Plata, Universidad Nacional de La Plata and CONICET, La Plata, Argentina*
- ⁷²*Physics Department, Lancaster University, Lancaster, United Kingdom*
- ^{73a}*INFN Sezione di Lecce, Italy*
- ^{73b}*Dipartimento di Matematica e Fisica, Università del Salento, Lecce, Italy*
- ⁷⁴*Oliver Lodge Laboratory, University of Liverpool, Liverpool, United Kingdom*
- ⁷⁵*Department of Physics, Jožef Stefan Institute and University of Ljubljana, Ljubljana, Slovenia*
- ⁷⁶*School of Physics and Astronomy, Queen Mary University of London, London, United Kingdom*
- ⁷⁷*Department of Physics, Royal Holloway University of London, Surrey, United Kingdom*
- ⁷⁸*Department of Physics and Astronomy, University College London, London, United Kingdom*
- ⁷⁹*Louisiana Tech University, Ruston LA, United States of America*
- ⁸⁰*Laboratoire de Physique Nucléaire et de Hautes Energies, UPMC and Université Paris-Diderot and CNRS/IN2P3, Paris, France*
- ⁸¹*Fysiska institutionen, Lunds universitet, Lund, Sweden*
- ⁸²*Departamento de Física Teórica C-15, Universidad Autónoma de Madrid, Madrid, Spain*
- ⁸³*Institut für Physik, Universität Mainz, Mainz, Germany*
- ⁸⁴*School of Physics and Astronomy, University of Manchester, Manchester, United Kingdom*
- ⁸⁵*CPPM, Aix-Marseille Université and CNRS/IN2P3, Marseille, France*
- ⁸⁶*Department of Physics, University of Massachusetts, Amherst MA, United States of America*
- ⁸⁷*Department of Physics, McGill University, Montreal QC, Canada*
- ⁸⁸*School of Physics, University of Melbourne, Victoria, Australia*
- ⁸⁹*Department of Physics, The University of Michigan, Ann Arbor MI, United States of America*
- ⁹⁰*Department of Physics and Astronomy, Michigan State University, East Lansing MI, United States of America*
- ^{91a}*INFN Sezione di Milano, Italy*
- ^{91b}*Dipartimento di Fisica, Università di Milano, Milano, Italy*

- ⁹²*B.I. Stepanov Institute of Physics, National Academy of Sciences of Belarus, Minsk, Republic of Belarus*
- ⁹³*National Scientific and Educational Centre for Particle and High Energy Physics, Minsk, Republic of Belarus*
- ⁹⁴*Department of Physics, Massachusetts Institute of Technology, Cambridge MA, United States of America*
- ⁹⁵*Group of Particle Physics, University of Montreal, Montreal QC, Canada*
- ⁹⁶*P.N. Lebedev Institute of Physics, Academy of Sciences, Moscow, Russia*
- ⁹⁷*Institute for Theoretical and Experimental Physics (ITEP), Moscow, Russia*
- ⁹⁸*National Research Nuclear University MEPhI, Moscow, Russia*
- ⁹⁹*D.V. Skobeltsyn Institute of Nuclear Physics, M.V. Lomonosov Moscow State University, Moscow, Russia*
- ¹⁰⁰*Fakultät für Physik, Ludwig-Maximilians-Universität München, München, Germany*
- ¹⁰¹*Max-Planck-Institut für Physik (Werner-Heisenberg-Institut), München, Germany*
- ¹⁰²*Nagasaki Institute of Applied Science, Nagasaki, Japan*
- ¹⁰³*Graduate School of Science and Kobayashi-Maskawa Institute, Nagoya University, Nagoya, Japan*
- ^{104a}*INFN Sezione di Napoli, Italy*
- ^{104b}*Dipartimento di Fisica, Università di Napoli, Napoli, Italy*
- ¹⁰⁵*Department of Physics and Astronomy, University of New Mexico, Albuquerque NM, United States of America*
- ¹⁰⁶*Institute for Mathematics, Astrophysics and Particle Physics, Radboud University Nijmegen/Nikhef, Nijmegen, Netherlands*
- ¹⁰⁷*Nikhef National Institute for Subatomic Physics and University of Amsterdam, Amsterdam, Netherlands*
- ¹⁰⁸*Department of Physics, Northern Illinois University, DeKalb IL, United States of America*
- ¹⁰⁹*Budker Institute of Nuclear Physics, SB RAS, Novosibirsk, Russia*
- ¹¹⁰*Department of Physics, New York University, New York NY, United States of America*
- ¹¹¹*Ohio State University, Columbus OH, United States of America*
- ¹¹²*Faculty of Science, Okayama University, Okayama, Japan*
- ¹¹³*Homer L. Dodge Department of Physics and Astronomy, University of Oklahoma, Norman OK, United States of America*
- ¹¹⁴*Department of Physics, Oklahoma State University, Stillwater OK, United States of America*
- ¹¹⁵*Palacký University, RCPTM, Olomouc, Czech Republic*
- ¹¹⁶*Center for High Energy Physics, University of Oregon, Eugene OR, United States of America*
- ¹¹⁷*LAL, Université Paris-Sud and CNRS/IN2P3, Orsay, France*
- ¹¹⁸*Graduate School of Science, Osaka University, Osaka, Japan*
- ¹¹⁹*Department of Physics, University of Oslo, Oslo, Norway*
- ¹²⁰*Department of Physics, Oxford University, Oxford, United Kingdom*
- ^{121a}*INFN Sezione di Pavia, Italy*
- ^{121b}*Dipartimento di Fisica, Università di Pavia, Pavia, Italy*
- ¹²²*Department of Physics, University of Pennsylvania, Philadelphia PA, United States of America*
- ¹²³*National Research Centre “Kurchatov Institute” B.P.Konstantinov Petersburg Nuclear Physics Institute, St. Petersburg, Russia*
- ^{124a}*INFN Sezione di Pisa, Italy*
- ^{124b}*Dipartimento di Fisica E. Fermi, Università di Pisa, Pisa, Italy*
- ¹²⁵*Department of Physics and Astronomy, University of Pittsburgh, Pittsburgh PA, United States of America*
- ^{126a}*Laboratório de Instrumentação e Física Experimental de Partículas—LIP, Lisboa, Portugal*
- ^{126b}*Faculdade de Ciências, Universidade de Lisboa, Lisboa, Portugal*
- ^{126c}*Department of Physics, University of Coimbra, Coimbra, Portugal*
- ^{126d}*Centro de Física Nuclear da Universidade de Lisboa, Lisboa, Portugal*
- ^{126e}*Departamento de Física, Universidade do Minho, Braga, Portugal*
- ^{126f}*Departamento de Física Teórica y del Cosmos and CAFPE, Universidad de Granada, Granada, Spain*
- ^{126g}*Dep Física and CEFITEC of Faculdade de Ciências e Tecnologia, Universidade Nova de Lisboa, Caparica, Portugal*
- ¹²⁷*Institute of Physics, Academy of Sciences of the Czech Republic, Praha, Czech Republic*
- ¹²⁸*Czech Technical University in Prague, Praha, Czech Republic*
- ¹²⁹*Faculty of Mathematics and Physics, Charles University in Prague, Praha, Czech Republic*
- ¹³⁰*State Research Center Institute for High Energy Physics, Protvino, Russia*
- ¹³¹*Particle Physics Department, Rutherford Appleton Laboratory, Didcot, United Kingdom*
- ^{132a}*INFN Sezione di Roma, Italy*
- ^{132b}*Dipartimento di Fisica, Sapienza Università di Roma, Roma, Italy*
- ^{133a}*INFN Sezione di Roma Tor Vergata, Italy*
- ^{133b}*Dipartimento di Fisica, Università di Roma Tor Vergata, Roma, Italy*

- ^{134a}*INFN Sezione di Roma Tre, Italy*
- ^{134b}*Dipartimento di Matematica e Fisica, Università Roma Tre, Roma, Italy*
- ^{135a}*Faculté des Sciences Ain Chock, Réseau Universitaire de Physique des Hautes Energies—Université Hassan II, Casablanca, Morocco*
- ^{135b}*Centre National de l’Energie des Sciences Techniques Nucleaires, Rabat, Morocco*
- ^{135c}*Faculté des Sciences Semlalia, Université Cadi Ayyad, LPHEA-Marrakech, Morocco*
- ^{135d}*Faculté des Sciences, Université Mohamed Premier and LPTPM, Oujda, Morocco*
- ^{135e}*Faculté des sciences, Université Mohammed V, Rabat, Morocco*
- ¹³⁶*DSM/IRFU (Institut de Recherches sur les Lois Fondamentales de l’Univers), CEA Saclay (Commissariat à l’Energie Atomique et aux Energies Alternatives), Gif-sur-Yvette, France*
- ¹³⁷*Santa Cruz Institute for Particle Physics, University of California Santa Cruz, Santa Cruz CA, United States of America*
- ¹³⁸*Department of Physics, University of Washington, Seattle WA, United States of America*
- ¹³⁹*Department of Physics and Astronomy, University of Sheffield, Sheffield, United Kingdom*
- ¹⁴⁰*Department of Physics, Shinshu University, Nagano, Japan*
- ¹⁴¹*Fachbereich Physik, Universität Siegen, Siegen, Germany*
- ¹⁴²*Department of Physics, Simon Fraser University, Burnaby BC, Canada*
- ¹⁴³*SLAC National Accelerator Laboratory, Stanford CA, United States of America*
- ^{144a}*Faculty of Mathematics, Physics & Informatics, Comenius University, Bratislava, Slovak Republic*
- ^{144b}*Department of Subnuclear Physics, Institute of Experimental Physics of the Slovak Academy of Sciences, Kosice, Slovak Republic*
- ^{145a}*Department of Physics, University of Cape Town, Cape Town, South Africa*
- ^{145b}*Department of Physics, University of Johannesburg, Johannesburg, South Africa*
- ^{145c}*School of Physics, University of the Witwatersrand, Johannesburg, South Africa*
- ^{146a}*Department of Physics, Stockholm University, Sweden*
- ^{146b}*The Oskar Klein Centre, Stockholm, Sweden*
- ¹⁴⁷*Physics Department, Royal Institute of Technology, Stockholm, Sweden*
- ¹⁴⁸*Departments of Physics & Astronomy and Chemistry, Stony Brook University, Stony Brook NY, United States of America*
- ¹⁴⁹*Department of Physics and Astronomy, University of Sussex, Brighton, United Kingdom*
- ¹⁵⁰*School of Physics, University of Sydney, Sydney, Australia*
- ¹⁵¹*Institute of Physics, Academia Sinica, Taipei, Taiwan*
- ¹⁵²*Department of Physics, Technion: Israel Institute of Technology, Haifa, Israel*
- ¹⁵³*Raymond and Beverly Sackler School of Physics and Astronomy, Tel Aviv University, Tel Aviv, Israel*
- ¹⁵⁴*Department of Physics, Aristotle University of Thessaloniki, Thessaloniki, Greece*
- ¹⁵⁵*International Center for Elementary Particle Physics and Department of Physics, The University of Tokyo, Tokyo, Japan*
- ¹⁵⁶*Graduate School of Science and Technology, Tokyo Metropolitan University, Tokyo, Japan*
- ¹⁵⁷*Department of Physics, Tokyo Institute of Technology, Tokyo, Japan*
- ¹⁵⁸*Department of Physics, University of Toronto, Toronto ON, Canada*
- ^{159a}*TRIUMF, Vancouver BC, Canada*
- ^{159b}*Department of Physics and Astronomy, York University, Toronto ON, Canada*
- ¹⁶⁰*Faculty of Pure and Applied Sciences, University of Tsukuba, Tsukuba, Japan*
- ¹⁶¹*Department of Physics and Astronomy, Tufts University, Medford MA, United States of America*
- ¹⁶²*Centro de Investigaciones, Universidad Antonio Narino, Bogota, Colombia*
- ¹⁶³*Department of Physics and Astronomy, University of California Irvine, Irvine CA, United States of America*
- ^{164a}*INFN Gruppo Collegato di Udine, Sezione di Trieste, Udine, Italy*
- ^{164b}*ICTP, Trieste, Italy*
- ^{164c}*Dipartimento di Chimica, Fisica e Ambiente, Università di Udine, Udine, Italy*
- ¹⁶⁵*Department of Physics, University of Illinois, Urbana IL, United States of America*
- ¹⁶⁶*Department of Physics and Astronomy, University of Uppsala, Uppsala, Sweden*
- ¹⁶⁷*Instituto de Física Corpuscular (IFIC) and Departamento de Física Atómica, Molecular y Nuclear and Departamento de Ingeniería Electrónica and Instituto de Microelectrónica de Barcelona (IMB-CNM), University of Valencia and CSIC, Valencia, Spain*
- ¹⁶⁸*Department of Physics, University of British Columbia, Vancouver BC, Canada*
- ¹⁶⁹*Department of Physics and Astronomy, University of Victoria, Victoria BC, Canada*
- ¹⁷⁰*Department of Physics, University of Warwick, Coventry, United Kingdom*
- ¹⁷¹*Waseda University, Tokyo, Japan*
- ¹⁷²*Department of Particle Physics, The Weizmann Institute of Science, Rehovot, Israel*

¹⁷³*Department of Physics, University of Wisconsin, Madison WI, United States of America*

¹⁷⁴*Fakultät für Physik und Astronomie, Julius-Maximilians-Universität, Würzburg, Germany*

¹⁷⁵*Fachbereich C Physik, Bergische Universität Wuppertal, Wuppertal, Germany*

¹⁷⁶*Department of Physics, Yale University, New Haven CT, United States of America*

¹⁷⁷*Yerevan Physics Institute, Yerevan, Armenia*

¹⁷⁸*Centre de Calcul de l'Institut National de Physique Nucléaire et de Physique des Particules (IN2P3), Villeurbanne, France*

[†]Deceased.

^aAlso at Department of Physics, King's College London, London, United Kingdom,

^bAlso at Institute of Physics, Azerbaijan Academy of Sciences, Baku, Azerbaijan,

^cAlso at Novosibirsk State University, Novosibirsk, Russia,

^dAlso at TRIUMF, Vancouver BC, Canada,

^eAlso at Department of Physics, California State University, Fresno, CA, USA.

^fAlso at Department of Physics, University of Fribourg, Fribourg, Switzerland.

^gAlso at Departamento de Física e Astronomia, Faculdade de Ciências, Universidade do Porto, Portugal.

^hAlso at Tomsk State University, Tomsk, Russia.

ⁱAlso at CPPM, Aix-Marseille Université and CNRS/IN2P3, Marseille, France.

^jAlso at Università di Napoli Parthenope, Napoli, Italy.

^kAlso at Institute of Particle Physics (IPP), Canada.

^lAlso at Particle Physics Department, Rutherford Appleton Laboratory, Didcot, United Kingdom.

^mAlso at Department of Physics, St. Petersburg State Polytechnical University, St. Petersburg, Russia.

ⁿAlso at Louisiana Tech University, Ruston, LA, USA.

^oAlso at Institutio Catalana de Recerca i Estudis Avancats, ICREA, Barcelona, Spain.

^pAlso at Department of Physics, The University of Michigan, Ann Arbor, MI, USA.

^qAlso at Graduate School of Science, Osaka University, Osaka, Japan.

^rAlso at Department of Physics, National Tsing Hua University, Taiwan.

^sAlso at Department of Physics, The University of Texas at Austin, Austin, TX, USA.

^tAlso at Institute of Theoretical Physics, Ilia State University, Tbilisi, Georgia.

^uAlso at CERN, Geneva, Switzerland.

^vAlso at Georgian Technical University (GTU), Tbilisi, Georgia.

^wAlso at Manhattan College, New York, NY, USA.

^xAlso at Hellenic Open University, Patras, Greece.

^yAlso at Institute of Physics, Academia Sinica, Taipei, Taiwan.

^zAlso at LAL, Université Paris-Sud and CNRS/IN2P3, Orsay, France.

^{aa}Also at Academia Sinica Grid Computing, Institute of Physics, Academia Sinica, Taipei, Taiwan.

^{bb}Also at School of Physics, Shandong University, Shandong, China.

^{cc}Also at Moscow Institute of Physics and Technology State University, Dolgoprudny, Russia.

^{dd}Also at Section de Physique, Université de Genève, Geneva, Switzerland.

^{ee}Also at International School for Advanced Studies (SISSA), Trieste, Italy.

^{ff}Also at Department of Physics and Astronomy, University of South Carolina, Columbia, SC, USA.

^{gg}Also at School of Physics and Engineering, Sun Yat-sen University, Guangzhou, China.

^{hh}Also at Faculty of Physics, M.V.Lomonosov Moscow State University, Moscow, Russia.

ⁱⁱAlso at National Research Nuclear University MEPhI, Moscow, Russia.

^{jj}Also at Department of Physics, Stanford University, Stanford, CA, USA.

^{kk}Also at Institute for Particle and Nuclear Physics, Wigner Research Centre for Physics, Budapest, Hungary.

^{ll}Also at University of Malaya, Department of Physics, Kuala Lumpur, Malaysia.